DESIGN AND CHARACTERIZATION OF ABSORBENT POLYMERS FOR TWO-PHASE PARTITIONING BIOREACTOR APPLICATIONS

by

Stuart Lloyd Bacon

A thesis submitted to the Department of Chemical Engineering

in conformity with the requirements for

the degree of Doctor of Philosophy

Queen's University

Kingston, Ontario, Canada

(February, 2017)

Abstract

The production of fuels and chemicals from renewable biomass feedstocks can reduce our reliance on petroleum resources and help mitigate environmental issues associated with their use. However, many bioprocesses are limited by end-product inhibition, leading to lower product titer and reduced bioreactor productivity. Introducing a carefully selected solid absorbent polymer can reduce end-product inhibition by removing the product as it is formed and enriching it within the polymer phase. To be effective, the polymer must possess (1) a high affinity for the target solute, measured by its partition coefficient (PC), (2) a preference for solute absorption over water uptake, measured by selectivity (α), (3) biocompatibility towards the microorganism, and (4) sufficient physical strength to withstand the high shear bioreactor environment.

The present work begins with an evaluation of thermodynamic activity models for *a priori* polymer phase selection. Accurate PC predictions were demonstrated for a range of target solutes in rubbery, amorphous materials. Further, polymer selection based on PC was shown to favor low molecular weight (MW) materials, whereas higher MW polymer yielded stronger, more solid-like absorbents. Compromises between absorptive and physical properties inherent to unimodal molecular weight distribution (MWD) polymers were mitigated by developing novel bimodal MWD formulations, made from mixing very low MW material (organic solvent or oligomer) with a high MW polymer. Solute absorption was also sensitive towards polymer crystallinity and water uptake; these factors were captured qualitatively by the thermodynamic models but with significantly reduced prediction accuracy.

Remarkable improvements in both PC and α for n-butanol and n-octanol were realized by covalently tethering small amounts of imidazolium ionic functionality to a hydrophobic polymer, yielding an ionomer. Further improvements were achieved by preparing high ionic content polyelectrolytes, polymerized from reactive imidazolium ionic liquids (IL). The polyelectrolytes registered excellent PC values for several alcohols (n-butanol, iso-butanol, ethanol) as well as good solute/water selectivity. Importantly, both ionomer and hydrophobic polyelectrolyte formulations substantially eliminated cytotoxicity and water-solubility concerns associated with analogous ILs. These findings advance the state-of-the-art in absorbent materials for bioprocess separations and represent a promising avenue for future partitioning bioreactor research.

Co-Authorship

Chapters 2 to 5 have been published in refereed journals and were co-authored by Professor Andrew J. Daugulis and Professor J. Scott Parent, who provided technical and editorial advice. Dr. Eric Peterson made a significant contribution to Chapter 4 with his work on butyric acid absorption and melting point depression, in addition to technical and editorial advice. Chapter 6 has been prepared in draft manuscript form and was co-authored by Professor Andrew J. Daugulis and Professor J. Scott Parent, who provided technical and editorial advice, as well as Rachel Ross, who assisted with ionic liquid (IL) and polyelectrolyte synthesis.

Acknowledgements

I would like to thank my supervisors, Andrew Daugulis and Scott Parent, for their support and guidance throughout my graduate degree. I am particularly grateful for their countless ideas that are embedded throughout this work, for their technical guidance on all things polymer/thermo/fermentation and for their patience and persistence in helping me develop the craft of technical writing.

I would also like to thank my lab-mates past and present for their help along the way. From the Daugulis lab, many thanks to Dr. Eric Peterson, Dr. Julian Dafoe, Eduardo Poleo and Jake Alexiou for their insights and technical guidance on cell culture and analytics. From the Parent lab, I'd like to thank Chris Twigg, Mike Bodley and Kyle Ozols for their assistance with organic synthesis and polymer modification. I'd also like to thank Rachel Ross for her work on polyelectrolyte synthesis during the summer.

Finally, I'd like to thank my family and Hannah for their enduring support throughout this journey.

Table of Contents

List of Figures

List of Tables

Chapter 1

Introduction

1.1 Overview

Increasing energy costs, emergent environmental issues and national energy independence have contributed to interest in producing chemicals and fuels from renewable biomass feedstocks. However, the bioprocesses that yield these chemical and fuels are often limited by end-product inhibition, leading to reduced product titre and volumetric productivity. Commercially, end-product inhibition can affect bioprocess economics by increasing fermenter costs, downstream processing costs and wastewater treatment costs.[1] *In-situ* product recovery (ISPR) technologies can mitigate these effects by removing and enriching the products as they are produced. Bioprocesses of particular interest for use with ISPR include alcohol and organic acid fermentations, as well as biotransformations producing flavours/fragrance compounds, neutraceuticals and pharmaceutical intermediates.[2–5]

1.2 *In-situ* product recovery (ISPR)

Depending on the properties of the target fermentation end product, competing technologies for ISPR can include gas stripping, liquid-liquid extraction, adsorption, solid-liquid extraction (i.e. polymeric absorption), pervaporation and perstraction, for which there are several recent and comprehensive reviews.[6–9] The applicability and economic viability of each ISPR technique requires careful analysis of target molecule properties, bioprocessing strategy and operational configuration. In all ISPR strategies, successful implementation can depend on selection of an appropriate secondary phase (gas, liquid or solid) to sequester and enrich the target molecule. The present work is focussed on advancing the selection and design of polymeric *absorbents* for solid-liquid extraction. The following review provides background information on the current state-of-

the-art pertaining to liquid-liquid extraction (Section 1.3) and solid-liquid systems, covering both *adsorptive* and *absorptive* materials (Section 1.4). Particular attention will be given to the pre-existing frameworks and methodologies used to select liquid and solid extractants as the foundation for the scientific contributions described in this thesis.

1.3 Liquid-liquid systems

Immiscible liquid extractants sequester the toxic solute from the aqueous fermentation medium into a distinct organic phase, a technology platform commonly referred to as a 'two-phase partitioning bioreactor' (TPPB). Liquid extractants can include: organic solvents, oligomeric liquids including silicone oil (polydimethyl siloxane, PDMS) and poly(propylene glycol), and, more recently, ionic liquids (ILs). Liquid-liquid extraction implementations have been previously studied in great depth in both in internal or external configurations (see reviews[6,9,12]), categorized on the basis of whether product is recovered within the bioreactor or in an external unit.[1] In internal configurations, the liquid extractant is contacted with the aqueous fermentation broth directly in the bioreactor. External configurations require an extractant contactor module to yield a product-rich extractant stream sent for regeneration and product recovery. In either configuration, the target molecule is transferred from aqueous fermentation broth to the extractant according to thermodynamic equilibrium, commonly quantified by the solute's partition coefficient (PC_i) (Equation 1), the ratio of solute mass fraction in the extractant phase ($w_i^{extract}$) and the aqueous broth ($w_i^{aqeuous}$).

$$\boldsymbol{PC_i = \frac{w_i^{extract}}{w_i^{aqeuous}}} \quad (1)$$

Larger PCs influence bioreactor volumetric productivity by requiring less polymer to remove a given quantity of product, thereby occupying less fermentor volume and reducing fixed process

costs. In contrast, the cost effectiveness and energy requirements of downstream product purification processes (e.g. distillation) are particularly sensitive to the extractant's preference for solute absorption over water uptake, quantified by solute/water selectivity (Equation 2).

$$\alpha_{i/w} = \frac{PC_i}{PC_{water}} \quad (2)$$

In addition to PC and selectivity, there are a number of operational factors that must be considered when screening liquid extractants for TPPB applications, summarized in Table 1, for which more detailed descriptions are available.[6]

Table 1 - Extractant property considerations for liquid-liquid extraction

Large equilibrium partition coefficient (PC)
High product/water selectivity ($\alpha_{i/w}$)
Biocompatibility
Non-bioavailability
Water insolubility
Easy separation
Low volatility, flammability
Low cost

1.3.1 Organic solvents and oligomers

The use of organic solvents and oligomers in liquid-liquid extraction ISPR configurations has been investigated over the past several decades,[15] and has been successfully applied to a wide range of two-phase fermentation and biotransformation processes. The selection of organic solvents for TPPBs has been well-established, most notably the development of a predictive

extractant screening program (ESP) to rank organic solvents based on solute affinity (PC) and selectivity ($\alpha_{i/w}$) using the UNIFAC group contribution activity model.[16] These PC and selectivity predictions are qualitatively accurate and, in conjunction with consideration of the extractant criteria outlined in Table 1, have been used successfully for the selection of appropriate solvent extractants in many systems.[17,18] In contrast, the use of viscoelastic liquid oligomers, namely poly(propylene glycol) and silicone oil (PDMS) has been limited to heuristics.[19,20]

The study of organic solvent biocompatibility is also well established, with the 'critical log $K_{o/w}$' concept a quantitative means of predicting biocompatibility for a wide range of microbes.[18] In general, the critical log $K_{o/w}$ is a microorganism-specific value for which organic solvents that possess Log $K_{o/w}$ values above the critical point are biocompatible, and solvents with log $K_{o/w}$ values below the critical point are generally cytotoxic. More generally, the critical log $K_{o/w}$ value is representative of the organic solvent's hydrophobicity, and consequently, its water solubility. Biocompatibility of oligomers is less well understood, and the log $K_{o/w}$ concept is not strictly held for these systems.[21] It has been suggested that the molecular weight distribution of certain oligomeric extractants and the effect of oligomer molecular weight on Log $K_{o/w}$ and water solubility may limit this type of analysis.[21]

1.3.2 Ionic liquids

Ionic liquids have shown great promise for their use in separations,[23,24] ability to break azeotropes[25] and as solvents for enzyme catalysis (recently reviewed by Potdar et al.[22]). Separation processes based on ionic liquids (IL)[26–29] have benefited greatly from their low vapour pressure and ability to adjust solute affinity by varying cation and anion structure.[23,25,30–33] For polar fermentation solutes such as n-butanol, PC values for ILs can exceed[34] those for comparable organic solvents[19] due to strong hydrogen bonding and ion-dipole interactions.

Selection of ILs for their use in ISPR has generally been limited to heuristics.[6,35] Recent work using the COSMO-RS model has demonstrated the *a priori* prediction of PC and α values for various organic-organic liquid-liquid systems, however, the quantitative accuracy of COSMO-RS for water-containing systems is system dependent.[36–39] Nevertheless, investigation into the predictive capabilities of COSMO-RS represents a unique opportunity for qualitative IL screening that would be otherwise impossible using UNIFAC-derived activity models used for non-ionic organic solvents.

While the use of ILs has gained recent interest in many fields, their utility in whole cell and enzyme biocatalysis and ISPR has been limited to date by microbe cytotoxicity[40–44] and enzyme destabilization/deactivation.[45,46] While strategies such as lower extractant phase ratios and less toxic cation/anion combinations have identified some biocompatible options,[47–49] the compatibility of ILs with ISPR techniques that rely on direct contact between extractant and fermentation medium remains uncertain. Related to biocompatibility, water solubility remains another concern for many routinely studied ILs.[50,51] In addition, two-phase stability and the potential for emulsions are concerns for surfactant-like ILs, however, this can be overcome through careful IL selection.[24,27]

1.4 Solid-liquid systems

Two separate classes of solid extractants differ by their mechanism of solute sequestration, namely, adsorptive or absorptive materials. Adsorptive resins are typically hard, glassy and porous, providing solute sequestration based on surface-based interactions. In contrast, absorptive materials tend to be rubbery amorphous bulk solids, removing solute according to absorptive thermodynamic equilibrium akin to a liquid solvent. In solid-liquid extraction, absorbent or adsorbent particles can be separated from the bioreactor medium using a coarse mesh, centrifuge or cyclone separator. Solid extractants can offer operational benefits over liquid extractants as

they do not emulsify or interact with bioreactor internals. Additional benefits of solid particles include their lack of volatility and decreased water solubility.

1.4.1 Adsorptive resins

Adsorptive resins are glassy ($T_g > T_{bioreactor}$) materials that function *via* surface interactions between solute and interaction sites on the polymer. The amount of solute adsorbed is described according to a Freundlich or Langmuir isotherm.[52] They are most commonly composed of inorganic zeolites (e.g. silicalite), activated and mesoporous carbons or poly(styrene-co-divinylbenene) based resins, as recently reviewed.[53] Hydrophobic adsorptive polymeric resins are selected based on their specific surface area (m^2/g), specific loading (mmol/kg) and selectivity towards the target solute. Due to the solid-liquid, surface interaction-based equilibrium dynamics of adsorptive processes, solute adsorption (PC) is highly dependent on material characteristics such as specific surface area and aqueous solute concentration. As a result, adsorbent resins tend to exhibit higher PC values at lower aqueous concentrations.

Adsorbent resins are typically selected for use in ISPR applications using both heuristics and a trial-and-error approach. At present, there does not appear to be a systematic methodology to predict the performance of an adsorbent resin based on its structure and/or properties. Adsorbent resins are generally considered inherently biocompatible toward microbes,[54] however, glassy adsorbents with rough surfaces can reduce cell viability when used under agitation *in-situ* due to physical cell disruption.[55] Furthermore, glassy adsorptive resins can fracture and lose mechanical integrity due to the shear stress experienced in a stirred-tank bioreactor,[54] favoring the use of *ex-situ* expanded bed adsorption column configurations to minimize shear environments.[56,57] However, the abundant surface area and rough surfaces establish conditions for which adsorptive performance can be limited by surface fouling, biofilm formation and competitive adsorption.[58,59]

1.4.2 Absorptive polymers

Use of absorptive polymers in TPPBs has gained interest in recent years due to their inherent biocompatibility, low cost, lack of volatility and non-bioavailability.[17] Polymers possess complex structure-property relationships, which makes polymer selection a challenging task. In general terms, a polymer's structure encompasses the material's chemical composition and molecular weight distribution. Chemical composition refers to both mer and end-group structure, the latter being particularly influential at low molecular weight. Polymer molecular weight distribution refers to the fact that polymers do not have a single molecular weight (MW) in the manner of organic solvents, but a distribution of MWs that can influence physical and chemical properties.

Selection criteria based on polymer properties are similar to those listed for liquid extractants in Table 1, with some minor changes due to several unique polymer characteristics. While volatility, flammability, water-solubility and emulsion formation can be mitigated by using solid polymer absorbents, shear forces throughout the bioprocess introduce the criterion of a tough, solid polymer capable of facile solid/liquid separation. Additionally, product absorption throughout the polymer's bulk requires amorphous, rubbery domains. In semi-crystalline materials, absorption is limited to the amorphous phase due to the non-absorptive properties of intact crystallites.[61–63] Similarly, glassy materials possessing a glass transition temperature (T_g) above the operating temperature ($T_{bioreactor}$) are non-absorptive, limiting product sequestration to surface-based interactions (as in adsorptive resins). Thus, polymer T_g, degree of crystallinity and melting temperature (T_m) must be considered as additional polymer selection criteria.

Selection of absorptive polymers has been previously limited to heuristics, however, recent studied have begun the development of a first principles' approach to rational polymeric extractant selection.[60,61,64] These approaches have identified the thermodynamic equilibrium existing between polymer and aqueous phase, providing qualitative assessments of polymer

performance based on T_g and thermodynamic affinity (PC), estimated using solubility parameter and polymer functional groups analysis (UNIFAC).

1.5 Scope of thesis

For effective use in a TPPB applications, an absorbent polymer must have: (1) a high affinity for the inhibitory solute (PC), (2) a low affinity for water ($\alpha_{i/w}$), (3) biocompatibility with the microorganisms and (4) solid-like physical properties to enable facile separation from the fermentation medium. This thesis advances the state-of-the-art in absorbent selection and design to satisfy these four requirements.

The objective of Chapters 2 through 4 was to develop a first principles' approach to polymer selection based on the structure-property relationships that govern the absorption of inhibitory solutes. Chapter 2 provides a thorough investigation into polymer-solute thermodynamic affinity based on solute and polymer chemical composition. A rigorous analysis of the thermodynamic equilibrium that exists between the polymer extractant and the aqueous phase is performed, resulting in a reliable thermodynamic framework to predict solute PC using polymer-solute activity models. This framework was validated using a range of experimental solute absorption data in poly(butyl acrylate), an amorphous, rubbery, non-ionic polymer.

Chapter 3 expands on this work by investigating the effect of polymer molecular weight and molecular weight distribution (MWD) on absorbent selection. This study demonstrated that solute PC can increase significantly as polymer's number average molecular weight (M_n) is lowered. Importantly, MWD is shown to have no effect on solute uptake, with both unimodal and bimodal distributions generating the same PC at a given M_n. Given the dependence on polymer physical properties on both M_n and MWD, we demonstrated that highly bimodal polymer mixtures can be formulated to provide high PC values (low M_n) as well as satisfactory material strength.

Two other important considerations for absorbent polymer selection, the material's glass transition temperature and degree of crystallinity, are investigated in Chapter 4. This work identifies the importance of these polymer properties on both the extent (i.e. PC) and rate of solute absorption. The thermodynamic framework developed in Chapter 2 is reapplied to polar semi-crystalline polymers that take up significant amounts of water, demonstrating a qualitative ability to rank these more complex materials based on predicted PC.

Chapters 5 and 6 shift focus from the selection of commercially available polymers to the synthesis and derivatization of novel ionic absorbents. This work was founded on the discovery in Chapter 5 that a small amount of imidazolium bromide functionality incorporated within an isobutylene-rich matrix provides significant improvements in both PC and selectivity for polar solutes (i.e. butanol, octanol). Interestingly, while ionic liquid (IL) analogs were not biocompatible towards the three microorganisms tested, covalent tethering of the imidazolium ionic functionality to the insoluble polymer backbone largely eliminated cytotoxicity. Furthermore, although the ionomers were biocompatible with suspended cells, the materials demonstrated antimicrobial surface properties, preventing the proliferation of some microorganisms under sustained, direct contact.

Given the inherently low level of ionic functionality present in ionomers, Chapter 6 focused on developing a novel polyelectrolyte absorbent synthesized by polymerization of a reactive imidazolium IL. This work demonstrated that polymerization of ILs into insoluble gels and linear thermoformable materials can successfully eliminate cytotoxicity while simultaneously providing excellent absorptive properties for polar fermentation products. Finally, Chapter 7 briefly outlines the main conclusions from this work and highlights the most promising areas for future research.

1.6 References

1 W. Van Hecke, G. Kaur and H. De Wever, *Biotechnol. Adv.*, 2014, **32**, 1245–1255.

2 C. S. López-Garzón and A. J. J. Straathof, *Biotechnol. Adv.*, 2014, **32**, 873–904.

3 T. C. Ezeji, N. Qureshi and H. P. Blaschek, *Curr. Opin. Biotechnol.*, 2007, **18**, 220–7.

4 I. Faizal, M. Ohba, A. Juroda, N. Takigughi, H. Ohtake, K. Honda and J. Kato, *J. Environ. Biotechnol.*, 2007, **7**, 39–44.

5 T. Craig and A. J. Daugulis, *Biochem. Eng. J.*, 2014, **82**, 97–104.

6 J. T. Dafoe and A. J. Daugulis, *Biotechnol. Lett.*, 2014, **36**, 443–60.

7 W. Van Hecke, T. Hofmann and H. De Wever, *Bioresour. Technol.*, 2013, **129**, 421–9.

8 H.-J. Huang, S. Ramaswamy, U. W. Tschirner and B. V. Ramarao, *Sep. Purif. Technol.*, 2008, **62**, 1–21.

9 L. M. Vane, *Biofuels, Bioprod. Biorefining*, 2008, **2**, 553–588.

10 H. Fujita, *Adv. Polym. Sci.*, 1961, **3**, 1–47.

11 J. G. Wijmans and R. W. Baker, *J. Memb. Sci.*, 1995, **107**, 1–21.

12 J. J. Malinowski, *Biotechnol. Adv.*, 2001, **19**, 525–38.

13 J. Polák and G. C. Benson, *J. Chem. Thermodyn.*, 1971, **3**, 235–242.

14 M. Matsumura, H. Kataoka, M. Sueki and K. Araki, *Bioprocess Eng.*, 1988, **3**, 93–100.

15 A. J. Daugulis, D. E. Swaine, F. Kollerup and C. A. Groom, *Biotechnol. Lett.*, 1987, **9**, 425–430.

16 F. Kollerup and A. J. Daugulis, *Can. J. Chem. Eng.*, 1985, **63**, 919–927.

17 G. Quijano, M. Hernandez, F. Thalasso, R. Muñoz and S. Villaverde, *Appl. Microbiol. Biotechnol.*, 2009, **84**, 829–46.

18 L. J. Bruce and A. J. Daugulis, *Biotechnol. Prog.*, 1991, **7**, 116–24.

19 W. E. Barton and A. J. Daugulis, *Appl. Microbiol. Biotechnol.*, 1992, **36**, 632–639.

20 P. Parnian, S. M. Zamir and S. A. Shojaosadati, *Chem. Eng. J.*, 2016, **284**, 926–933.

21 J. Harris and A. J. Daugulis, *Biotechnol. Bioeng.*, 2015, **112**, 2450–2458.

22 M. K. Potdar, G. F. Kelso, L. Schwarz, C. Zhang and M. T. W. Hearn, *Molecules*, 2015, **20**, 16788–16816.

23 P. Steltenpohl and E. Graczová, *Acta Chim. Slovaca*, 2014, **7**, 129–133.

24 C. F. Poole and S. K. Poole, *J. Chromatogr. A*, 2010, **1217**, 2268–2286.

25 A. B. Pereiro, J. M. M. Araujo, J. M. S. S. Esperanca, I. M. Marrucho and L. P. N. Rebelo, *J. Chem. Thermodyn.*, 2012, **46**, 2–28.

26 M. Zawadzki, F. A. e Silva, U. Domańska, J. A. P. Coutinho and S. P. M. Ventura, *Green Chem.*, 2016, **18**, 3527–3536.

27 R. J. Cornmell, C. L. Winder, S. Schuler, R. Goodacre and G. Stephens, *Green Chem.*, 2008, **10**, 685–691.

28 U. Domańska and M. Królikowski, *J. Chem. Thermodyn.*, 2012, **53**, 108–113.

29 K. S. Khachatryan, S. V. Smirnova, I. I. Torocheshnikova, N. V. Shvedene, A. A. Formanovsky and I. V. Pletnev, *Anal. Bioanal. Chem.*, 2005, **381**, 464–470.

30 W. Y. Lou, M. H. Zong and T. J. Smith, *Green Chem.*, 2006, **8**, 147–155.

31 L. D. Simoni, A. Chapeaux, J. F. Brennecke and M. A. Stadtherr, *Comput. Chem. Eng.*, 2010, **34**, 1406–1412.

32 H. Zhao, S. Xia and P. Ma, *J. Chem. Technol. Biotechnol.*, 2005, **80**, 1089–1096.

33 P. Dehury, U. Mahanta and T. Banerjee, *Fluid Phase Equilib.*, 2016, (In Press).

34 L. Y. Garcia-chavez, C. M. Garsia, B. Schuur and A. B. De Haan, *Ind. Eng. Chem. Res.*, 2012, **51**.

35 S. H. Ha, N. L. Mai and Y.-M. Koo, *Process Biochem.*, 2010, **45**, 1899–1903.

36 F. S. Oliveira, J. M. M. Araújo, R. Ferreira, L. P. Rebelo and I. M. Marrucho, *Sep. Purif. Technol.*, 2012, **85**, 137–146.

37 C. M. S. S. Neves, J. F. O. Granjo, M. G. Freire, A. Robertson, N. M. C. Oliveira and J. A. P. Coutinho, *Green Chem.*, 2011, **13**, 1517–1526.

38 M. Diedenhofen and A. Klamt, *Fluid Phase Equilib.*, 2010, **294**, 31–38.

39 D. Rabari and T. Banerjee, *Ind. Eng. Chem. Res.*, 2014, **53**, 18935–18942.

40 R. Melgarejo-Torres, C. O. Castillo-Araiza, P. López-Ordaz, N. V. Calleja-Castañeda, J. L. Cano-Velasco, R. M. Camacho-Ruíz, G. J. Lye and S. Huerta-Ochoa, *Chem. Eng. J.*, 2015, **279**, 379–386.

41 O. Dipeolu, E. Green and G. Stephens, *Green Chem.*, 2009, **11**, 397.

42 M. Matsumoto, K. Mochiduki, K. Fukunishi and K. Kondo, *Sep. Purif. Technol.*, 2004, **40**, 97–101.

43 A. Romero, A. Santos, J. Tojo and A. Rodríguez, *J. Hazard. Mater.*, 2008, **151**, 268–273.

44 K. M. Docherty and C. F. Kulpa, Jr., *Green Chem.*, 2005, **7**, 185.

45 H. Zhao, O. Olubajo, Z. Song, A. L. Sims, T. E. Person, R. A. Lawal and L. A. Holley, *Bioorg. Chem.*, 2006, **34**, 15–25.

46 H. Zhao, *J. Mol. Catal. B Enzym.*, 2005, **37**, 16–25.

47 S. Mao, B. Hua, N. Wang, X. Hu, Z. Ge, Y. Li, S. Liu and F. Lu, *J. Chem. Technol. Biotechnol.*, 2013, **88**, 287–292.

48 R. J. Cornmell, C. L. Winder, G. J. T. Tiddy, R. Goodacre and G. Stephens, *Green Chem.*, 2008, **10**, 836.

49 A. Lenourry, J. M. Gardiner and G. Stephens, *Biotechnol. Lett.*, 2005, **27**, 161–165.

50 A. Hasanoğlu, *Desalin. Water Treat.*, 2015, **3994**, 1–13.

51 M. Matsumoto, K. Mochiduki and K. Kondo, *J. Biosci. Bioeng.*, 2004, **98**, 344–7.

52 M. Wiehn, Arizona State University, 2013.

53 K. W. Staggs and D. R. Nielsen, *Process Biochem.*, 2015, **50**, 1487–1498.

54 D. R. Nielsen and K. J. Prather, *Biotechnol. Bioeng.*, 2009, **102**, 811–21.

55 S.-H. Lee, M.-H. Eom, J.-D.-R. Choi, S. Kim, J. Kim, Y.-A. Shin and K. H. Kim, *Bioprocess Biosyst. Eng.*, 2016, **39**, 695–702.

56 M. Wiehn, K. Staggs, Y. Wang and D. R. Nielsen, *Biotechnol. Prog.*, 2014, **30**, 68–78.

57 X. Lin, J. Wu, X. Jin, J. Fan, R. Li, Q. Wen, W. Qian, D. Liu, X. Chen, Y. Chen, J. Xie, J. Bai and H. Ying, *Biotechnol. Prog.*, 2012, **28**, 962–972.

58 R. Ranjan, S. Thust, C. E. Gounaris, M. Woo, C. A. Floudas, M. von Keitz, K. J. Valentas, J. Wei and M. Tsapatsis, *Microporous Mesoporous Mater.*, 2009, **122**, 143–148.

59 M. A. Mirata, D. Heerd and J. Schrader, *Process Biochem.*, 2009, **44**, 764–771.

60 J. T. Dafoe, J. S. Parent and A. J. Daugulis, *J. Chem. Technol. Biotechnol.*, 2014, **89**, 1304–1310.

61 J. S. Parent, M. Capela, J. T. Dafoe and A. J. Daugulis, *J. Chem. Technol. Biotechnol.*, 2012, **87**, 1059–1065.

62 A. S. Michaels and H. J. Bixler, *J. Polym. Sci.*, 1961, **50**, 393–412.

63 R. M. Hodge, G. H. Edward and G. P. Simon, *Polymer (Guildf).*, 1996, **37**, 1371–1376.

64 E. E. Poleo and A. J. Daugulis, *J. Chem. Technol. Biotechnol.*, 2014, **89**, 88–96.

Chapter 2

A framework to predict and experimentally evaluate polymer-solute thermodynamic affinity for two-phase partitioning bioreactor (TPPB) applications

With minor changes to fulfill formatting requirements, this chapter is substantially as it appears in:

S. L. Bacon, J. S. Parent and A. J. Daugulis, *J. Chem. Technol. Biotechnol.*, 2014, **89**, 948–956.

2.1 Abstract

BACKGROUND:

Selection of a polymer for two-phase partitioning bioreactor (TPPB) applications has previously been limited to heuristics, however recent interest has focused on first principles' methods based on polymer crystallinity, glass transition temperature and polymer-solute thermodynamic affinity. In this work, a framework is proposed to evaluate and predict polymer-solute thermodynamic affinity *via* the polymer-phase activity coefficient.

RESULTS:

Polymer screening *via* thermodynamic affinity was shown to be most effective at very dilute concentrations, where partition coefficients can be estimated using infinite dilution activity coefficients. In the absence of published values, UNIFAC-vdW-FV or Flory-Huggins based activity models can provide very good predictions for the polymer-phase activity coefficient, significantly improving upon previous approaches using Hildebrand and Hansen solubility parameter differences. For non-dilute systems, however, the activity models failed to consider the full effects of concentration on partition coefficient. Additionally, a reduction in polymer molecular weight resulted in improved partition coefficients, a phenomena well described by the activity models.

CONCLUSION:

Predicting and experimentally quantifying polymer-solute thermodynamic affinity at very dilute concentrations will aid future attempts at TPPB polymer selection. Furthermore, experimental partition coefficient data at a range of operational concentrations will indicate how TPPB effectiveness will change throughout the fermentation course. Finally, reduction of polymer molecular weight to improve solute partitioning should be investigated further for a range of polymers.

2.2 Introduction

Bioprocess productivity is commonly hindered by substrate and/or product inhibition. Benefits have been previously demonstrated by introducing a non-aqueous phase (NAP), used to sequester the toxic target molecule and lower its aqueous concentration to sub-inhibitory levels. This technology platform, commonly referred to as a two-phase partitioning bioreactor (TPPB), has been successfully demonstrated with a variety of NAPs including small molecule solvents,[1,2] viscoelastic oligomeric liquids (polypropylene glycol, silicone oil)[3–6] and solid co-polymer beads.[7–11] In addition to their need to be non-bioavailable and biocompatible, NAPs are screened based on substrate/product affinity *via* the partition coefficient.[12] Previous work has established a predictive screening program to rank liquid solvents based on solute affinity using the UNIFAC group contribution activity model.[13] Polymers, on the other hand, have been limited to selection through heuristic methods, prompting recent efforts to investigate first principles approaches to screening polymers on the basis of crystallinity, glass transition temperature (T_g) and thermodynamic affinity.[9,14] To fully realize the benefits of using polymers in TPPBs,[5,15] the present study provides the required framework to rationally select and evaluate a polymer based on its thermodynamic affinity for the target substrate and/or product.

Quantifying polymer-solute interactions can be achieved by finding an expression for the Gibbs free energy of mixing. Favorable polymer-solute affinity is characterized by a negative Gibbs free-energy of mixing, ΔG_M, which can be related to the enthalpy and entropy of mixing, ΔH_M and ΔS_M, by Equation 3.

$$\Delta G_M = \Delta H_M - T\Delta S_M \tag{3}$$

The Flory-Huggins solution theory is the most widely used thermodynamic framework for quantifying the enthalpic and entropic contributions to the Gibbs free energy of mixing, ΔG_M.[16]

Other contributions to polymer-solute mixing which could not be directly attributed as being purely enthalpic (ΔH_M) or entropic (ΔS_M) such as the free-volume effect, were later discovered.[17] Therefore, we are proposing a shift in the discussion of polymer-solute affinity from using the enthalpy and entropy of mixing to more quantifiable and conceptually available contributions. They include 1) the combinatorial entropy of mixing, 2) intermolecular interactions between solute and polymer molecules and 3) the free volume effect.[17,18] These three main contributions describe polymer-solute affinity by contributing to ΔS_M, ΔH_M or both.

A very thorough description of these three contributions has been provided by Patterson,[18] briefly reviewed here with respect to their overall contribution to ΔG_M. The **combinatorial entropy of mixing**, ΔS_M^{comb}, results from increases in positional disorder/randomness through mixing, that is, an increase in the number of possible molecular configurations from mixing two pure substances. Combinatorial entropy is always positive and is a main component of the overall entropy of mixing, ΔS_M, from Equation 3. Therefore, greater combinatorial entropy will result in more energetically favorable mixing by reducing ΔG_M. An important contribution to ΔS_M which is not included in ΔS_M^{comb} is the entropic contribution from the conformational changes associated with polymer chains unfolding.[19] This contribution is particularly significant when polymer-solute mixing induces the melting of crystals in semi-crystalline polymers.[20]

Patterson's[18] discussion of polymer-solute **intermolecular interactions** focuses on dispersive and specific interactions between polymer chains and solute molecules. The main contribution of these interactions is toward the enthalpy of mixing, ΔH_M. Dispersion forces and/or random dipole-induced dipole interactions always lead to a positive contribution to ΔH_M and ΔG_M and therefore are not favorable to mixing. In the rarer case of specific interactions, negative contributions to ΔH_M and ΔG_M can result from strong hydrogen bonding forces or charge transfer between polymer and solute molecules.[18]

The **free volume effect** results from polymer chains having fewer degrees of freedom and more restricted mobility compared to small molecules. This lack of mobility causes polymer chains to have smaller free volumes than small molecules, which have more "free volume" to wander around their equilibrium positions as they are not tied to an adjacent polymer segment.[20] When polymers and small molecules mix, the polymer's small free volume causes a net contraction in total mixture volume and forces the polymer and solute molecules closer together.[18] This leads to a negative contribution to ΔH_M (favorable to mixing) and a negative contribution to ΔS_M (unfavorable to mixing). These two effects do not cancel out, and the free volume effect leads to a net positive contribution in ΔG_M which is unfavorable for mixing.[18]

A large body of research has been devoted to quantifying these three contributions to polymer-solute mixing by means of the activity coefficient, γ_i. The activity coefficient is related by Equation 4 to the *excess* Gibbs free energy of mixing, ΔG_M^E, the difference between ΔG_M of a non-ideal system compared to that of its ideal counterpart, ΔG_M^{ideal}. Analogous to ideal small molecule solutions, an ideal polymer-solute solution has equal solute-solute, polymer-solute and polymer-polymer interactions. ΔG_M^{ideal} can be theoretically calculated, with its only contribution being an *idealized* representation of the combinatorial entropy of mixing.

$$\Delta G_M^E = \Delta G_M - \Delta G_M^{ideal} = RT \sum_i x_i \ln \gamma_i \tag{4}$$

$$\Delta G_M^{ideal} = -T\Delta S_M^{ideal} \tag{5}$$

Conceptually, the activity coefficient provides a measure to account for the deviations from ideality that result from mixing small solute molecules and long polymer chains. The activity coefficient provides a direct indication of polymer-solute affinity, with smaller activity coefficients indicating more favorable mixing. In the case of TPPBs, a polymer or small molecule solvent NAP is best suited for a target molecule when the activity coefficient of the target

molecule in the NAP is small. The present work explores the practical benefits of using activity coefficients to quantify polymer-solute affinity, including a convenient approach for experimental activity coefficient evaluation and several easily-accessible prediction methods.

Previous first principles' methods to screen and rank polymer-solute thermodynamic affinity have been limited to analysis of the intermolecular interactions through the use of Hildebrand and Hansen solubility parameters differences.[9,14] Such methods can be effective with polymer solutions due to their significantly lower combinatorial entropy of mixing when compared to small molecules.[21] However, the combinatorial entropy becomes more significant as the molecular weight decreases, as seen in small molecule and oligomeric NAPs, thereby increasing the favorability of mixing by reducing ΔG_M. Due to the significance of molecular weight on ΔG_M, activity models or alternative approaches to predicting polymer-solute affinity can benefit from considering intermolecular interactions, combinatorial entropy and the free volume effect as described above.[16,22,23]

This study uses activity coefficients to characterize the thermodynamic affinity of a polymeric NAP for a range of solutes. A simple and direct correlation between activity coefficients and partition coefficient establishes a framework for polymer screening and evaluation for TPPB applications. The study begins with a demonstration of the influence of solute concentration on partition coefficient for three target molecules specifically selected to posses varying hydrophobicity and aqueous solubility (methyl *tert*-butyl ether, *n*-pentanol, *n*-butyl acetate). Very dilute conditions are shown to be effective for the prediction and experimental evaluation of partition coefficients, with the predictive activity coefficient models demonstrating less precision at higher concentrations.

The use of published infinite dilution activity coefficients is examined for polymer screening applications before evaluating three predictive polymer-phase activity coefficient models for use

in cases where literature values are not available. Alternatively, a brief exploration of two surrogate approaches[9,14] to ranking polymer-solute affinity is provided. Both the activity coefficient estimation approach, and the surrogate approaches are evaluated using experimental partition coefficient data collected for 16 solutes (alcohols, ketones, ethers, esters, aromatics) absorbing into poly(*n*-butyl acrylate) at very dilute conditions. This polymer is an amorphous viscoelastic liquid with a glass transition temperature below 25°C (T_g=-54°C)[24] that does not present complications associated with crystallinity or an unabsorptive glassy state, thereby isolating polymer-solute thermodynamic affinity.[9,14]

The report concludes with a demonstration of the influence of NAP molecular weight on partition coefficients, highlighting the importance of the combinatorial entropy contribution towards ΔG_M, and establishing a bridge between small molecule, oligomeric and polymeric TPPB systems. Throughout the work, the activity coefficient based framework for analyzing polymer-solute thermodynamic affinity is discussed in the context of improving polymer NAP screening methods, TPPB processes and operational understanding.

2.3 Experimental

2.3.1 Materials and Material Preparation

All chemicals were purchased from either Sigma–Aldrich (Canada) or Fisher Scientific (Canada). High molecular weight (M_w≈100,000 g/mol) poly(*n*-butyl acrylate) was purchased from Scientific Polymer Products (Ontario, NY) and isolated from toluene solution by solvent evaporation at 60°C. Low molecular weight (M_w=6,200 g/mol) poly(*n*-butyl acrylate) was prepared by atom transfer radical polymerization (ARGET ATRP) in anisole solution as outlined previously,[25] and purified from residual copper by passing through a silica column before isolating by solvent evaporation at 60°C.

2.3.2 Partition coefficient tests

Partition coefficient tests were performed in triplicate using three polymer masses, ranging from 0.5 to 1.5 g of dry mass. Each target molecule was prepared in separate aqueous solutions using Type I ultrapure water. In addition to the polymer mass, 10 mL aliquots of aqueous solution were added to each scintillation vial, sealed tightly with a foil lined cap and allowed to equilibrate in an Innova 4400 incubator shaker for 6 days at 30^{o}C at 180 rpm. Aqueous concentrations before and after equilibration were measured using either a Varian 450-GC gas chromatography unit equipped with a CP-8410 AutoInjector, VF-5ms 30m column and FID detector or a Varian Pro Star HPLC with UV/VIS detection and separated on a Polaris C18 150x4.6mm 5 µm column with a mobile phase of 50:50 water/acetonitrile at 1 mL/min. A mass balance was performed to determine the solute concentration in the polymer. Experimental partition coefficients were calculated using aqueous and polymer phase weight fractions, w_i^{aq} and w_i^{poly}, in Equation 6. Reported mean and standard deviation (n=3) values were calculated from triplicate data.

$$\text{Partition Coefficient} = \frac{w_i^{poly}}{w_i^{aq}} \tag{6}$$

2.4 Results and discussion

2.4.1 Partition coefficient prediction

The partition coefficient is defined as the ratio of the equilibrium solute concentration in the non-aqueous phase (NAP) to that in the aqueous phase. In general, a higher partition coefficient is desired in TPPB applications, as it indicates an increased ability to sequester toxic substrates/products within the NAP. Since phase equilibrium is achieved when a solute's activity is equal in each phase, the partition coefficient can be expressed as a ratio of activity coefficients. Therefore, given appropriate correlations and/or predictions of activity coefficient values for the

aqueous phase and the polymeric NAP, partition coefficients can be calculated for any polymer/solute system.

$$a_i^{aq} = a_i^{poly} \tag{7}$$

$$a_i^{\alpha} = \gamma_i^{\alpha} x_i^{\alpha} = \Omega_i^{\alpha} w_i^{\alpha} \tag{8}$$

Therefore

$$\text{Partition Coefficient} = \frac{\Omega_i^{aq}}{\Omega_i^{poly}} \tag{9}$$

where a_i^{α} is the activity, x_i^{α} is the mole fraction, w_i^{α} is the weight fraction, γ_i^{α} is the mole fraction activity coefficient, and Ω_i^{α} is the weight fraction activity coefficient which can be converted from the mole fraction activity coefficient as follows

$$\boldsymbol{\Omega_i = \gamma_i \frac{x_i}{w_i}} \tag{10}$$

Information on the activity of solutes in aqueous solution is widely available, both in terms of experimental data[26–29] and in the form of correlations such as NRTL[30] and UNIQUAC.[31] Where data and correlative model parameters[32] are lacking, fully predictive models such as UNIFAC or modified-UNIFAC may be used to predict activity based on molecular structure. Note that while aqueous-phase activity coefficients are reported on a mole fraction basis, Equation 10 converts them to the weight fraction basis normally used for TPPB systems employing a polymeric NAP. Compared to aqueous solutions, polymer-phase activity coefficient data are scarce.[33–35] However, there are a number of correlative and fully predictive models available for polymer-phase activity coefficient estimation, several of which have been reviewed by Costa et al.[36] Unfortunately, correlative parameters are lacking for the poly(*n*-butyl acrylate) mixtures of present interest,

necessitating the use of predictive models such as UNIFAC-vdW-FV[23] and the Flory-Huggins model in conjunction with pure component Hildebrand and Hansen solubility parameters.[21,37] A simpler approach to gauging polymer-solute affinity which does not involve activity coefficient calculations, utilizes surrogate parameters in their place. Common surrogates include the Hildebrand solubility parameter differences[9,38] and the Hansen 'Ra Distance',[9,21] whose simplicity warrants their use in TPPB polymer screening, but at the expense of thermodynamic rigour.

2.4.2 Effect of solute concentration on partition coefficients

The process of selecting a polymeric NAP for a target molecule often begins with consideration of the solute's published Log $K_{o/w}$ value. This is a measure of the solute's partition coefficient in an *n*-octanol/water system, with high values indicative of a hydrophobic molecule that is best suited to a non-polar NAP. Note that the guidelines for Log $K_{o/w}$ estimation established by the Organization for Economic Co-operation and Development (OECD) require solute concentrations to be <0.01 M in both the aqueous and *n*-octanol phases.[39] This restriction on solute concentrations ensures that both phases abide by a dilute-ideal solution assumption, and that the system as a whole abides by the Nernst distribution law.[39] The Nernst distribution law states *"the distribution ratio of a solute between two liquid phases at equilibrium is a constant, provided that the solute forms a dilute-ideal solution in each phase.*"[40] In a dilute-ideal solution, the solvent approaches ideality and can be represented by Raoult's law ($\gamma_2 \rightarrow 1$) while the solute follows Henry's law ($\gamma_1 \rightarrow \gamma_1^{\infty}$). Therefore, Log $K_{o/w}$ values measured under these conditions are single-point constants that describe solute partitioning under dilute conditions, but they may not reflect the partition coefficient at higher solute concentrations.

Similar arguments pertain to the NAP/water systems of present interest, in that partition coefficients can be concentration dependent, and single-point constants may apply only where both phases abide by a dilute-ideal solution assumption. Consider the data presented in Figure 1,

in which equilibrium MTBE, *n*-pentanol and *n*-butyl acetate concentrations in the aqueous and poly(butyl acrylate) phase are plotted. Using Equation 6, we can identify the ratio of the solute concentration in the polymer (y-axis) to the aqueous concentration (x-axis) as the partition coefficient. Single point partition coefficient (PC) values at minimum and maximum solute concentrations have been extended over the concentration range to form the PC_{min} and PC_{max} lines (.....), illustrating the lower and the upper bounds of experimental phase composition. The upward trends for the experimental data in Figure 1, from PC_{min} to PC_{max}, suggest that increased equilibrium concentrations correspond to higher partition coefficients, that is, larger ratios of polymer phase to aqueous phase concentrations. The inlays in Figure 1 show that in the very dilute regime, partition coefficients are nearly constant (i.e., constant slope) and are at the lower PC_{min} boundary. In contrast, partition data at higher concentrations are generally near the upper PC_{max} boundary, indicating higher partition coefficients. The model predictions shown in Figure 1 are discussed below in Section 2.4.4.3 *'Partition coefficient prediction for non-dilute systems'*.

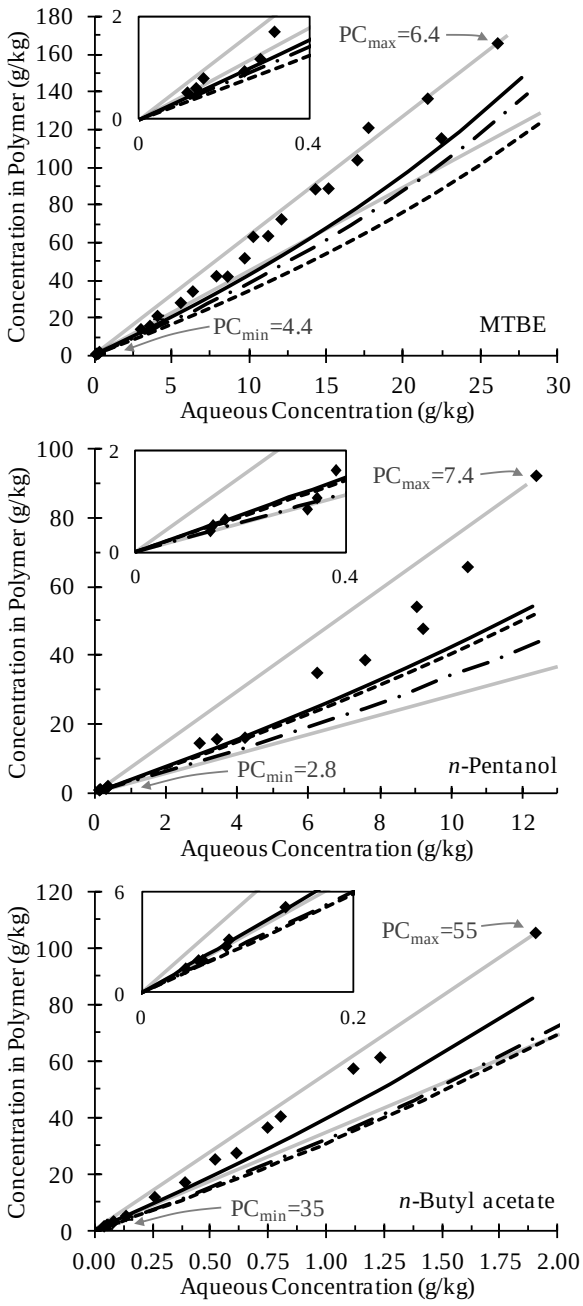

Figure 1 - Equilibrium phase composition data (◆) and model predictions for (a) MTBE, (b) *n*-pentanol and (c) *n*-butyl acetate in poly(*n*-butyl acrylate) (M_w≈100,000 g/mol). Upper and lower bounds of phase composition (.....) are based upon partition coefficient (*PC*) values at maximum and minimum solute concentration. Inlays show an enlarged view of the very dilute concentration region. Model predictions shown are using UNIFAC-vdW-FV (— . -), FH-HSP (——) and FH-Hildebrand (– – –).

Most partition coefficients for TPPB applications are determined near the inhibitory substrate and/or product concentration,[10,41,42] which may exceed the dilute-ideal solution limit, although this is not always the case.[43] The implications of a concentration-dependent partition coefficient are twofold. In the first place, single-point partition coefficients should be measured and reported at infinitely dilute conditions. Second, recognizing that many TPPB processes operate under conditions that exceed the dilute-ideal solution limit, partition coefficient data should also be provided as a function of solute concentration where these conditions may arise. For example, single phase biodegradation is completely inhibited when exposed to greater than 130 mg/L of 2,4-dichlorophenol,[10] while ethanol production with *Zymomonas mobilis* is inhibited only when concentrations reach 120 g/L.[44] Based on the relationships illustrated in Figure 1, a NAP's absorptive capacity may change during batch fermentation as product concentration increases and/or substrate concentration is reduced. Therefore, TPPB process design requires knowledge of partition coefficient variation with aqueous phase and NAP compositions. However, where the objective is limited to the selection of a polymeric NAP for a given solute, dilute-ideal solution values are likely to suffice.

2.4.3 Evaluation of partition coefficients at infinite dilution

The benefits of infinitely dilute concentrations for initial screening and selection of a polymeric NAP are twofold: 1) partition coefficients can be more easily predicted using single point infinite dilution activity coefficients and 2) experimental partition coefficients can be analyzed to yield an experimental estimate of the polymer phase activity coefficient.

The first benefit is generally limited to the aqueous phase, for which a wide range of published molar infinite dilution activity coefficients, $\gamma_i^{aq,\infty}$, are available[26–29] and can be converted to the weight fraction activity coefficient using Equation 11. These experimental published values are preferred over predictive or correlative activity models when operating within the infinitely dilute

concentration regime. On the other hand, data for polymer-phase activity coefficients, $\Omega_i^{poly,\infty}$, are generally more scarce.[33] For the poly(*n*-butyl acrylate) systems of present interest, polymer phase infinite dilution activity data are unavailable, necessitating the use of activity models to achieve partition coefficient predictions.

$$\boldsymbol{\Omega_i^{aq,\infty} = \gamma_i^{aq,\infty} \frac{MW_{H2O}}{MW_i}} \tag{11}$$

The second benefit of using infinitely dilute conditions arises when evaluating polymer phase activity model predictions. When analyzing a wide range of solutes, each with a unique aqueous activity coefficient, $\Omega_i^{poly,pred}$ cannot be directly compared to experimental partition coefficients. However, experimental partition coefficients can be normalized using the solute's aqueous infinite dilution activity coefficient, $\Omega_i^{aq,\infty}$, to yield an experimental estimate of the polymer phase activity coefficient, $\Omega_i^{poly,expt}$. Thus, a direct comparison between experimental and predicted polymer phase activity coefficients is possible.

$$\boldsymbol{\Omega_i^{poly,expt} = \frac{\Omega_i^{aq,\infty}}{Partition\ Coefficient}} \tag{12}$$

The recommended threshold for the accepted dilute-ideal concentration threshold (<0.01 M) likewise affects the concentration range for which Equation 12 remains valid. For the remainder of this work, partition coefficients were determined at sufficiently dilute conditions such that the aqueous phase concentrations were always <0.01 M, enabling the use of $\Omega_i^{aq,\infty}$. However, in many cases, particularly when the polymer had a high affinity for the solute, the solute was concentrated in the polymer and exceeded the 0.01 M limit. In these cases, the experimental

polymer phase activity coefficient could not be considered infinitely dilute, $\Omega_i^{poly,\infty}$, and is instead indicated by the experimental equilibrium conditions, $\Omega_i^{poly,expt}$. Table 2 identifies the polymer phase solute concentrations at which the partition data were collected. Efforts were made to obtain partition coefficient data at the lowest possible concentrations, however, analytic detection limits prevented the <0.01 M condition from holding in some cases.

2.4.4 Estimation of polymer-phase activity coefficients

2.4.4.1 Activity model identification and implementation

We have examined three polymer-phase activity coefficient models that can be used towards partition coefficient predictions. They include Flory-Huggins solution theory[16] in conjunction with Hildebrand solubility parameters (FH-Hildebrand),[21] Flory-Huggins solution theory in conjunction with Hansen solubility parameters (FH-HSP)[37] and UNIFAC-vdW-FV.[23] The Flory-Huggins solution model[16] considers combinatorial entropy in the first three terms in Equation 13 and by convention, any contribution to ΔG^{mix} which is non-combinatorial (intermolecular interactions and free volume effects) is included in the Flory-Huggins interaction parameter, χ_{12} (where *i* and *j* refer to the solute and polymer, respectively).[18] A set of sample calculations for the FH-Hildebrand and FH-HSP models is included in Appendix A1.

$$\ln \gamma_i^{pred} = \underbrace{\ln \frac{\varphi_i}{x_i} + 1 - \frac{\varphi_i}{x_i}}_{combinatorial} + \underbrace{\chi_{ij}\varphi_j^2}_{non\text{-}comb} \tag{13}$$

Equation 13 was used to evaluate the mole fraction activity coefficient (γ_i^{pred}) which was subsequently converted to weight fraction activity coefficient ($\Omega_i^{poly,pred}$) using Equation 10.

The use of χ_{ij} is advantageous because binary interaction parameters are specific to the polymer-solute pair of interest. Unfortunately, Flory-Huggins interaction parameters for poly(*n*-butyl acrylate) and the solutes of interest were not available, necessitating the use of the semi-empirical correlations that predict the binary mixture parameter from pure-component data. FH-Hildebrand calculations utilized Equation 14 to provide χ_{ij} estimates from solute and polymer Hildebrand solubility parameters, δ_1 and δ_2, where V_1 is the molar volume of the solute, and β =0.34.[21]

$$\boldsymbol{\chi_{12} = \frac{V_1}{RT}(\delta_1 - \delta_2)^2 + \beta} \quad (14)$$

Greater insight into the non-combinatorial contributions to polymer-solute mixing can be gained using Hansen solubility parameters to separate the total Hildebrand solubility parameter into three components: atomic dispersion forces (δ_d), polar dipole-dipole forces (δ_p) and hydrogen bonding interactions (δ_h).[21] FH-HSP calculations were derived from χ_{ij} estimates based on Hansen solubility parameters. The α value is an adjustable parameter which can be used to fit the model to an experimental dataset with sufficient data points, e.g., more than 6.[45] The α parameter was originally prescribed by Lindvig et al.[37] to be α=0.6, however we found that α=1.0 resulted in better predictions for the poly(*n*-butyl acrylate) systems of present interest.

$$\boldsymbol{\chi_{12} = \alpha \frac{V_1}{RT}\left[(\delta_{d1} - \delta_{d2})^2 + 0.25(\delta_{p1} - \delta_{p2})^2 + 0.25(\delta_{h1} - \delta_{h2})^2\right]} \quad (15)$$

In contrast to the Flory-Huggins based models, which use component solubility parameters to quantify polymer-solute interactions, the UNIFAC-vdW-FV model captures how each functional group within the solute molecule and polymer chain interact. Each pair of functional groups present corresponds to an experimentally regressed binary functional group interaction parameter. As outlined by Kannan et al.,[23] UNIFAC-vdW-FV is a free volume based activity model akin to

the original UNIFAC-FV,[22] that considers combinatorial entropy, intermolecular interactions and free volume effects. The 'UNIFAC-vdW-FV' computer program[46] was used to run calculations with input of polymer and solute molecular structures, bulk densities, polymer molecular weight and solute vapour pressure.

2.4.4.2 Activity model comparison

Figure 2 presents a comparison of experimental activity coefficient data to predictions derived from the three thermodynamic models. The near 1:1 ratio of predicted vs. experimental results (indicated by the dashed line) demonstrates the very good predictability of several solute classes in poly(*n*-butyl acrylate) by all three models. Trends for the primary alcohols (*n*-butanol to *n*-octanol) are most effectively captured by direct activity coefficient estimation methods. It is likely that the parallel structures of the primary alcohols made this series more predictable, whereas the more diverse structures tested within groups such as ethers (THF, MTBE, anisole) or ketones (acetone, MIBK, cyclohexanone) complicated our attempts to predict their phase partitioning behaviour.

The greater thermodynamic rigour employed by considering group contributions in the UNIFAC-vdW-FV model is thought to provide a more fundamental foundation for future polymer screening efforts compared to the semi-empirical correlations relating Hildebrand and Hansen solubility parameters to the Flory-Huggins interaction parameter 'χ_{12}'. However, the Flory-Huggins based models are considerably quicker to compute and may provide adequate results for initial polymer NAP screening for TPPB applications.

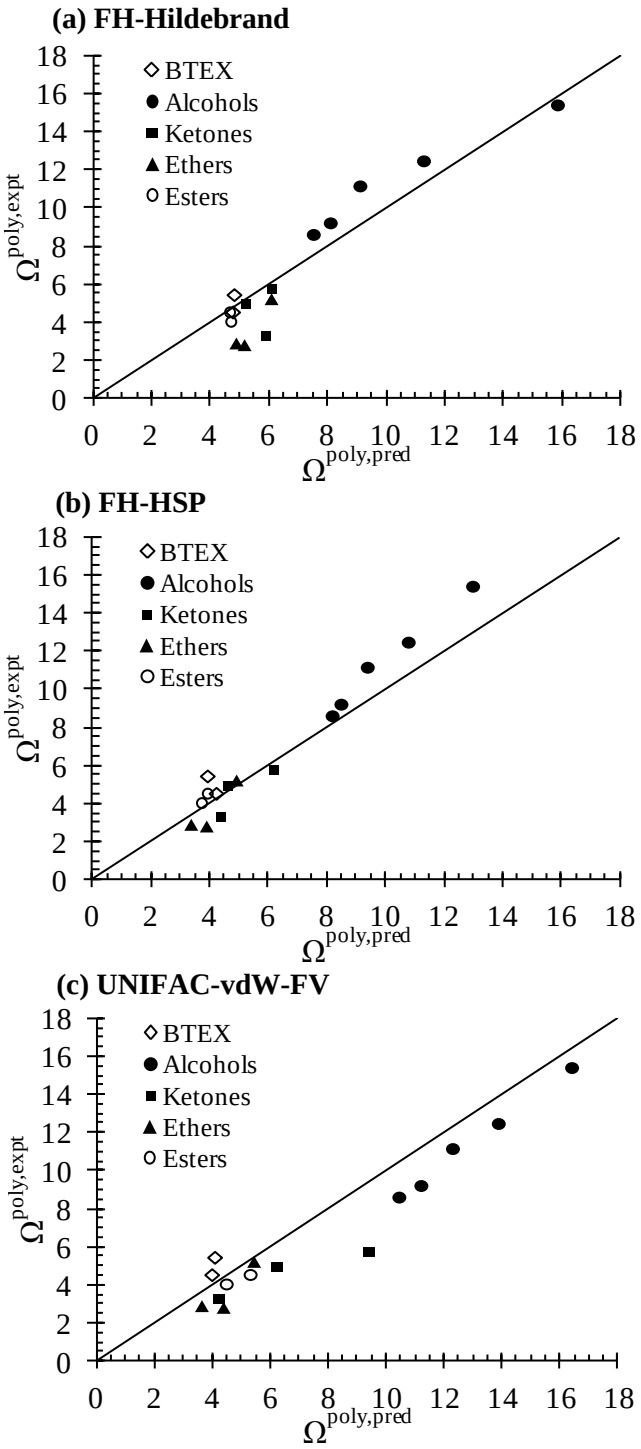

Figure 2 - Comparison of weight fraction activity coefficient predictions using (a) FH-Hildebrand, (b) FH-HSP and (c) UNIFAC-vdW-FV with experimental estimates for the weight fraction activity coefficient of various target molecules in poly(*n*-butyl acrylate) (M_w≈100,000 g/mol).

Table 2 - Summary of partition coefficients, experimental polymer phase solute activity coefficients, Hansen Ra and Hildebrand solubility parameter differences, and activity coefficient predictions using Flory-Huggins theory and UNIFAC-vdW-FV. Partition coefficients were determined using poly(*n*-butyl acrylate) (M_w≈100,000 g/mol). Errors shown are +/- one standard deviation.

Solute	Partition Coefficient	$\Omega^{aq,\infty}$	$\Omega^{poly,expt}$	Hildebrand $\|\Delta\delta\|$ ($MPa^{1/2}$)	Hansen 'Ra' Distance ($MPa^{1/2}$)	FH-Hildebrand $\Omega^{poly,pred}$	FH-HSP $\Omega^{poly,pred}$	UNIFAC-vdW-FV $\Omega^{poly,pred}$
Benzene	117 ± 12	538 [d,e,f,g]	4.6 ± 0.7 [c]	0.90	4.94	4.8	4.2	4.0
Toluene	328 ± 66	1806 [d,e,f,g]	5.5 ± 1.1 [c]	0.56	3.71	4.8	3.9	4.1
n-Butanol	0.8 ± 0.4	12.3 [d,e,f,g]	15.4 ± 7.8 [b]	5.59	11.85	15.9	13.0	16.5
n-Pentanol	3.3 ± 0.9	41 [d,e,f,g]	12.5 ± 3.4 [c]	4.32	10.12	11.3	10.8	13.9
n-Hexanol	12 ± 2	134 [d,e,f,g]	11.2 ± 2.1 [c]	3.43	8.79	9.1	9.4	12.3
n-Heptanol	58 ± 4	525 [d,e,f,g]	9.2 ± 1.1 [c]	2.91	7.85	8.1	8.5	11.3
n-Octanol	207 ± 8	1784 [e,f,g]	8.6 ± 0.8 [c]	2.55	7.29	7.5	8.2	10.5
Acetone	0.4 ± 0.2	2.3 [d,e,f,g]	5.8 ± 2.9 [b]	2.33	8.35	6.1	6.2	9.4
Cyclohexanone	3.0 ± 0.4	9.9 [g]	3.3 ± 0.5 [c]	2.73	5.89	5.9	4.4	4.3
Methyl *iso*-butyl ketone	10.6 ± 0.9	53 [f,g]	5.0 ± 0.6 [c]	0.63	4.40	5.2	4.6	6.3
Tetrahydrofuran	1.5 ± 0.3	4.2 [e,f]	2.8 ± 0.6 [b]	1.85	4.56	5.2	3.9	4.4
Methyl *tert*-butyl ether	4.4 ± 0.8	23 [e,f,g]	5.2 ± 1.0 [c]	1.40	4.28	6.1	4.9	5.5
Anisole	208 ± 2	606 [g]	2.9 ± 0.2 [c]	1.98	3.54	4.9	3.4	3.7
Ethyl acetate	2.9 ± 0.3	13 [e,f,g]	4.6 ± 0.6 [b]	0.55	4.20	4.7	3.9	5.3
n-Butyl acetate	35 ± 2	144 [d,e,f,g]	4.1 ± 0.9 [c]	0.20	2.87	4.7	3.7	4.5
iso-Pentyl acetate	113 ± 12	412 [e,f,g]	3.6 ± 0.5 [c]	0.50	3.97	4.8	4.2	4.3

[a] Aqueous phase concentration < 0.01 M ($\Omega_i^{aq,\infty}$) in all cases

[b] Polymer phase concentration < 0.01 M ($\Omega_i^{poly,\infty}$)

[c] Polymer phase concentration < 0.1 M ($\Omega_i^{poly,expt}$)

Aqueous phase activity references: [d: 26; e: 27; f: 28; g:29]

2.4.4.3 Partition coefficient prediction for non-dilute systems

Equilibrium phase composition predictions using FH-Hildebrand, FH-HSP and UNIFAC-vdW-FV are shown with experimental data in Figure 1 for MTBE, *n*-pentanol and *n*-butyl acetate in poly(*n*-butyl acrylate). The NRTL model was used to predict the aqueous phase activity coefficient at varying concentrations using experimentally regressed binary model parameters.[32] In accordance with the results in Figure 2, the three activity models provided good approximations of polymer phase activity coefficients and partition coefficients at very dilute concentrations. However, it is evident in Figure 1 that the models fail to consider the full effects of phase composition on partition coefficient as the concentrations increase. When compared to the infinitely dilute case in which solute-polymer and polymer-polymer interactions dominate, the additional effect of solute-solute intermolecular interactions at higher concentrations may have contributed to the activity models' poorer precision. These results suggest that the use of these activity models is currently limited to polymer screening applications at infinitely dilute conditions, and that they cannot reliably be used in the place of experimental data to quantify the effects of changing concentrations on TPPB operation.

When predicting partition coefficients for non-dilute systems, activity coefficient evaluation must be performed in conjunction with a system mass balance in an approach equivalent to that of a flash calculation. Contrary to the case in which activity coefficients are fixed at their infinite dilution values, activity coefficients in non-dilute systems vary with composition. In the non-dilute case, an iterative 'flash calculation' approach is required using composition dependent activity models to determine the polymer and aqueous phase concentrations which satisfy the equi-activity requirement in Equation 7.

2.4.5 Surrogate approach to ranking polymer-solute affinity

Two methods of providing a surrogate to polymer-solute thermodynamic affinity were identified as 1) Hildebrand solubility parameter difference and 2) Hansen 'Ra distance'. Hansen solubility parameters used in the 'Ra distance' approach were readily available for all systems using the HSPiP v4.0.04 computer program,[47] which contains a large database of experimental solubility parameter estimates. Compilations of published Hildebrand solubility parameters exist, however for consistency, the Hildebrand solubility parameter was found as the sum of squares of Hansen solubility parameters.

2.4.5.1 Hildebrand solubility parameter differences

When the difference between a solute's and a polymer's solubility parameters is small, the non-combinatorial contribution to mixing is reduced, resulting in a higher polymer-solute affinity, i.e., a smaller activity coefficient, seen in Figure 3. Therefore, a simplified surrogate for polymer-solute affinity can be estimated by the Hildebrand solubility parameter difference in Equation 16.

$$|\boldsymbol{\Delta\delta}| = |\boldsymbol{\delta_{poly} - \delta_{solute}}| \tag{16}$$

2.4.5.2 Hansen 'Ra distance'

The Hansen 'Ra distance' defined in Equation 17 is analogous to the Hildebrand difference, with lower values indicating more favorable mixing between the solute and polymer. The constant '4' before the dispersive parameter produces spherical regions of solubility, thereby simplifying correlations to Hansen solubility parameter differences.[21] A more complete discussion of this corrective constant is available.[21]

$$\boldsymbol{Ra} = \sqrt{\boldsymbol{4}(\boldsymbol{\delta_{d1}} - \boldsymbol{\delta_{d2}})^{\boldsymbol{2}} + \left(\boldsymbol{\delta_{p1}} - \boldsymbol{\delta_{p2}}\right)^{\boldsymbol{2}} + (\boldsymbol{\delta_{h1}} - \boldsymbol{\delta_{h2}})^{\boldsymbol{2}}} \quad (17)$$

2.4.5.3 Comparison of surrogate approaches

Figure 3 reveals a strong correlation between the experimental infinite dilution polymer-phase activity coefficient and the two surrogate approaches: Hildebrand solubility parameter difference and Hansen 'Ra distance'. The data show that the Hildebrand surrogate approach does not provide a direct (1:1) estimate of activity coefficient, however a reasonable trend is evident from which a general ranking of polymer-solute affinity can be made. Consistent with a recent report,[9] Figure 3 indicates that Hansen 'Ra Distance' values provide a more direct (1:1) and linear (R^2) correlation with experimental polymer-phase activity coefficients compared to Hildebrand solubility parameter differences.

By testing a single polymer with a variety of solutes at relatively constant concentration, the combinatorial entropy contribution remains similar between systems. Therefore, Figure 3 is likely a 'best case' result of the Hildebrand and Hansen surrogate approaches, which does not consider any entropic effects.

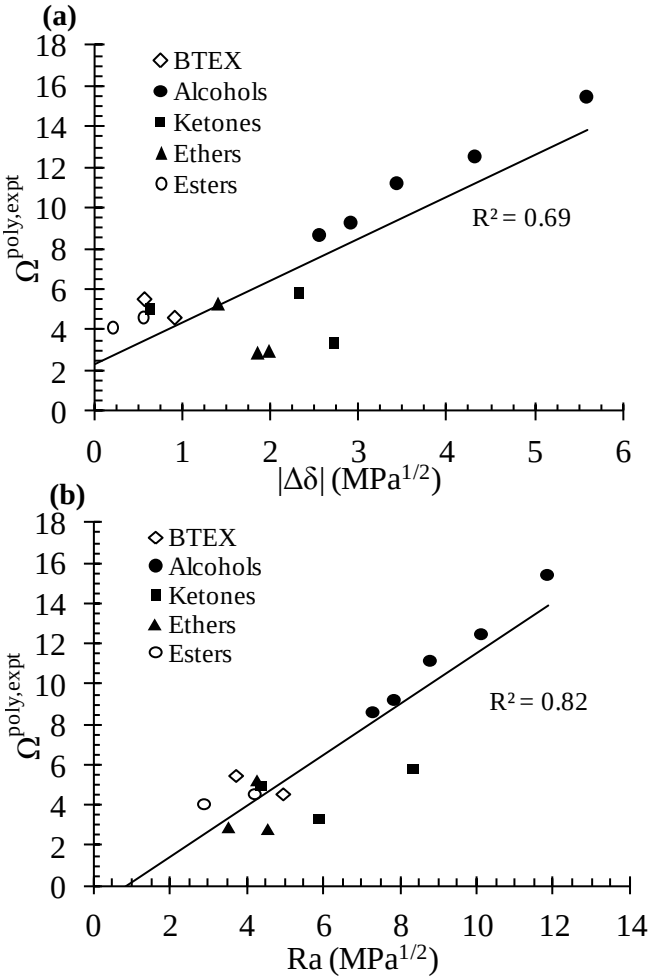

Figure 3 - Comparison of (a) absolute Hildebrand solubility parameter difference and (b) Hansen 'Ra distance' with experimental estimates for the weight fraction activity coefficient of various target molecules in poly(*n*-butyl acrylate) (M_w≈100,000 g/mol).

2.4.6 Effect of molecular weight on partition coefficient

Experimental partition coefficients were also measured for solutes from three chemical classes (alcohol, aromatic, ester) absorbing into poly(*n*-butyl acrylate) of two different molecular weights, as well as a representative small molecule (dibutyl adipate). The applicability of dibutyl adipate as a model for low molecular weight poly(*n*-butyl acrylate) was evaluated by comparing activity coefficient predictions for the three solutes in poly(*n*-butyl acrylate) (M_w=258 g/mol) with those estimated for dibutyl adipate (M_w=258 g/mol). Differences in polymer-solute activity

coefficient predictions varied between the activity model used, with an average absolute deviation for FH-Hildebrand=1.8%, FH-HSP=12.6% and UNIFAC-vdW-FV=3.8%. These comparisons suggest that the composition of dibutyl adipate is a reasonable low molecular weight proxy for our polymer system.

The data listed in Table 3 show that the partition coefficients measured for *n*-butanol, *n*-butyl acetate and benzene increased with decreasing NAP molecular weight. By reducing molecular weight from 100,000 to 258 g/mol, the partition coefficients increased 85% for benzene, 156% for *n*-butyl acetate and 160% for *n*-butanol. This molecular weight effect was captured by both Flory-Huggins based methods (FH-Hildebrand and FH-HSP) and the UNIFAC-vdW-FV model. A closer analysis of the Flory-Huggins equation (Equation 13) suggests that the effect of poly(*n*-butyl acrylate) molecular weight is largely captured within the model as an increase in combinatorial entropy. Previous observations on poly(propylene glycol) have also shown molecular weight effects to be significant,[4] as the partition coefficient for *n*-butanol in this system increased from 3.0 to 4.8 as the polymer molecular weight was reduced from 4000 to 1000 g/mol. Due to the pronounced effect of molecular weight, partition coefficients published in the future will also benefit from reporting the oligomer/polymer molecular weight used. Further insight into the influence of molecular weight averages (i.e. M_n vs. M_w) and molecular weight distribution on PC is provided in Chapter 3.

Table 3 - Comparison of three activity models' abilities to capture the effect of poly(*n*-butyl acrylate) molecular weight on solute activity coefficient in the polymer phase. Aqueous phase infinite dilution activity coefficients were used as reported in Table 2. Errors shown are +/- one standard deviation.

Solute	Polymer M_w (g/mol)	Partition Coefficient [c]	$\Omega^{poly,expt}$	FH-Hildebrand $\Omega^{poly,pred}$	FH-HSP $\Omega^{poly,pred}$	UNIFAC-vdW-FV $\Omega^{poly,pred}$
n-Butanol	258 [a]	2.1 ± 0.2	5.9 ± 0.6 [d]	10.5 [b]	6.8 [b]	8.3 [b]
	6,200	1.3 ± 0.1	9.5 ± 0.9 [d]	15.6	12.8	15.9
	100,000	0.8 ± 0.4	15.4 ± 7.8 [d]	15.9	13.0	16.5
n-Butyl Acetate	258 [a]	86 ± 3	1.7 ± 0.4 [e]	2.6 [b]	1.9 [b]	2.0 [b]
	6,200	37 ± 1	3.9 ± 0.8 [e]	4.6	3.6	4.4
	100,000	35 ± 2	4.1 ± 0.9 [e]	4.7	3.7	4.5
Benzene	258 [a]	216 ± 16	2.5 ± 0.3 [e]	3.1 [b]	2.7 [b]	2.2 [b]
	6,200	125 ± 6	4.3 ± 0.5 [e]	4.7	3.7	3.9
	100,000	117 ± 12	4.6 ± 0.7 [e]	4.8	3.8	4.0

[a] Dibutyl adipate (M_w=258.4 g/mol) was used as a low molecular weight model compound for poly(*n*-butyl acrylate)
[b] Predictions were made for dibutyl adipate
[c] Aqueous phase concentration < 0.01 M ($\Omega_i^{aq,\infty}$) in all cases
[d] Polymer phase concentration < 0.01 M ($\Omega_i^{poly,\infty}$)
[e] Polymer phase concentration < 0.1 M ($\Omega_i^{poly,expt}$)

The effect of molecular weight on the polymer-phase activity coefficient is most pronounced in the low molecular weight region. In some cases lower molecular weight small molecules/oligomers may exhibit operational challenges in TPPBs such as increased foaming,[48] more challenging extractant recovery,[48] and decreased biocompatibility,[4] however the potential for molecular weight to improve solute partitioning merits further investigation.

A major limitation of the surrogate approaches is that their consideration of polymer-solute affinity cannot capture the combinatorial entropy contribution to mixing. As previously discussed, this contribution is significant in describing how changes in molecular weight affect polymer-solute affinity. Furthermore, in the case of poly(*n*-butyl acrylate), molecular weight has

very little effect on Hildebrand and Hansen solubility parameters, and as such, the influence of polymer molecular weight cannot be described by these methods.

2.5 Conclusions

The present study demonstrated that UNIFAC-vdW-FV and Flory-Huggins-based models provide accurate activity coefficient estimates for dilute solutions of small molecule solutes in poly(*n*-butyl acrylate). However, significant deviations between model predictions and experimental activity coefficients were observed at higher solute concentrations, indicating that partition coefficients should be reported along with the solute concentration used to produce the measurement. Furthermore, the sensitivity of partition coefficients to poly(*n*-butyl acrylate) molecular weight was demonstrated experimentally and through thermodynamic modeling, suggesting that partition coefficient values for polymeric systems should be accompanied by molecular weight information.

2.6 Acknowledgements

We gratefully acknowledge the financial support of DuPont Canada and the Natural Sciences and Engineering Research Council of Canada.

2.7 References

1 A. J. Daugulis, D. E. Swaine, F. Kollerup and C. A. Groom, *Biotechnol. Lett.*, 1987, **9**, 425–430.

2 A. J. Daugulis, *Curr. Opin. Biotechnol.*, 1997, **8**, 169–74.

3 J. M. Aldric, J. P. Lecomte and P. Thonart, *Appl. Biochem. Biotechnol.*, 2009, **153**, 67–79.

4 W. E. Barton and A. J. Daugulis, *Appl. Microbiol. Biotechnol.*, 1992, **36**, 632–639.

5 H. Fam and A. J. Daugulis, *Bioprocess Biosyst. Eng.*, 2012, **35**, 1367–74.

6 L. Rehmann and A. J. Daugulis, *Biotechnol. Bioeng.*, 2008, **99**, 1273–80.

7 B. G. Amsden, J. Bochanysz and A. J. Daugulis, *Biotechnol. Bioeng.*, 2003, **84**, 399–405.

8 J. V Littlejohns and A. J. Daugulis, *Biotechnol. Bioeng.*, 2009, **103**, 1077–86.

9 E. E. Poleo and A. J. Daugulis, *J. Chem. Technol. Biotechnol.*, 2014, **89**, 88–96.

10 M. C. Tomei, M. C. Annesini and A. J. Daugulis, *New Biotechnol.*, 2012, **30**, 44–50.

11 M. C. Tomei, M. C. Annesini, S. Rita and A. J. Daugulis, *Environ. Sci. Technol.*, 2010, **44**, 7254–9.

12 G. Quijano, M. Hernandez, F. Thalasso, R. Muñoz and S. Villaverde, *Appl. Microbiol. Biotechnol.*, 2009, **84**, 829–46.

13 F. Kollerup and A. J. Daugulis, *Can. J. Chem. Eng.*, 1985, **63**, 919–927.

14 J. S. Parent, M. Capela, J. T. Dafoe and A. J. Daugulis, *J. Chem. Technol. Biotechnol.*, 2012, **87**, 1059–1065.

15 A. J. Daugulis, M. C. Tomei and B. Guieysse, *Appl. Microbiol. Biotechnol.*, 2011, **90**, 1589–1608.

16 P. J. Flory, *Principles of Polymer Chemistry*, Cornell University Press, New York, 1953.

17 D. Patterson, *Pure Appl. Chem.*, 1972, **31**, 133–149.

18 D. Patterson, *Polym. Eng. Sci.*, 1982, **22**, 64–73.

19 G. H. Fredrickson, A. J. Liu and F. S. Bates, *Macromolecules*, 1994, **27**, 2503–2511.

20 M. A. van Dijk and A. Wakker, *Polymer Thermodynamics Library, Vol. 2: Concepts of polymer thermodynamics*, Technomic Publishing Company, Lancaster, PA, 1997.

21 C. M. Hansen, *Hansen Solubility Parameters: A User's Handbook*, Taylor & Francis Group, Boca Raton, FL, 2nd edn., 2007.

22 T. Oishi and J. M. Prausnitz, *Ind. Eng. Chem. Process Des. Dev.*, 1978, **17**, 333–339.

23 D. C. Kannan, J. L. Duda and R. P. Danner, *Fluid Phase Equilib.*, 2005, **228**–**229**, 321–328.

24 J. Brandrup, E. H. Immergut and E. A. Grulke, *Polymer Handbook*, John Wiley & Sons, Ltd, New York, 4th edn., 2003.

25 K. A. Payne, M. F. Cunningham and R. A. Hutchinson, in *Progress in Controlled Radical Polymerization: Mechanisms and Techniques*, eds. K. Matyjaszewski, B. Sumerlin and N. Tsarevsky, American Chemical Society, Washington, DC, 2012, pp. 182–202.

26 J. Gmehling, J. Menke and M. Schiller, *Activity coefficients at infinite dilution*, DECHEMA, Frankfurt, 1994.

27 K. Kojima, S. Zhang and T. Hiaki, *Fluid Phase Equilib.*, 1997, **131**, 145–179.

28 E. Estrada, G. a Díaz and E. J. Delgado, *J. Comput. Aided. Mol. Des.*, 2006, **20**, 539–48.

29 B. E. Mitchell and P. C. Jurs, *J. Chem. Inf. Comput. Sci.*, 1998, **38**, 200–209.

30 H. Renon and J. M. Prausnitz, *AIChE J.*, 1968, **14**, 135–144.

31 D. Abrams and J. M. Prausnitz, *AIChE J.*, 1975, **21**, 116–128.

32 W. Arlt, M. E. A. Macedo, P. Rasmussen and J. M. Sorensen, *Liquid-Liquid Equilibrium Data Collection*, DECHEMA, Frankfurt, 1979.

33 W. Hao, H. S. Elbro and P. Alessi, *Polymer Solution Data Collection, Part 2+3*, DECHEMA, Frankfurt, 1992.

34 R. A. Orwoll and P. A. Arnold, in *Physical Properties of Polymers Handbook*, ed. J. E. Mark, Springer, New York, 2007, pp. 233–257.

35 R. P. Danner and M. S. High, *Handbook of Polymer Solution Thermodynamics*, American Institute of Chemical Engineers, New York, 1993.

36 G. M. N. Costa, T. Dias, M. Cardoso, Y. Guerrieri, F. L. P. Pessoa, S. A. B. Vieira de Melo and M. Embiruçu, *Fluid Phase Equilib.*, 2008, **267**, 140–149.

37 T. Lindvig, M. L. Michelsen and G. M. Kontogeorgis, *Fluid Phase Equilib.*, 2002, **203**, 247–260.

38 J. Hildebrand and R. L. Scott, *The Solubility of Nonelectrolytes*, Reinhold Publishing Corp, New York, 3rd edn., 1950.

39 OECD, *OECD Guideline for the Testing of Chemicals - Partition Coefficient (n-octanol/water): Shake Flask Method*, Paris, 1995.

40 Y. Marcus, in *Solvent Extraction Principles and Practice*, eds. J. Rydberg, M. Cox, C. Musikas and G. Choppin, Marcel Dekker, Inc, New York, 2004, pp. 27–80.

41 J. J. Malinowski and A. J. Daugulis, *AIChE J.*, 1994, **40**, 1459–1465.

42 D. R. Nielsen, G. S. Amarasiriwardena and K. L. J. Prather, *Bioresour. Technol.*, 2010, **101**, 2762–9.

43 S. Tanaka, Y. Tashiro, G. Kobayashi, T. Ikegami, H. Negishi and K. Sakaki, *Bioresour. Technol.*, 2012, **116**, 448–52.

44 Y. Lin and S. Tanaka, *Appl. Microbiol. Biotechnol.*, 2006, **69**, 627–42.

45 H. Modarresi, E. Conte, J. Abildskov, R. Gani and P. Crafts, *Ind. Eng. Chem. Res.*, 2008, **47**, 5234–5242.

46 UNIFAC-vdW-FV Computer Program, A. Jones, D. Kannan and R. Danner, 2005.

47 HSPiP Computer Program v. 5.0.04, S. Abbott and H. Yamamoto, 2013.

48 G. Quijano, M. Hernandez, S. Villaverde, F. Thalasso and R. Muñoz, *Appl. Microbiol. Biotechnol.*, 2010, **85**, 543–51.

Chapter 3

Effect of polymer molecular weight distribution on solute sequestration in two-phase partitioning bioreactors

With minor changes to fulfill formatting requirements, this chapter is substantially as it appears in:

S. L. Bacon, A. J. Daugulis and J. S. Parent, *Chem. Eng. J.*, 2016, **299**, 56–62.

3.1 Abstract

Polymeric solids are effective absorbents in two-phase partitioning bioreactors (TPPBs) when they provide adequate absorptive capacity for the target solute, as well as the physical properties required by solid-liquid TPPB operations. This study demonstrates the influence of molecular weight distribution (MWD) on solute uptake, as measured by solute partition coefficient (PC), and mechanical strength, as measured by the polymer's complex modulus (G*). Experimental PC data for n-octanol absorption from aqueous solution by poly(dimethyl siloxane) (PDMS) demonstrate a decline in absorptive capacity with increasing number average molecular weight (M_n), in agreement with Flory-Huggins solution theory predictions. Importantly, MWD is shown to have no effect on solute uptake, with both unimodal and bimodal distributions generating the same PC at a given M_n. This is in contrast to G*, whose MWD sensitivity is exploited to formulate bimodal mixtures of poly(isobutylene) (PIB) that provide high n-octanol PC values as well as satisfactory material strength. This bimodal MWD strategy to TPPB absorbent design is extended to miscible solutions of high MW PIB and cyclohexylbenzene, which are shown to generate superior n-octanol PC at a given G*.

3.2 Introduction

Two-phase partitioning bioreactor (TPPB) technology is a proven means of improving bioreactor productivity by reducing substrate and/or product cytotoxicity. The first TPPB processes employed an organic solvent[1–5] or oligomeric liquid (e.g. silicone oil, poly(propylene glycol))[6–11] as an immiscible second phase to selectively sequester inhibitory compounds from fermentation media. However, low molecular weight absorbents can suffer from biocompatibility and bioavailability issues, as well as operational challenges stemming from volatility, flammability, emulsification and foaming.[1,12–17] Viscoelastic polymers are a potential solution to these challenges,[18–20] provided they possess the necessary absorptive capacity, and the physical integrity needed to survive within a bioreactor environment.

A principal polymer selection criterion is thermodynamic affinity for the target solute, as quantified by the partition coefficient (PC) between the polymer and an aqueous phase. The influence of chemical structure, crystallinity and phase transition temperatures on PC has been investigated in detail,[22,23] as has the effect of these polymer characteristics on solute diffusivity and mass transfer rate.[19,24–31] The present work advances our understanding of the effect of polymer molecular weight distribution (MWD) on solute absorption. Our preliminary studies have shown that lowering the MW of poly(n-butyl acrylate)[22] and poly(propylene glycol)[9] has a positive effect on PC, presumably due to associated increases in the entropy of mixing.[32] These examples involved unimodal MWD's of linear polymer chains, leaving the potential advantages provided by other polymer architectures largely unexplored in the context of TPPB applications.

The central question addressed by this study is whether unimodal MWD polymers and bimodal MWD polymers differ appreciably in terms of solute uptake and material strength. We begin with PC measurements of n-octanol absorption by poly(dimethyl siloxane) (PDMS, silicone oil) samples of varying molecular weight and MWD. Both substances are well represented in the

bioprocessing literature, with n-octanol forming the basis of tabulated log $K_{o/w}$ data, and silicone oil finding frequent application in TPPB systems.[6–8,10,11,33] These data are discussed in the context of Flory-Huggins solution theory to provide a thermodynamic basis for observed MW effects.

The joint influence of MWD on solute uptake and material strength is examined using poly(isobutylene) (PIB), which provides the mechanical strength that is generally lacking in uncured PDMS materials. Measurements of n-octanol PC and complex modulus (G*) reveal important differences between unimodal and bimodal MWD samples of linear PIB chains. Insights gained through these studies are used to formulate mixtures of high MW PIB with a high-boiling organic solvent, cyclohexylbenzene, which are designed to exploit the absorptive capacity of a low MW compound as well as the physical strength of a high MW polymer. The results are relevant to TPPB bioproduction/biodegradation processes and polymer-based product recovery processes that require solute affinity and mechanical rigidity, such as pervaporation, perstraction and vapour permeation.

3.3 Materials and methods

3.3.1 Materials and material preparation

All chemicals (purity ≥ 98%) were purchased from either Sigma-Aldrich (Canada) or Fisher Scientific (Canada). All poly(dimethyl siloxane) (PDMS) samples (S-UM-1 to S-UM-5) were purchased from Scientific Polymer Products (Ontario, NY). PIB Samples IB-UM-1 to IB-UM-4 were provided by TPC group (Houston, TX). PIB samples IB-UM-5 and IB-UM-6 were provided by Shandong Hongrui Petrochemical Co., Ltd (Jinan, China). Samples IB-UM-7 to IB-UM-9 were purchased from Scientific Polymer Products (Ontario, NY). Number average (M_n) and weight average (M_w) molecular weight data for each polymer are listed in Table 4 and Table 5, experimentally determined as per Section 3.3.2.

Bimodal PDMS samples were prepared by adding varying quantities of S-UM-1 to S-UM-5 and agitated in an Innova 4400 incubator shaker at 30°C and 180 rpm until the solution was homogeneous (one week). The solution was vortexed at least daily under high power to facilitate homogeneity. Bimodal PIB mixtures (IB-BM) were prepared by dissolving varying quantities of IB-UM-1 and IB-UM-9 as a ~15 wt% solution in hexanes in a sealed glass tube. The resultant polymer cement was agitated at 180 rpm in an Innova 4400 incubator shaker at 60°C until the solution was homogenous (one week). The solution was vortexed at least daily under high power to facilitate homogeneity. Aliquots of the polymer mixtures were transferred to scintillation vials and allowed to dry at 60°C for one week followed by atmospheric conditions for one additional week.

Bimodal mixtures of high MW PIB and cyclohexylbenzene (IB-CHB) were prepared by adding varying quantities of cyclohexylbenzene (CHB) to IB-UM-9 and agitated in an Innova 4400 incubator shaker at 30°C and 180 rpm until the solution was homogeneous (two weeks). The solution was vortexed at least daily under high power to facilitate homogeneity. The rational for selecting CHB is provided in considerable detail in the Results and Discussion section. Low molecular weight component fractions (wt/wt) were calculated by determining the weight loss from a sample after drying in a 110^{o}C oven.

Table 4 - M_n and M_w values for unimodal PDMS samples (S-UM) and bimodal mixtures of high MW PDMS mixed with oligomeric PDMS (S-BM). S-BM samples were made by combining S-UM-1 and S-UM-5.

Sample ID	**Low MW Component**	**Low MW Fraction**	**M_n** (g/mol)	**M_w** (g/mol)
S-UM-1	n/a[a]	0	100[b]	105[b]
S-UM-2	n/a[a]	0	1150	1,200
S-UM-3	n/a[a]	0	9220	15,500
S-UM-4	n/a[a]	0	21,600	48,400
S-UM-5	n/a[a]	0	69,700	135,300
S-BM-1	PDMS oligomer	0.95	105	6580
S-BM-2	PDMS oligomer	0.90	110	13,300
S-BM-3	PDMS oligomer	0.75	130	34,400
S-BM-4	PDMS oligomer	0.50	200	67,700
S-BM-5	PDMS oligomer	0.25	400	101,500
S-BM-6	PDMS oligomer	0.10	980	121,800
S-BM-7	PDMS oligomer	0.05	1880	128,300

[a] unimodal sample

[b] nominal value from supplier

Table 5 - M_n and M_w values for unimodal PIB samples (IB-UM), bimodal mixtures of high MW PIB with oligomeric PIB (IB-BM) and bimodal mixtures of high MW PIB with CHB (IB-CHB). IB-BM samples were made by combining IB-UM-1 and IB-UM-9. IB-CHB samples made were made by combining IB-UM-9 with CHB.

Sample ID	**Low MW Component**	**Low MW Fraction**	**M_n** (g/mol)	**M_w** (g/mol)
IB-UM-1	n/a[a]	0	670	1100
IB-UM-2	n/a[a]	0	920	1790
IB-UM-3	n/a[a]	0	1470	3110
IB-UM-4	n/a[a]	0	2670	8490
IB-UM-5	n/a[a]	0	9490	51,400
IB-UM-6	n/a[a]	0	18,400	65,500
IB-UM-7	n/a[a]	0	21,200	119,800
IB-UM-8	n/a[a]	0	85,700	503,800
IB-UM-9	n/a[a]	0	320,000	4,912,000
IB-BM-1	PIB oligomer	0.75	890	1,229,000
IB-BM-2	PIB oligomer	0.50	1320	2,446,000
IB-BM-3	PIB oligomer	0.25	2640	3,677,000
IB-BM-4	PIB oligomer	0.10	6490	4,416,000
IB-BM-5	PIB oligomer	0.05	12,500	4,659,000
IB-BM-6	PIB oligomer	0.01	50,400	4,857,000
IB-CHB-1	Cyclohexylbenzene	0.25	640	3,684,000
IB-CHB-2	Cyclohexylbenzene	0.11	1520	4,396,000
IB-CHB-3	Cyclohexylbenzene	0.04	3860	4,710,000
IB-CHB-4	Cyclohexylbenzene	0.02	9160	4,828,000

[a] unimodal sample

3.3.2 Molecular weight determination

Unimodal PIB and PDMS samples with M_n<100,000 g/mol were characterized by size exclusion chromatography (SEC) using a Waters 2960 separation module with Styragel packed columns HR 0.5, HR 1, HR 3, HR 4, and HR 5E (Waters Division Millipore) coupled with a refractive index (RI) detector operating at 35°C. Tetrahydrofuran (THF) was used as eluent and the flow rate was set to 1.0 mL/min.

Unimodal PIB samples with M_n>100,000 g/mol were characterized by SEC using a Viscotek 270max separation module with an RI detector. A set of two porous PolyAnalytik columns with an exclusion limit molecular weight of 20×10^6 g/mol were used in series at 40°C. Distilled THF was used as the eluent at a flow rate of 1.0 mL/min.

In both cases, the unimodal weight average molecular weight (M_w), number average molecular weight (M_n) and polydispersity index (PDI) were obtained by universal calibration using Mark-Houwink parameters.[34]

M_n and M_w values for the homogenous bimodal mixtures were calculated using the following equations using data from unimodal samples:

$$M_{n,blend} = \frac{1}{\frac{w_{lo}}{M_{n,lo}} + \frac{w_{hi}}{M_{n,hi}}} \tag{18}$$

$$M_{w,blend} = w_{lo}M_{w,lo} + w_{hi}M_{w,hi} \tag{19}$$

$$w_{lo} = 1 - w_{hi} \tag{20}$$

where:

w_i is the weight fraction of component '*i*' in the mixture

3.3.3 Experimental partition coefficients (PCexpt)

Partition coefficient tests were performed in triplicate using three polymer masses, ranging from 0.25 to 1.5 g. n-Octanol was prepared in aqueous solution (0.4 g/L) using Type I ultrapure water. In addition to the polymer mass, a 20 mL aliquot of aqueous solution were added to each scintillation vial, sealed tightly with a foil lined cap and allowed to equilibrate in an Innova 4400 incubator shaker at 30°C at 180 rpm for 1 week (PDMS) or 2 weeks (PIB). Equilibration times were determined from time-course absorption experiments for each material. n-Octanol concentrations before and after equilibration with the polymer were measured using a Varian 450-GC gas chromatography unit equipped with a CP-8410 AutoInjector, VF-5ms 30m capillary column and FID detector. Using this method, 0.4 g/L control n-octanol solutions (left to equilibrate without polymer) had a standard deviation of 6.7% (n=3).

A mass balance was performed to determine the solute concentration in the polymer. Experimental *PC* values were calculated using aqueous and polymer phase weight fractions, w_i^{aq} and w_i^{poly}, in Equation 21. Standard deviation (n=3) values were calculated from triplicate samples to establish a mean value for the equilibrium *PC*.

$$PC = \frac{w_i^{poly}}{w_i^{aq}} \tag{21}$$

3.3.4 Partition coefficients predictions (PCpred)

Partition coefficients (*PC*) can be predicted for systems only at thermodynamic equilibrium, for which the PC has be defined as [22]

$$PC = \frac{w_i^{poly}}{w_i^{aq}} = \frac{\Omega_i^{aq}}{\Omega_i^{poly}} \quad (22)$$

In this study, the non-random two liquid (NRTL) model (Equation 23) [35] was selected to estimate aqueous phase weight fraction activity coefficients (Ω_i^{aq}) at experimental conditions.

$$a_1^{aq} = w_1\Omega_1^{aq} = x_1\gamma_1^{aq} = x_1 \exp\left(x_2^2\left(\tau_{21}\frac{exp(-2\alpha_{12}\tau_{21})}{[x_1+x_2\,exp(-\alpha_{12}\tau_{21})]^2} + \tau_{12}\frac{exp(-\alpha_{12}\tau_{12})}{[x_2+x_1\,exp(-\alpha_{12}\tau_{12})]^2}\right)\right) \quad (23)$$

where a_1^{aq} is the activity of n-octanol in the aqueous phase, γ_1^{aq} is the mole fraction activity coefficient and x_i is the mole fraction of 'i'. Temperature dependent LLE binary interaction parameters were provided by the Dortmund Data Bank[36] for n-octanol (1)/water (2): $\alpha_{12} = \alpha_{21} = 0.2$; $\Delta g_{12}[K] = -3902.9 + 24.68 \cdot T - 0.0388 \cdot T^2$; $\Delta g_{21}[K] = 2099.1 - 0.316 \cdot T + 0.00882 \cdot T^2$. Note that according to DDB convention $\tau_{i,j} = \frac{\Delta g_{i,j}}{T}$ and $G_{i,j} = \exp(-\alpha \cdot \tau_{i,j})$.

As described in our previous work,[22,23] polymer phase activity coefficients (Ω_i^{poly}) were predicted using the Flory-Huggins solution theory [32] in conjunction with Hansen solubility parameters (FH-HSP).[37] The system-dependent adjustable parameter in the FH-HSP model was set to a default value of α=1.[22,23,37] Solubility parameters were sourced from the database provided in the HSPiP v.4.0.04 computer program.[38] Octanol [MPa$^{1/2}$]: (δ_D, δ_P, δ_H: 16.0, 5.0, 11.2) and PDMS [MPa$^{1/2}$]: (δ_D, δ_P, δ_H: 12.3, 0.4, 0.3).

3.3.5 Rheological analysis

Polymer samples were tested for complex modulus G* at 37°C in an Advanced Polymer Analyzer 2000 (Alpha Technologies) controlled-strain rheometer equipped with biconical discs operating at 1 Hz and 3° arc.

3.4 Results and discussion

3.4.1 Unimodal and Bimodal MWD Absorbents

Polymeric materials, either by design or inherent from their method of preparation, do not have a single molecular weight (MW) in the manner of organic solvents, but a distribution of MWs that can be tailored to satisfy different physical and chemical property requirements. In the majority of cases, the complete MWD is not specified, but rather is summarized by the first two moments of the distribution. The number average MW, M_n, is calculated based on the *number* of each chain of a given molecular weight, while the weight average MW, M_w, is calculated on the *mass* of each chain of a given molecular weight. The ratio of M_w to M_n is the polydispersity, PD= M_w/M_n, a measure of the breadth of the distribution ranging from a value of 1 for a completely monodisperse material to very large values for materials possessing chains of widely ranging MWs.

The critical molecular weight of a polymer (M_c), which defines the MW at which chain entanglements contribute to physical properties, is particularly important to this work. Below M_c, material viscosity is dominated by intermolecular forces, whereas above M_c, polymer chains entangle with one another to produce the viscoelasticity associated with elastomeric behaviour. The polymer samples used in this study spanned a very wide range of MWs, as illustrated in Figure 4-a for “as received” PIB materials, and in Figure 4-b for bimodal PIB samples prepared by mixing different proportions of PIB oligomer and high MW PIB polymer. Taken together,

these unimodal and bimodal samples shed light on the influence of MW and MWD on solute uptake and material physical properties, leading to a better understanding of how polymeric absorbents can be designed to meet the demands of TPPB systems.

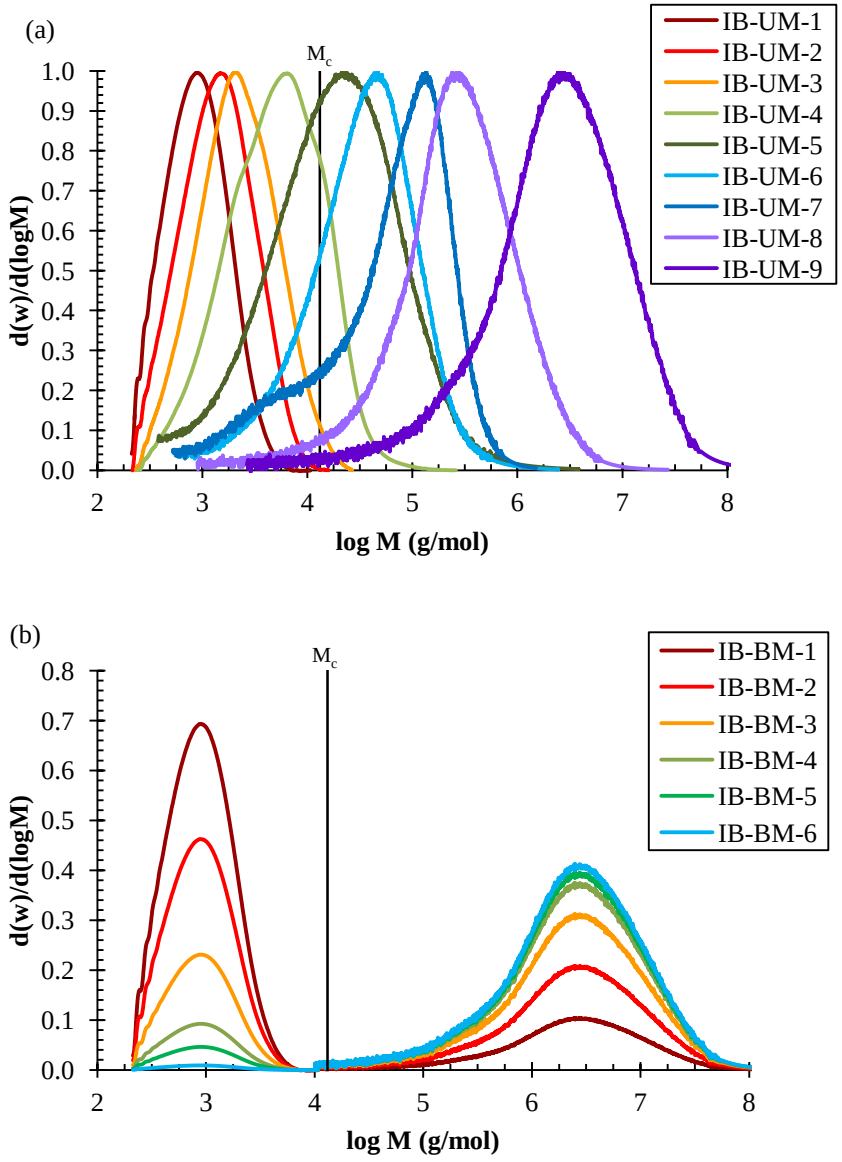

Figure 4 –Normalized representative GPC curves of (a) unimodal and (b) bimodal PIB samples.

3.4.2 Influence of PDMS M_n, M_w and MWD on n-octanol absorption

The selection of an absorptive phase for TPPB applications is normally concerned with chemical composition. Generalized statements such as "like dissolves like", and empirical frameworks such as the Hildebrand solubility parameter[39] and the Hansen parameters[40] are expressions of the need to minimize the enthalpy of mixing generated by a prospective solute/solvent system. Semi-empirical expressions for the thermodynamic activity of a solute in a polymer phase, such as the Flory-Huggins solution model, also address the enthalpic contributions to the Gibbs energy directly through binary interaction parameters estimated from experimental data.[32,37] Note, however, that the Flory-Huggins equation has additional terms describing the entropic contributions to the Gibbs energy of mixing, wherein the molecular weight of the polymer phase factors prominently.

Equation 24 is a common presentation of the Flory-Huggins equation governing the activity coefficient of solute i in polymer j;

$$\boldsymbol{a_i^{poly} = w_i \Omega_i^{poly} = x_i \gamma_i^{poly} = x_i \cdot \exp\left(\underbrace{\ln \frac{\varphi_i}{x_i} + 1 - \frac{\varphi_i}{x_i}}_{combinatorial} + \underbrace{\chi_{ij} \varphi_j^2}_{non\text{-}comb} \right)} \qquad (24)$$

where γ_i is the mole fraction activity coefficient, x_i is the mole fraction and φ_i is the volume fraction. Non-combinatorial (enthalpic) contributions to mixing are captured by the Flory-Huggins interaction parameter, χ_{ij},[41] while combinatorial (entropic) contributions are a function of the volume fraction and the mole fraction of the solute in the mixture – the latter being directly related to the molecular weight of the polymer.[32,37]

Figure 5 provides a semi-log plot of predicted n-octanol PC values in PDMS derived from Flory-Huggins solution theory (See Experimental Section), as well as experimental PC data for our

unimodal MWD and bimodal MWD samples. The data show that decreasing the M_n of PDMS from 69,700 to 100 g/mol results in a 2-fold increase in PC. According to the Flory-Huggins equation, decreasing polymer M_n lowers the solute mole fraction (x_1) relative to solute volume fraction (φ_i). Accordingly, the net contribution to solute activity (a_i) is negative, indicating more favourable mixing and improved PC. At M_n values above about 1000 g/mol, the combinatorial contribution becomes negligible compared to the enthalpic term, resulting in a plateau for PC that agrees well with experiment. Inaccuracy in measuring the MW of PDMS oligomers may account for some of the deviation between model and experiment at low M_n.

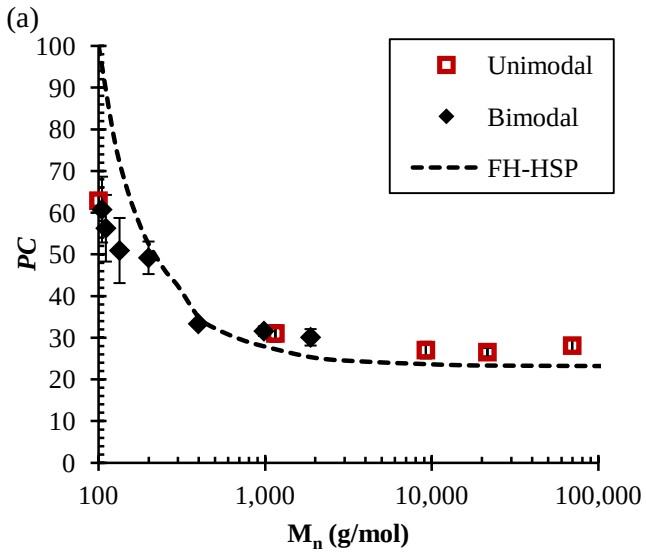

Figure 5 - n-Octanol partition coefficient versus M_n for unimodal (S-UM) and bimodal (S-BM) PDMS

The results presented in Figure 5 have two important consequences for selecting polymers for TPPB applications. First, the influence that polymer MW has on PC is a predictable function of M_n, so the reporting of PC data, and their use in polymer selection, should make explicit reference to number average molecular weight, particularly at low M_n. Second, the influence of

M_n on PC is independent of molecular weight distribution, applying equally well to unimodal and bimodal MWDs. Therefore, given the sensitivity of most physical properties to MWD and chain architecture, polymeric absorbents can be formulated to meet a PC/M_n target while simultaneously meeting mechanical strength targets. This opportunity is demonstrated below for the PIB polymer system, which provides superior mechanical strength to uncured PDMS.

3.4.3 Influence of PIB MWD on octanol uptake and material strength

As discussed above, the selection of a polymeric absorbent for TPPB applications requires consideration of its thermodynamic affinity for the target solute and its mechanical strength/toughness. Given the wide range of MWs of our samples and the resulting breadth of their physical properties, oscillatory rheometry was used as a standard measure of material strength. The complex modulus (G*) is the magnitude of the dynamic stress response by the polymer to an oscillatory applied strain. In contrast to a continuous strain rate measurement such as static tensile testing, it provides accurate data for oligomeric materials (viscous liquids) as well as high MW polymers (viscoelastic solids). Since PDMS requires crosslinking to infinite molecular weight to exhibit solid-like mechanical properties, it is not appropriate for studies of M_n/PC and M_n/G* relationships. PIB was, therefore, selected for use in the remainder of the work.

The data plotted in Figure 6 confirm that n-octanol partitioning into an amorphous elastomer improves as polymer M_n is lowered, as PC values for PIB increased nearly 4-fold (10.7 ± 1.3 to 39.5 ± 0.6) as M_n decreased from 320,000 to 670 g/mol. Furthermore, the MWD of the material had no bearing on solute uptake capacity (PC), consistent with our PDMS/n-octanol results. Note that the end-groups of our PIB and PDMS samples were chemically similar to the polymer backbone. However, when the polarity and H-bonding strength of end-groups differ significantly

from those of the main chain, the relationship between PC and oligomer MW can be dominated by enthalpic contributions as opposed to entropic effects, leading to deviations from Flory-Huggins solution theory predictions. The enthalpic effect of end-group composition on solute absorption in low MW oligomers has been demonstrated previously.[42]

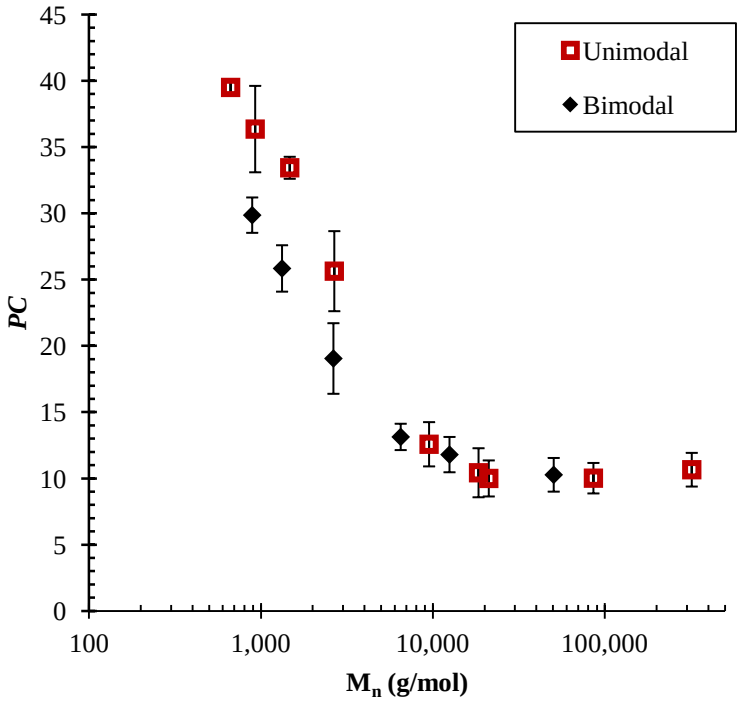

Figure 6 - Partition coefficient (*PC*) values plotted against (a) M_n and (b) M_w for unimodal and bimodal PIB

Our PDMS and PIB results showed that two chemically identical samples with a given M_n will provide the same PC, irrespective of MWD. In sharp contrast, the data plotted in Figure 7 demonstrate the sensitivity of G* to chain populations larger than the critical MW of the polymer (M_c). The unimodal MWD samples generated very low G* values until a fraction of PIB chains

had MW greater than M_c = 13,100 g/mol,[43,44] whereupon the material strength improved greatly as polymer chain entanglement heightened the material's resistance to an applied deformation.[45,46] Very different behaviour was observed for the bimodal MWD samples that were prepared by mixing low MW PIB with high MW PIB (see Figure 4). Since each bimodal mixture contained a population of chains larger than M_c, the bimodal materials provided greater G*values at a given M_n than the unimodal materials. Consider that at M_n ~ 2650 g/mol, the bimodal mixture generated a G* 25-times that of the corresponding unimodal material (Figure 7).

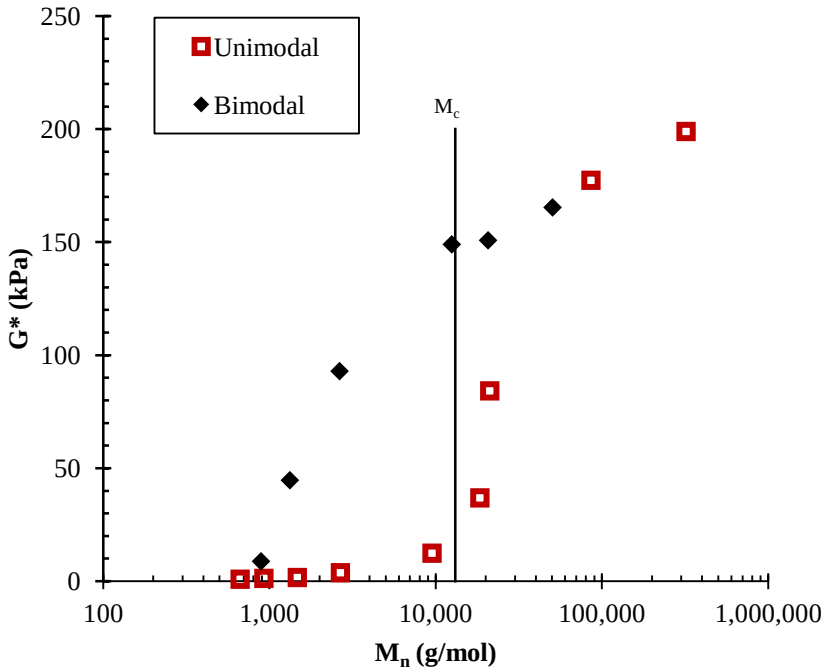

Figure 7 - Effect of M_n on complex modulus (G*) for unimodal and bimodal MWD PIB materials

In the context of TPPB polymer selection, it is clear that thermodynamic affinity for the target solute (PC) encourages the selection of low M_n elastomer, while mechanical strength (G*) favours high M_n material. Fortunately, compromises between PC and G* that are inherent to conventional unimodal MWD polymers can be mitigated using bimodal MWD materials made

from mixing very low and very high MW material. Semi-log plots of PC versus G* (Figure 8) confirm that a bimodal mixture can combine much of the absorptive benefits derived from a small M_n with the strength derived from a polymer chain population with MW>M_c. In TPPB applications where liquid-like materials exhibit operational challenges such as foaming and emulsification, bimodal molecular weight distributions may provide desirable viscoelastic solid properties without incurring significant losses of solute absorptive capacity. Note that further benefits may be realised with a high MW component that contains long-chain branching, wherein chain entanglements effects are further amplified.

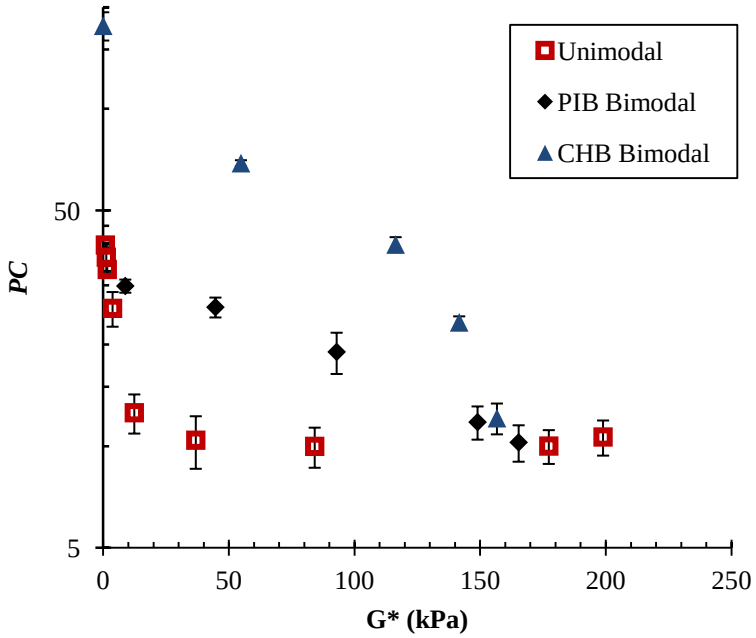

Figure 8 - Comparison of PC and G* for unimodal PIB, bimodal PIB oligomer + PIB polymer, and bimodal CHB + PIB polymer samples

3.4.4 Formulation of Polymer + Solvent Absorbents

The benefits of bimodal MWD materials outlined above can be used to design interesting TPPB absorbents from miscible mixtures of a low MW organic solvent and high MW polymer. According to this approach, the polymer's primary role in the mixture is to provide the requisite material strength to mitigate operational challenges (e.g. foaming, emulsification) associated with pure organic solvents. The solvent is then selected to maximize the solute PC through both enthalpic and entropic contributions. Building upon our knowledge of the n-octanol/PIB system, we sought an organic solvent to serve as the low MW component for bimodal samples that provide a more favourable PC versus G* relationship than that generated by combining low and high MW PIB alone. The development of a two-component formulation introduces additional material selection criteria, a list of which can be found in Table 6. Note that an organic solvent within polymer solution will exhibit a reduced volatility and water solubility compared to the solvent alone.

Table 6 - Ideal properties of a low molecular weight component in bimodal MWD absorbents

Property	**Selection Criterion**
Affinity for the target molecule	High n-octanol PC
Miscibility with polymer	Hansen solubility parameters
Low volatility	Boiling point / Vapour pressure
Biocompatibility	Critical Log $K_{o/w}$ of microorganism
Must not leach into bioreactor broth preventing losses and causing cytotoxic effects	Water solubility
Commercial availability and cost	

Cyclohexylbenzene (CHB) was chosen on the basis of its high boiling point (B_p=239-240°C) [47], low vapour pressure (6.1 Pa at 25°C), low water solubility (11.3 mg/L at 25°C), as well as a log $K_{o/w}$ (4.8) high enough to ensure biocompatibility with most industrially-pertinent microorganisms.[10,15,21] A predicted PC value of 212 for n-octanol was generated using the UNIFAC-vdW-FV model,[48,49] which was later supplemented with an experimental value of PC_{expt}=176 ± 17. Note that this is considerably greater than the PC generated by oligomeric PIB (M_n=670, PC=39.5 ± 0.6).

High MW PIB (M_n=320,000) was mixed in different proportions with either CHB or oligomeric PIB (M_n=670) to generate the materials whose properties are illustrated in Figure 9. At all concentrations, samples containing CHB as the low MW component yielded higher n-octanol PCs than the corresponding oligomeric PIB containing controls, with the greatest gains corresponding to the highest loadings of low MW component (Figure 9-a). The effect of the low molecular component (CHB or oligomeric PIB) on G* was similar at low concentrations (Figure 9-b). However, above a low MW component fraction of 0.2 (wt/wt), declines of G* were steeper for the CHB loaded material, owing to the lower viscosity of the organic solvent relative to the PIB oligomer.

A summary of the PC versus G* relationships explored in this work is provided in Figure 8, which illustrates the benefits of using a mixture of CHB + high MW PIB for n-octanol sequestration. More generally, it demonstrates the potential of a TPPB polymer formulation based upon carefully selected mixtures of organic solvent and high MW polymer to provide high absorptive capacity while maintaining viscoelastic solid properties.

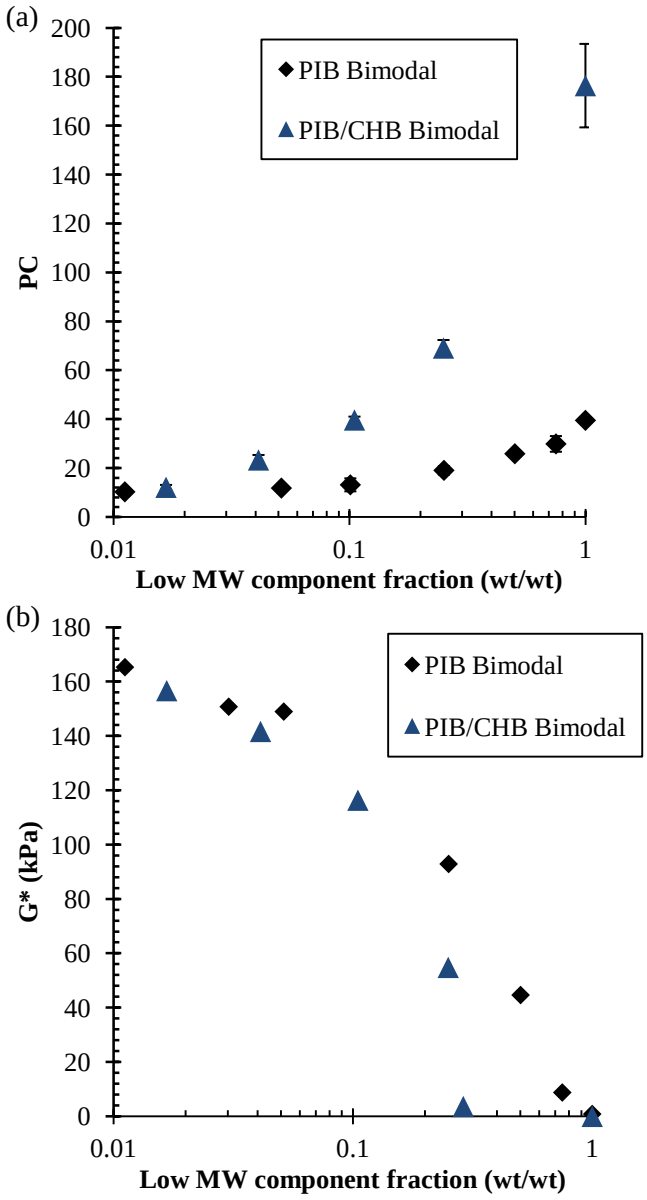

Figure 9 - Effect of low MW component fraction (oligomeric PIB or cyclohexylbenzene) on the absorption of n-octanol (PC) and polymer mixture stiffness G*

3.5 Conclusions

Solute absorption by a polymer is a predictable function of the material's *number average* molecular weight (M_n). However, it is independent of MWD (e.g. unimodal, bimodal). In the context of TPPB polymer selection, thermodynamic affinity for the target solute (PC) encourages

the selection of low M_n material, while mechanical strength (G*) favours high M_n polymer. Compromises between PC and G* inherent to unimodal MWD polymers can be mitigated using bimodal MWD formulations, made from mixing very low MW material (organic solvent or oligomer) with a high MW polymer. The low MW material is selected to maximize solute PC through both entropic and enthalpic contributions, while the high MW polymer's role is to provide the requisite material strength to the mixture.

3.6 Acknowledgements

We gratefully acknowledge the financial support of DuPont Canada and the Natural Sciences and Engineering Research Council of Canada. We also wish to thank the Dortmund Data Bank Software & Separation Technology GmbH for their help with NRTL parameter regression.

3.7 References

1 A. Arca-Ramos, G. Eibes, M. T. Moreira, G. Feijoo and J. M. Lema, *Chem. Eng. J.*, 2014, **240**, 281–289.

2 M. Minier and G. Goma, *Biotechnol. Bioeng.*, 1982, **24**, 1565–1579.

3 H. C. Cheng and F. S. Wang, *Chem. Eng. J.*, 2010, **162**, 809–820.

4 A. J. Daugulis, D. E. Swaine, F. Kollerup and C. A. Groom, *Biotechnol. Lett.*, 1987, **9**, 425–430.

5 J. Marcoux, E. Déziel, R. Villemur, F. Lépine, J. G. Bisaillon and R. Beaudet, *J. Appl. Microbiol.*, 2000, **88**, 655–662.

6 J. Rocha-Rios, S. Bordel, S. Hernández and S. Revah, *Chem. Eng. J.*, 2009, **152**, 289–292.

7 S. M. Zamir, S. Babatabar and S. A. Shojaosadati, *Chem. Eng. J.*, 2015, **268**, 21–27.

8 P. Parnian, S. M. Zamir and S. A. Shojaosadati, *Chem. Eng. J.*, 2016, **284**, 926–933.

9 W. E. Barton and A. J. Daugulis, *Appl. Microbiol. Biotechnol.*, 1992, **36**, 632–639.

10 S. Arriaga, R. Muñoz, S. Hernández, B. Guieysse and S. Revah, *Environ. Sci. Technol.*, 2006, **40**, 2390–2395.

11 R. Muñoz, S. Arriaga, S. Hernández, B. Guieysse and S. Revah, *Process Biochem.*, 2006,

41, 1614–1619.

12 J. Harris and A. J. Daugulis, *Biotechnol. Bioeng.*, 2015, **112**, 2450–2458.

13 T. B. Janikowski, D. Velicogna, M. Punt and A. J. Daugulis, *Appl. Microbiol. Biotechnol.*, 2002, **59**, 368–76.

14 A. J. Daugulis and M. C. Tomei, *Appl. Microbiol. Biotechnol.*, 2011, **90**, 1589–1608.

15 L. D. Collins and A. J. Daugulis, *Biotechnol. Bioeng.*, 1997, **55**, 155–162.

16 J. L. Rols, J. S. Condoret, C. Fonade and G. Goma, *Biotechnol. Bioeng.*, 1990, **35**, 427–35.

17 G. Quijano, M. Hernandez, F. Thalasso, R. Muñoz and S. Villaverde, *Appl. Microbiol. Biotechnol.*, 2009, **84**, 829–46.

18 B. G. Amsden, J. Bochanysz and A. J. Daugulis, *Biotechnol. Bioeng.*, 2003, **84**, 399–405.

19 G. Quijano, M. Hernandez, S. Villaverde, F. Thalasso and R. Muñoz, *Appl. Microbiol. Biotechnol.*, 2010, **85**, 543–51.

20 M. C. Tomei, M. C. Annesini, S. Rita and A. J. Daugulis, *Environ. Sci. Technol.*, 2010, **44**, 7254–9.

21 J. L. Ramos, E. Duque, M.-T. Gallegos, P. Godoy, M. I. Ramos-Gonzalez, A. Rojas, W. Teran and A. Segura, *Annu. Rev. Microbiol.*, 2002, **56**, 743–768.

22 S. L. Bacon, J. Scott Parent and A. J. Daugulis, *J. Chem. Technol. Biotechnol.*, 2014, **89**, 948–956.

23 S. L. Bacon, E. C. Peterson, A. J. Daugulis and J. S. Parent, *Biotechnol. Prog.*, 2015, **31**, 1500–7.

24 J. Rocha-Rios, G. Quijano, F. Thalasso, S. Revah and R. Muñoz, *J. Chem. Technol. Biotechnol.*, 2011, **86**, 353–360.

25 M. Hernández, G. Quijano, F. Thalasso, A. J. Daugulis, S. Villaverde and R. Muñoz, *Biotechnol. Bioeng.*, 2010, **106**, 731–740.

26 J. M. Aldric, J. P. Lecomte and P. Thonart, *Appl. Biochem. Biotechnol.*, 2009, **153**, 67–79.

27 A. Arwa, S. Baup, N. Gondrexon, J.-P. Magnin and J. Willison, *Biotechnol. Bioprocess Eng.*, 2011, **16**, 413–418.

28 H. Fam and A. J. Daugulis, *Bioprocess Biosyst. Eng.*, 2012, **35**, 1367–74.

29 R. Muñoz, M. Chambaud, S. Bordel and S. Villaverde, *Appl. Microbiol. Biotechnol.*, 2008, **79**, 33–41.

30 M. Hernández, G. Quijano, R. Muñoz and S. Bordel, *Chem. Eng. J.*, 2011, **172**, 961–969.

31 M. J. Pittman, M. W. Bodley and A. J. Daugulis, *J. Chem. Technol. Biotechnol.*, 2015, **90**, 1391–1399.

32 P. J. Flory, *Principles of Polymer Chemistry*, Cornell University Press, New York, 1953.

33 B. Guieysse and C. B. Mattiasson, *Appl. Microbiol. Biotechnol.*, 2001, **56**, 796–802.

34 O. Chiantore, in *Encyclopedia of Chromatography*, ed. J. Cazes, Taylor & Francis Group, Boca Raton, FL, 2nd edn., 2005.

35 H. Renon and J. M. Prausnitz, *AIChE J.*, 1968, **14**, 135–144.

36 2015.

37 T. Lindvig, M. L. Michelsen and G. M. Kontogeorgis, *Fluid Phase Equilib.*, 2002, **203**, 247–260.

38 S. Abbott and H. Yamamoto, 2013.

39 J. Hildebrand and R. L. Scott, *The Solubility of Nonelectrolytes*, Reinhold Publishing Corp, New York, 3rd edn., 1950.

40 C. M. Hansen, *Hansen Solubility Parameters: A User's Handbook*, Taylor & Francis Group, Boca Raton, FL, 2nd edn., 2007.

41 D. Patterson, *Polym. Eng. Sci.*, 1982, **22**, 64–73.

42 J. T. Dafoe, J. S. Parent and A. J. Daugulis, *J. Chem. Technol. Biotechnol.*, 2014, **89**, 1304–1310.

43 G. C. Berry and T. G. Fox, *Adv. Polym. Sci.*, 1968, **5**, 261–357.

44 L. J. Fetters, D. J. Lohse and R. H. Colby, in *Physical Properties of Polymers Handbook*, ed. J. E. Mark, Springer, 2nd edn., 2006, pp. 445–452.

45 W. Graessley, *Adv. Polym. Sci.*, 1974, **16**, 1–179.

46 J. D. Ferry, *Viscoelastic properties of polymers*, John Wiley & Sons, Ltd, New York, 3rd edn., 1980.

47 US EPA, 2015.

48 D. C. Kannan, J. L. Duda and R. P. Danner, *Fluid Phase Equilib.*, 2005, **237**, 86–88.

49 A. Jones, D. Kannan and R. Danner, 2005.

Chapter 4

Selecting polymers for two-phase partitioning bioreactors (TPPBs): Consideration of thermodynamic affinity, crystallinity and glass transition temperature

With minor changes to fulfill formatting requirements, this chapter is substantially as it appears in:

S. L. Bacon, E. C. Peterson, A. J. Daugulis and J. S. Parent, *Biotechnol. Prog.*, 2015, **31**, 1500–7.

4.1 Abstract

Two-phase partitioning bioreactor (TPPB) technology involves the use of a secondary immiscible phase to lower the concentration of cytotoxic solutes in the fermentation broth to sub-inhibitory levels. Although polymeric absorbents have attracted recent interest due to their low cost and biocompatibility, material selection requires the consideration of properties beyond those of small molecule absorbents (i.e. immiscible organic solvents). These include a polymer's: 1) thermodynamic affinity for the target compound, 2) degree of crystallinity (w_c) and 3) glass transition temperature (T_g).

We have examined the capability of three thermodynamic models to predict the partition coefficient (*PC*) for *n*-butyric acid, a fermentation product, in 15 polymers. Whereas *PC* predictions for amorphous materials had an average absolute deviation (AAD) of ≥ 16%, predictions for semi-crystalline polymers were less accurate (AAD ≥ 30%). Prediction errors were associated with uncertainties in determining the degree of crystallinity within a polymer and the effect of absorbed water on *n*-butyric acid partitioning. Further complications were found to arise for semi-crystalline polymers, wherein strongly-interacting solutes increased the polymer's absorptive capacity by actually dissolving the crystalline fraction. Finally, we determined that diffusion limitations may occur for polymers operating near their T_g, and that the glass transition temperature can be reduced by plasticization by water and/or solute. This study has demonstrated the impact of basic material properties that affect the performance of polymers as sequestering phases in TPPBs, and reflects the additional complexity of polymers that must be taken into account in material selection.

4.2 Introduction

Two-phase partitioning bioreactor (TPPB) technology can improve the efficiency and product titres of bioconversion processes by reducing substrate and/or product concentrations below cytotoxic levels.[1–3] TPPBs have led to process improvements in systems ranging from alcohol/organic acid fermentation[4–10] to the biodegradation of more hydrophobic xenobiotics.[11–15] This is accomplished by solute absorption into a non-aqueous phase (NAP) that provides a combination of high solute affinity and good biocompatibility. High molecular weight elastomers and semi-crystalline thermoplastics have recently been studied as alternatives to immiscible organic solvents and oligomeric liquids such as polypropylene glycol and silicone oil.[2] These materials offer advantages such as ease of handling, low cost, simple recovery from bioreactor media, and improved biocompatibility.[16] We have also previously described limitations of solid polymers, namely, their lower inherent diffusivities[17] and potential for negative hydrodynamic effects.[18] We have now concluded that differences in the absorptive[19–21] properties of rubbery, glassy and crystalline domains within solid polymers requires a retooling of previous liquid NAP selection approaches.[22]

Selecting a polymer for a TPPB process requires consideration of many of the same factors important in other separation processes such as pervaporation, perstraction and vapour permeation,[23–25] as well as food packaging applications[26,27] and protective clothing design.[28] These aspects include: 1) polymer-solute thermodynamic affinity, 2) degree of crystallinity (w_c) and 3) polymer glass transition temperature (T_g).[29,30] In the case of TPPBs, these considerations will determine the *rate* and *extent* to which a toxic solute will be absorbed/sequestered in the polymer phase, thereby reducing its inhibitory effects. A common quantitative measure to describe the absorption capacity of a polymer is the partition coefficient (*PC*), defined as the equilibrium concentration of a solute in the polymer phase divided by that in the aqueous phase.

As such, estimating the *PC* provided by a polymer for the target solute is central to TPPB development.[29,31]

Our recent study[30] of polymer-solute thermodynamics found that UNIFAC-vdW-FV and Flory-Huggins based models were able to predict the equilibrium absorption (*PC*) of solutes into a single amorphous material, poly(*n*-butyl acrylate). One purpose of the present study was to examine the ability of these same thermodynamic models to describe the sequestration of *n*-butyric acid (recently produced in a TPPB system[32]) into a broad range of amorphous materials that were screened from a standard polymer solubility database.[33] The bioproduction of *n*-butyric acid is an attractive alternative to current petrochemical processes to supply food, fragrance, pharmaceutical and chemical industries.[34–36] However, the accumulation of *n*-butyric acid results in low product titres and lost productivity,[9,37] and therefore a TPPB system may have practical utility.[38] The present work extends previous binary (solute+polymer) *PC* prediction methods[30] by incorporating experimental water sorption data, enabling ternary polymer phase activity predictions (water+*n*-butyric acid+polymer). In the biological production of *n*-butyric acid, as in all fermentation processes, water is an inevitable component, making this approach a necessary step towards more realistically representing an actual biological process.

In addition, practical limitations related to semi-crystalline polymers, whose crystalline domains are generally non-absorptive,[29,39,40] were experimentally quantified in this work. In particular, the challenges in determining and applying measurements of the degree of crystallinity (w_c) in *PC* predictions were examined through studies of *n*-butyric acid sorption into seven semi-crystalline polymers. In a related aspect, the ability of water and/or solute to affect the polymer's melting temperature (T_m) and degree of crystallinity were quantified with respect to the material's overall ability to sequester the toxic target molecule.

A third aspect when selecting a polymeric absorptive phase is the material's glass transition temperature (T_g). The difference between a bioreactor's operating temperature and the polymer's T_g can provide a general indication of a material's diffusivity for a target solute molecule.[41] In the production of biomolecules in TPPBs, solute uptake must be fast enough to prevent the accumulation of toxic metabolites, making materials with low T_gs particularly attractive.[29] This work therefore also included a study of water and *n*-octanol absorption into poly(vinyl acetate) (PVAc), a polymer selected for its T_g (45.7^{o}C) being near to typical fermentation temperatures. The abundance of log $K_{o/w}$ values in literature combined with *n*-octanol's low polarity, strong affinity for PVAc and large molecular size (compared to water) made it an ideal model compound. Partitioning experiments were conducted at two temperatures, above and below the material's as-received T_g (30^{o}C and 60^{o}C), to quantify the ability of water and *n*-octanol to reduce T_g by plasticization and by extension, their impact on diffusivity.

In all, this paper describes both the theory and implementation of three important criteria that need to be considered when selecting a polymer for toxic solute removal in TPPBs. These results enable a more efficient and focused approach to selecting effective absorptive polymers, while expanding upon previous studies by considering semi-crystalline materials and polymers that absorb water. These considerations are of particular importance for more hydrophilic biomolecules, such as organic acids and alcohols, due to their affinity for more polar polymers. Finally, in addition to polymer screening based exclusively on the extent of solute absorption (*PC*), the rate of absorption is considered with respect to a material's T_g and its proximity to a bioreactor's operating temperature.

4.3 Materials and methods

4.3.1 Materials and material preparation

All chemicals (purity ≥ 99%) were purchased from either Sigma-Aldrich (Canada) or Fisher Scientific (Canada). All polymers were purchased from Scientific Polymer Products (Ontario, NY).

For *n*-butyric acid partitioning tests, polymers were used as-received with the exception of poly(methyl acrylate), poly(ethyl acrylate), poly(*n*-propyl acrylate) and poly(*n*-butyl acrylate), which were isolated from toluene solution by solvent evaporation at room temperature for 48 h followed by 48 h at 60^{o}C.

Prior to T_g depression studies, poly(vinyl acetate) (PVAc) beads with a nominal molecular weight of 350 kg/mol and bead diameter of ~0.2 to 1.0 mm were gently heated in an aluminum pan and formed into a fused mass using a spatula. The fused polymer was cooled to room temperature and ground using a rotary mill. Two stainless steel wire mesh sieves with clear openings of 0.980 mm and 1.524 mm were utilized to normalize the PVAc particle size, and ensure a consistent diffusional path length between studies.

4.3.2 Differential scanning calorimetry

4.3.2.1 Glass transition temperature (T_g)

Determination of glass transition temperature was performed using a DSC Q 100 by TA Instruments. Shortly after the partition tests were initiated (< 12 h), the PVAc particles conjoined to form a flattened fused mass. DSC samples were prepared by cutting the polymer in quarters and removing the sample from the centre of the fused mass. Samples were scanned between -40 and 80^{o}C at a heating rate of 10^{o}C/min under a nitrogen purge. The midpoint T_g was determined according to ASTM Test Method D7426−08 using TA Universal Analysis software.

4.3.2.2 Melting temperature (T_m) and crystalline weight fraction (w_c)

Melting temperature (T_m) and crystalline weight fraction (w_c) were determined with a DSC Q 100 by TA Instruments operating between -85°C and 85°C at a heating rate of 10°C/min under a nitrogen purge. For poly(ethylene succinate) (T_m=102°C), the upper temperature limit was 300°C. The melting endotherm recorded upon the sample's first heating was integrated using TA Universal Analysis software and divided by the standard enthalpy of fusion (ΔH_f°) to calculate the weight fraction of the crystalline domain (w_c).

First heating scans were chosen to represent w_c and T_m, as this represents polymer samples as-received, which were subjected to partitioning tests with no further handling. For polymers for which the DSC melting endotherm spanned the operating temperature (T=30°C), only the crystalline fraction that existed > 30°C was considered. To determine the impact of water or a *n*-butyric acid solution (20 g/L) on polymer crystallinity and melting temperature, polymer samples were soaked at 30°C in an Innova 4400 incubator shaker at 180 rpm for seven days and tested alongside dry polymer samples as-received from the supplier. Poly(tetramethylene glycol) (PTMG) (2.9 kg/mol) samples were also tested at 10 and 30 g/L *n*-butyric acid to further investigate the atypical behaviour of this system.

4.3.3 Water uptake

Water absorption experiments were conducted on polymer samples equilibrated for a minimum of 48h in Type I ultrapure water at 30°C. Water soaked samples (8-15 mg) were pat dry to remove surface water and immediately heated in a TA Instruments Q500 thermogravimetric analyzer from ~25°C to 200°C (10°C/min). The samples were held at 200°C (octanol bp 195°C; butanol bp 118°C) until the rate of mass loss dropped below 0.05 wt%/min. An 11.4% average standard deviation on water absorption values was estimated from duplicate runs performed for five polymers (amorphous and semi-crystalline).

4.3.4 Experimental partition coefficients (PC_{expt})

Partition coefficient tests were performed in triplicate using three polymer masses, ranging from 0.25 to 1.5 g of dry mass. Each target molecule was prepared in separate aqueous solutions (0.4 g/L *n*-octanol or 20 g/L *n*-butyric acid) using Type I ultrapure water. In addition to the polymer mass, 10-20 mL aliquots of aqueous solution were added to each scintillation vial, sealed tightly with a foil lined cap and allowed to equilibrate in an Innova 4400 incubator shaker at 30°C or 60°C at 180 rpm.

Aqueous *n*-butyric acid concentrations before and after equilibrating for 7 days were measured by HPLC using a Varian Hi-Plex H column (300 × 7.7 mm) at 60°C with a 10 mM H_2SO_4 mobile phase at 0.7 mL/min, and a UV-Vis detector (Varian Prostar, PS325) at 220 nm. *n*-Octanol concentrations were measured using a Varian 450-GC gas chromatography unit equipped with a CP-8410 AutoInjector, VF-5ms 30m capillary column and FID detector. In T_g depression trials, control solutions (without polymer) were taken at every other time point. Aqueous *n*-butyric acid concentrations had a standard deviation of 1.4% (n=3) while *n*-octanol concentrations had a standard deviation of 6.7% (n=3).

A mass balance was performed to determine the solute concentration in the polymer. Swelling of the polymer by water and the simultaneous decrease in aqueous phase volume was accounted for using experimental water uptake data. Experimental *PC* values were calculated using aqueous and polymer phase weight fractions, w_i^{aq} and w_i^{poly}, in Equation 25. Standard deviation (n=3) values were calculated from triplicate samples to establish a mean value for the equilibrium *PC*.

$$\boldsymbol{PC} = \frac{\boldsymbol{w_i^{poly}}}{\boldsymbol{w_i^{aq}}} \tag{25}$$

In the case of T_g depression trials, where systems are not in a state of equilibrium, the ratio of solute concentrations in the polymer and aqueous phase (n=1) as a function of time, $PC^*(t)$, can be defined as follows

$$PC^*(t) = \frac{w_i^{poly^*}(t)}{w_i^{aq^*}(t)} \tag{26}$$

4.3.5 Partition coefficient predictions (PC_{pred})

Partition coefficients (*PC*) can be predicted for systems only at thermodynamic equilibrium, for which the *PC* has be defined as[30]

$$\boldsymbol{PC} = \frac{\boldsymbol{w_i^{poly}}}{\boldsymbol{w_i^{aq}}} = \frac{\boldsymbol{\Omega_i^{aq}}}{\boldsymbol{\Omega_i^{poly}}} \tag{27}$$

In this study, the non-random two liquid (NRTL) model[42] was selected to estimate aqueous phase activity coefficients (Ω_i^{aq}) at experimental conditions using parameters provided by the Dortmund Data Bank. As described in our previous work,[30] polymer phase activity coefficients (Ω_i^{poly}) were predicted using the Flory-Huggins solution theory[43] in conjunction with Hildebrand solubility parameters (FH-Hildebrand),[44] Hansen solubility parameters (FH-HSP)[45] or using UNIFAC-vdW-FV.[46] Water absorption was accounted for in the UNIFAC-vdW-FV model by setting the polymer phase water weight fraction to the value determined from experimental data. The adjustable parameters in the FH-HSP model was set to α=1 and for FH-Hildebrand β=0.34.[30,44]

The utility of these models is dependent on the accuracy of the inputs entered into the model, namely the polymer's density, molecular weight, solubility parameters (FH-Hildebrand and FH-

HSP) and functional groups (UNIFAC-vdW-FV). Amorphous polymer densities (where available) were sourced from Brandrup et al..[47] Where amorphous phase density values were not available, the group contribution method outlined by van Krevelen and te Nijenhuis[48] was used. Nominal molecular weights were provided by the supplier. Solubility parameters were sourced from the database provided in the HSPiP v.4.0.04 computer program.[33]

4.4 Results and Discussion

4.4.1 Thermodynamic affinity

Polymer candidates for the sequestration of *n*-butyric acid were screened using the FH-HSP method applied to a database of 650 polymers,[33] of which eight amorphous polymers were tested for their experimental partition coefficients (PC_{expt}). The data listed in Table 7 show values ranging from 1.4 to 2.6, with more hydrophilic polymers generally yielding higher *PC*s. Note that all three activity coefficient models, FH-Hildebrand, FH-HSP and UNIFAC-vdW-FV, predicted *n*-butyric acid's activity coefficient satisfactorily in each case. When combined with aqueous phase activity coefficient estimates generated with the NRTL model, the average absolute deviation (AAD%) between predicted *PC* estimates and experimental PC_{expt} data was 16.5% for FH-Hildebrand, 31.4% for FH-HSP, and 53.5% for UNIFAC-vdW-FV. Moreover, all three models correctly identified poly(*n*-hydroxybutyl methacrylate), poly(hydroxyethyl methacrylate) and poly(*n*-hydroxypropyl methacrylate) as the top-three performing polymers in terms of butyric acid absorption (*PC*).

Several polymers that exhibit a strong affinity for *n*-butyric acid also absorb water (Table 7). In theory, consideration of water absorption in *PC* predictions provides a more rigorous analysis of the polymer phase solute activity. In this respect, UNIFAC-vdW-FV is advantageous over Flory-Huggins models as it can predict activity in ternary (polymer+*n*-butyric acid+water) and higher

phase systems. However, although remaining qualitatively correct, refining the UNIFAC-vdW-FV model by including water absorption data resulted in a distinct reduction in predictive accuracy (AAD=343%), particularly for polymers with high water uptake (Table 7). Decreased prediction accuracy at higher water concentrations may be indicative of UNIFAC-vdW-FV's inability to account for the formation of polymer-bound and un-bound states of water.[49,50]

Table 7 - Experimental (PC_{expt}) and predicted (PC_{pred}) partition coefficient values for *n*-butyric acid with various amorphous polymers. Partition coefficient values were obtained at 30°C using an initial aqueous concentration of 20 g/L. Experimental errors shown are +/- one standard deviation.

					FH-Hildebrand		**FH-HSP**		**UNIFAC-vdW-FV**		**UNIFAC-vdW-FV (with H_2O)**	
Polymer	**MW**[a] (kg/ mol)	**Water uptake (wt%)**	**Water uptake** UNIFAC-vdW-FV **(wt%)**	***PC*$_{expt}$**	PC_{pred}	Rank	PC_{pred}	Rank	PC_{pred}	Rank	PC_{pred}	Rank
Poly(*n*-hydroxybutyl methacrylate)	100	31.0 ± 3.5	12.8	2.6 ± 0.2	2.5	1	3.1	2	4.7	1	14.2	1
Poly(hydroxyethyl methacrylate)	20	38.5 ± 4.4	22.8	2.3 ± 0.4	2.2	3	3.1	3	4.5	3	13.4	3
Poly(*n*-hydroxypropyl methacrylate)	400	32.0 ± 3.6	17.2	2.3 ± 0.4	2.5	2	3.2	1	4.7	2	13.5	2
Poly(ethyl acrylate)	100	4.9 ± 0.6	2.3	1.8 ± 0.3	2.0	6	2.1	5	1.9	5	5.4	6
Poly(*n*-propyl acrylate)	140	2.1 ± 0.2	0.9	1.7 ± 0.4	1.8	8	1.8	8	1.3	8	2.5	7
Poly(*n*-butyl acrylate)	100	1.0 ± 0.1	0.9	1.5 ± 0.3	1.9	7	1.9	7	1.5	7	2.1	8
Poly(methyl acrylate)	40	14.5 ± 1.6	3.1	1.4 ± 0.5	2.1	5	2.1	6	1.5	6	9.7	4
Poly(vinyl propionate)	30	4.4 ± 0.5	2.7	1.4 ± 0.3	2.2	4	2.3	4	2.2	4	5.6	5

[a] nominal values provided by supplier

4.4.2 Degree of crystallinity

Experimental *PC* values for semi-crystalline polymers can be expressed as a function of the amorphous partition coefficient (PC_{am}) and the crystalline phase fraction (w_c). Equation 28 is based on the well documented observation that intact crystallites in semi-crystalline materials are non-absorptive.[29,39,40]

$$PC_{expt} = PC_{am}(1 - w_c) \tag{28}$$

We have shown that PC_{am} can be estimated with a reasonably good degree of accuracy using activity coefficient models (PC_{pred}) (see Table 7). However, the degree of crystallinity (w_c), is dependent on a material's thermal history and, as such, it cannot be predicted accurately. It should also be noted that w_c values reported in the literature are generally measured for an as-received dry polymer, and may not reflect the material once exposed to an aqueous fermentation medium. Table 8 provides melting point (T_m) and w_c data for a range of semi-crystalline materials in their as-received states, as well as after soaking in water and a 2 wt% butyric acid solution. In most cases, neither water nor solute changed these properties. However, poly(tetramethylene glycol) (PTMG) proved to be highly sensitive to the presence of *n*-butyric acid, as w_c declined from 0.55 for the dry polymer to 0.38 for the acid-soaked sample. This loss of crystallinity within PTMG is illustrated in Figure 10, which shows the transition from a semi-crystalline solid to viscoelastic polymer melt upon immersion in an aqueous *n*-butyric acid solution. The polymer melt's increasingly liquid-like behaviour and increased tackiness as w_c is reduced could cause operational challenges in a TPPB, including more difficult handling, separation and adsorption to internal bioreactor components.[16]

Table 8 - Effect of H_2O and 2 wt% *n*-butyric acid solution on the crystalline weight fraction (w_c) and melting temperature (T_m) for various semi-crystalline polymers

Polymer	T_m (°C)			w_c		
	As-received	Water soaked	Acid soaked (2 wt%)	As-received	Water soaked	Acid soaked (2 wt%)
Poly(tetramethylene glycol)	47	45	42	0.55	0.50	0.38
Poly(ε-caprolactone)	69	67	64	0.73	0.73	0.70
Poly(butylene adipate)	61	59	60	0.62	0.62	0.62
Poly(trimethylene adipate)	40	45	44	0.40	0.44	0.40
Poly(ethylene adipate)	54	53	50	0.58	0.61	0.61
Poly(trimethylene succinate)	52	47	47	0.27	0.30	0.32
Poly(ethylene succinate)	102	101	97	0.42	0.41	0.44

Figure 10 - PTMG (2.9 kg/mol) as-received (left) and after soaking in pure water (centre) and in a *n*-butyric acid solution (2 wt%) (right)

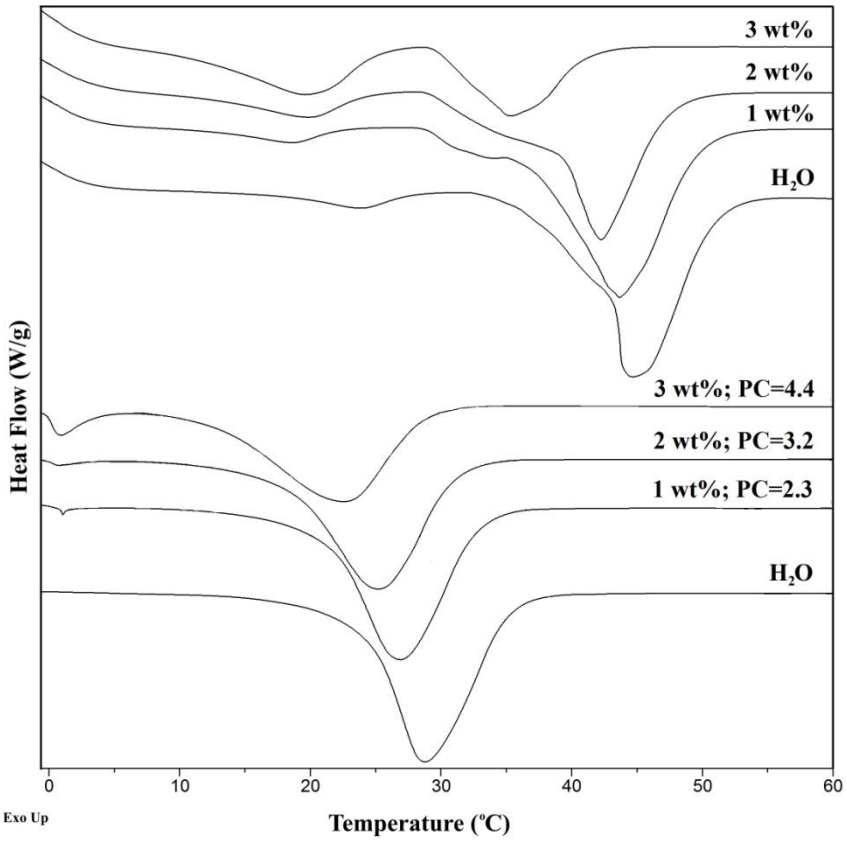

Figure 11 - First (top) and second (bottom) DSC heating scans of poly(tetramethylene glycol) (2.9 kg/mol) for samples after equilibration with pure water and aqueous *n*-butyric acid solutions with initial concentrations of 1 wt%, 2 wt% and 3 wt%. Melting temperature (T_m) values were derived from first heating scans.

Nevertheless, the loss of mechanical integrity as crystallinity is lowered is counteracted by the resultant increase in the amount of absorptive amorphous material. To demonstrate this, the unusual behavior of the PTMG+*n*-butyric acid system was further investigated by measuring *PC*, T_m and w_c for polymer exposed to a range of acid concentrations (Figure 11 and Table 9). Although soaking PTMG in 1 wt% *n*-butyric acid had no measurable impact on crystallinity, a 3 wt% solution reduced w_c to just 0.12. In addition, increasing the *n*-butyric acid concentration from 1 to 3 wt% increased PC_{expt} from 2.3 ± 0.2 to 4.4 ± 0.2 (Table 9), indicating an increase in the polymer's capacity to remove the acid. The observed relationship between *PC* and crystallinity is consistent with Equation 28, in that the correction of PC_{expt} for the degree of crystallinity

(using w_c found at each concentration: 1 wt%, 2 wt%, 3 wt%) yields the same amorphous phase partition coefficient (PC_{am} = 5.1 ± 0.1).

Table 9 - PTMG's crystalline weight fraction (w_c), melting temperature (T_m) and experimental (bulk polymer) partition coefficient (PC_{expt}) and corrected amorphous phase partition coefficient (PC_{am}) after equilibration with *n*-butyric acid at varying initial aqueous concentrations.

	w_c	T_m (°C)	PC_{expt}	PC_{am}
Dry (as-received)	0.55	47	-	-
Water soaked (100 wt%)	0.50	45	-	-
n-Butyric acid soaked (1 wt%)	0.56	44	2.3 ± 0.2	5.2 ± 0.5
n-Butyric acid soaked (2 wt%)	0.38	42	3.2 ± 0.2	5.2 ± 0.3
n-Butyric acid soaked (3 wt%)	0.12	35	4.4 ± 0.2	5.0 ± 0.2

From a material selection standpoint, lower crystallinity maximizes the absorptive amorphous phase and improves solute uptake. Table 10 further highlights the deleterious effect of crystallinity on *PC*, shown as the difference between PC_{am} (100% amorphous material) and PC_{expt} (semi-crystalline material). Table 10 also demonstrates the challenge in predicting the performance of semi-crystalline polymers, indicated by the generally poor agreement between predicted partition coefficients (PC_{pred}) and experimental measurements (PC_{am}). The amorphous phase activity coefficients are consistently over-predicted when water was not considered, with AAD% values of FH-Hildebrand (49%), FH-HSP (51%) and UNIFAC-vdW-FV (51%). In contrast, incorporating equilibrium water swelling data into UNIFAC-vdW-FV(H_2O) improved *PC* predictions to an AAD of 30%. In conjunction with *PC* predictions for amorphous polymers (Table 7), the results in Table 10 demonstrate the system-dependence of model accuracy and the benefits of employing a broad range of predictive tools for effective polymer identification.

Finally, uncertainty in w_c values undoubtedly contribute to errors in *PC* prediction, given the difficulty in integrating broad DSC melting endotherms, as well as variations in the morphology and quality of polymer

crystallites from those used to generate literature values for the heat of fusion. We conclude that the selection of semi-crystalline materials for TPPB applications is more qualitative than the selection of amorphous polymers, and more of an exercise in identifying promising candidates (by rank) than in predicting *PC* values accurately.

Table 10 - Experimental (PC_{expt}), corrected amorphous phase (PC_{am}) and predicted (PC_{pred}) partition coefficient values for *n*-butyric acid with various semi-crystalline polymers. Partition coefficient values were obtained at 30°C using an initial aqueous concentration of 20 g/L. Experimental errors shown are +/- one standard deviation.

Polymer	**MW[a] (kg/ mol)**	**Water uptake (wt%)**	**Water uptake** UNIFAC-vdW-FV **(wt%)**	***PC*$_{expt}$**	***PC*$_{am}$**	**FH-Hildebrand**		**FH-HSP**		**UNIFAC-vdW-FV**		**UNIFAC-vdW-FV (with H_2O)**	
						PC_{pred}	Rank	PC_{pred}	Rank	PC_{pred}	Rank	PC_{pred}	Rank
Poly(tetramethylene glycol)	2.9	4.9 ± 0.6	9.6	3.2 ± 0.2	5.2 ± 0.3	1.7	7	1.6	7	2.9	1	6.7	1
Poly(ε-caprolactone)	55	0.9 ± 0.1	2.0	1.5 ± 0.2	5.0 ± 0.7	1.9	6	1.9	5	1.9	2	2.4	7
Poly(butylene adipate)	12	1.9 ± 0.2	3.5	1.8 ± 0.2	4.7 ± 0.5	2.0	5	1.9	6	1.8	3	2.9	5
Poly(trimethylene adipate)	3.8	2.5 ± 0.3	2.1	2.2 ± 0.4	3.7 ± 0.7	2.1	2	2.0	4	1.8	4	3.4	3
Poly(ethylene adipate)	10	3.4 ± 0.4	2.2	1.2 ± 0.2	3.0 ± 0.5	2.1	3	2.1	3	1.6	5	3.6	2
Poly(trimethylene succinate)	9.5	3.2 ± 0.4	2.9	1.8 ± 0.4	2.6 ± 0.6	2.2	1	2.2	1	1.6	6	3.4	4
Poly(ethylene succinate)	10	2.4 ± 0.3	3.7	1.0 ± 0.2	1.7 ± 0.4	2.1	4	2.2	2	1.4	7	2.5	6

[a] nominal values provided by supplier

4.4.3 Glass transition temperature (T_g)

For a polymeric NAP to be effective, it must absorb/desorb the solute fast enough to maintain the desired aqueous phase concentration during TPPB operation. This generally requires a T_g that is significantly lower than the TPPB operating temperature, since this difference correlates strongly with polymer segment mobility, solute diffusivity[41] and absorption rate.[29] Poly(vinyl acetate) (PVAc) has a reported T_g of 46^{o}C and, as such, is expected to exist in a non-absorptive glassy state when used at 30°C, and an absorptive rubbery state when immersed in an aqueous *n*-octanol solution at 60°C. However, the data plotted Figure 12 show that PVAc exhibits good thermodynamic affinity for *n*-octanol at both test temperatures, with instantaneous partition coefficients ($PC^*(t)$) evolving to high equilibrium *PC* values, albeit at significantly different rates.

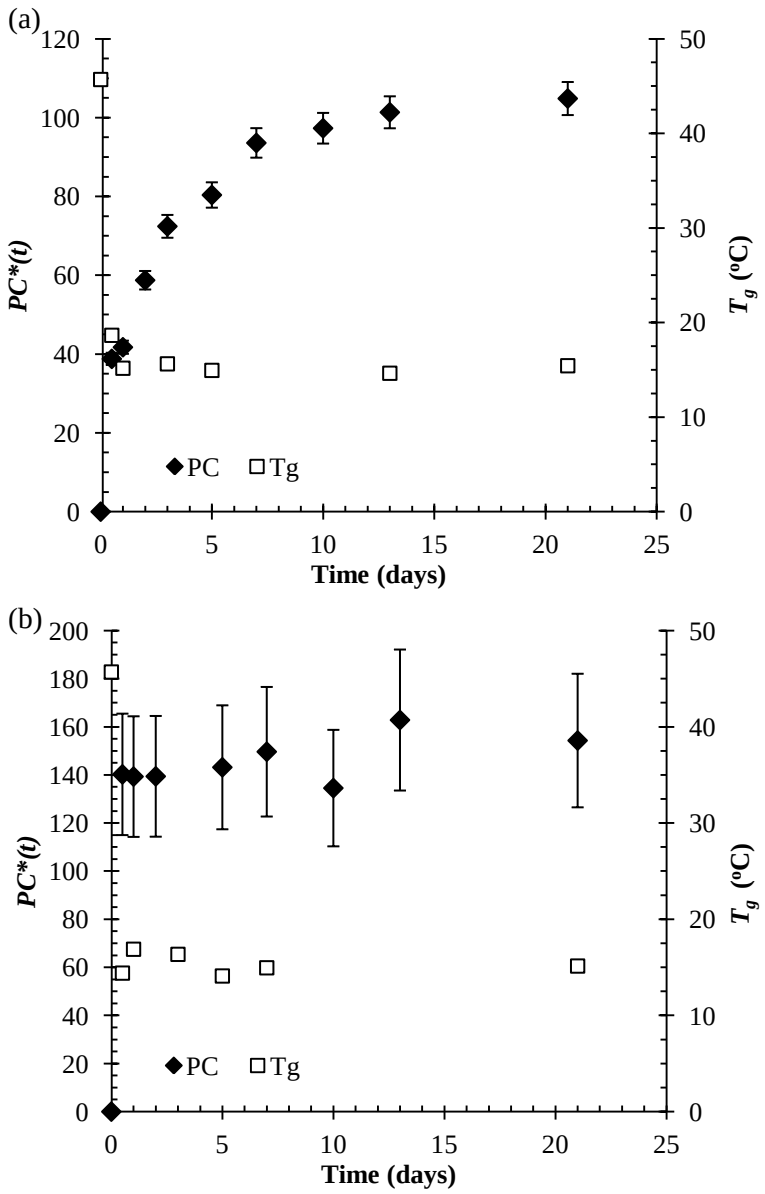

Figure 12 - Instantaneous T_g and *n*-octanol partition coefficient for PVAc (M_w≈350 kg/mol) at (a) 30°C and (b) 60°C.

Figure 12 also reports the T_g of the polymer phase as a function of time, revealing a rapid decline in glass transition temperature from 46°C in a dry sample to about 15°C upon immersion in an *n*-octanol solution. This T_g reduction accounts for the absorption observed at the 30°C test condition, but it is the speed of this decline at both 30°C and 60°C that is particularly interesting. Whereas *n*-octanol absorption rates were highly temperature dependent, polymer plasticization

was rapid in both experiments. The data listed in Table 11 confirm that plasticization results from a rapid uptake of a small amount of water, which in turn facilitates *n*-octanol absorption by improving polymer chain mobility. The high diffusivity of water has been noted for several polymers of relevance to aqueous-organic separations,[29,49,51–55] and the observed influence of penetrant size and shape on *n*-octanol uptake by PVAc is consistent with reports on several other polymer-solute systems.[56–58]

Table 11 - Plasticization of PVAc by water and *n*-octanol

	T_g (°C)[a]		
	PVAc (15 kg/mol)	**PVAc (100 kg/mol)**	**PVAc (350 kg/mol)**
As-received	33	49	46
***n*-Octanol**	37	51	52
Water	9	18	18
0.4 g *n*-Octanol/L	10	16	15

[a] 3 weeks immersion at 30°C

In the context of TPPB design, plasticization by water and/or solute can significantly improve absorption/desorption dynamics, allowing polymers with T_gs slightly above the bioprocess temperature to function effectively. In all cases, a large difference between the operating temperature and the *in situ* polymer phase T_g is advantageous, such that $T>>T_g$. In the PVAc/*n*-octanol system, operating 45°C above the plasticized glass transition temperature (T-T_g) (Figure 12-b) as opposed to T-T_g = 15°C (Figure 12-a) resulted in much faster solute equilibration, as well as a higher overall partition coefficient. However, when increasing a bioreactor's operating temperature is not technically feasible, polymers with low T_gs should be preferentially selected for their likelihood to achieve more rapid solute uptake.

4.5 Conclusions

Thermodynamic affinity, degree of crystallinity (w_c) and glass transition temperature (T_g) determine the suitability of a polymer as a non-aqueous phase (NAP) for a given TPPB application. We have shown that the thermodynamic affinity of amorphous polymers can be predicted with a good degree of accuracy using Flory-Huggins based models as well as UNIFAC-vdW-FV. However, challenges in quantifying crystallinity (w_c) under process operating conditions complicate similar analyses of semi-crystalline materials, and this makes prediction of solute affinity using the above thermodynamic methods less satisfactory. This is particularly true in situations in which water and/or solute depress T_m below the bioreactor operating temperature, rendering a semi-crystalline polymer amorphous. It should be noted that under such conditions, the polymer's amorphous phase fraction is increased, leading to higher overall *PC* values and a greater capacity to remove the toxic biomolecule.

UNIFAC-vdW-FV predictions were also highly sensitive to water uptake, however, accuracy improvements were largely system dependent. In this work, it was found that consideration of water uptake improved *PC* predictions for semi-crystalline materials but reduced predictive accuracy for amorphous polymers. Finally, interactions between the polymer and water and/or solute can greatly enhance absorption rates through polymer plasticization, and these effects should be considered where bioreactor operating temperatures are close to tabulated T_g values for dry, as-received polymer. However, in applications requiring very rapid absorption/desorption of target molecules, polymers with $T_g << T$ hold the most promise as they generally facilitate faster solute uptake. Overall, this work has contributed to establishing first-principles strategies for polymer selection in TPPB applications by evaluating the impact of several common polymer features and their effect on the extent and rate of solute uptake.

4.6 Acknowledgements

We gratefully acknowledge the financial support of DuPont Canada and the Natural Sciences and Engineering Research Council of Canada.

4.7 References

1 J. J. Malinowski, *Biotechnol. Adv.*, 2001, **19**, 525–38.

2 G. Quijano, M. Hernandez, F. Thalasso, R. Muñoz and S. Villaverde, *Appl. Microbiol. Biotechnol.*, 2009, **84**, 829–46.

3 C. S. López-Garzón and A. J. J. Straathof, *Biotechnol. Adv.*, 2014, **32**, 873–904.

4 A. J. Daugulis, D. E. Swaine, F. Kollerup and C. A. Groom, *Biotechnol. Lett.*, 1987, **9**, 425–430.

5 W. E. Barton and A. J. Daugulis, *Appl. Microbiol. Biotechnol.*, 1991, **36**, 632–639.

6 S. R. Roffler, J. Boudrant and C. R. Wilke, *Bioprocess Eng.*, 1987, **2**, 1–12.

7 S. Ishii, M. Taya and T. Kobayashi, *J. Chem. Eng. Japan*, 1985, **18**, 125–130.

8 M. Minier and G. Goma, *Biotechnol. Bioeng.*, 1982, **24**, 1565–1579.

9 Z. Wu and S.-T. Yang, *Biotechnol. Bioeng.*, 2003, **82**, 93–102.

10 P. J. Evans and H. Y. Wang, *Appl. Microbiol. Biotechnol.*, 1990, **32**, 393–397.

11 R. Muñoz, S. Arriaga, S. Hernández, B. Guieysse and S. Revah, *Process Biochem.*, 2006, **41**, 1614–1619.

12 A. Kohler, M. Schuttoff, D. Bryniok and H.-J. Knackmub, *Biodegradation*, 1994, **5**, 93–103.

13 J. Marcoux, E. Déziel, R. Villemur, F. Lépine, J. G. Bisaillon and R. Beaudet, *J. Appl. Microbiol.*, 2000, **88**, 655–662.

14 R. Villemur, E. Déziel, A. Benachenhou, J. Marcoux, E. Gauthier, F. Lépine, R. Beaudet and Y. Comeau, *Biotechnol. Prog.*, 2000, **16**, 966–972.

15 R. Muñoz, A. J. Daugulis, M. Hernández and G. Quijano, *Biotechnol. Adv.*, 2012, **30**, 1707–1720.

16 B. G. Amsden, J. Bochanysz and A. J. Daugulis, *Biotechnol. Bioeng.*, 2003, **84**, 399–405.

17 H. Fam and A. J. Daugulis, *Bioprocess Biosyst. Eng.*, 2012, **35**, 1367–74.

18 N. Boudreau and A. Daugulis, *Biotechnol. Bioeng.*, 2006, **94**, 607–615.

19 J. G. Wijmans and R. W. Baker, *J. Memb. Sci.*, 1995, **107**, 1–21.

20 R. Baker, *Controlled release of biologically active agents*, John Wiley & Sons, Ltd, New

York, 1987.

21 T. Craig and A. J. Daugulis, *Biotechnol. Bioeng.*, 2013, **110**, 1098–1105.

22 F. Kollerup and A. J. Daugulis, *Can. J. Chem. Eng.*, 1985, **63**, 919–927.

23 L. M. Vane, *J. Chem. Technol. Biotechnol.*, 2005, **80**, 603–629.

24 P. Peng, B. Shi and Y. Lan, *Sep. Sci. Technol.*, 2010, **46**, 234–246.

25 N. Qureshi and H. P. Blaschek, *Biomass and Bioenergy*, 1999, **17**, 175–184.

26 J. B. Konczal, B. R. Harte, P. Hoojjat and J. R. Giacin, *J. Food Sci.*, 1992, **57**, 967–970.

27 O. Vitrac and M. Hayert, *Ind. Eng. Chem. Res.*, 2006, **45**, 7941–7956.

28 K.-P. Chao, Y.-P. Hsu and S.-Y. Chen, *J. Hazard. Mater.*, 2008, **153**, 1059–66.

29 J. S. Parent, M. Capela, J. T. Dafoe and A. J. Daugulis, *J. Chem. Technol. Biotechnol.*, 2012, **87**, 1059–1065.

30 S. L. Bacon, J. Scott Parent and A. J. Daugulis, *J. Chem. Technol. Biotechnol.*, 2014, **89**, 948–956.

31 S. Tanaka, Y. Tashiro, G. Kobayashi, T. Ikegami, H. Negishi and K. Sakaki, *Bioresour. Technol.*, 2012, **116**, 448–52.

32 E. C. Peterson and A. J. Daugulis, *Biotechnol. Bioeng.*, 2014, **111**, 537–44.

33 S. Abbott and H. Yamamoto, 2013.

34 J. Zigova and E. Sturdik, *J. Ind. Microbiol. Biotechnol.*, 2000, **24**, 153–160.

35 J. D. Dziedzak, *Food Technol.*, 1986, **40**, 8–20.

36 I. Dolejš, M. Rebroš and M. Rosenberg, *Chem. Pap.*, 2013, **68**, 1–14.

37 E. C. Peterson and A. J. Daugulis, *Biotechnol. Bioeng.*, 2014, **111**, 2183–2191.

38 A. S. Kertes and C. J. King, *Biotechnol. Bioeng.*, 1985, **28**, 269–282.

39 A. S. Michaels and H. J. Bixler, *J. Polym. Sci.*, 1961, **50**, 393–412.

40 R. M. Hodge, G. H. Edward and G. P. Simon, *Polymer (Guildf).*, 1996, **37**, 1371–1376.

41 W. R. Brown and G. S. Park, *J. Paint Technol.*, 1970, **42**, 16–25.

42 H. Renon and J. M. Prausnitz, *AIChE J.*, 1968, **14**, 135–144.

43 P. J. Flory, *Principles of Polymer Chemistry*, Cornell University Press, New York, 1953.

44 C. M. Hansen, *Hansen Solubility Parameters: A User's Handbook*, Taylor & Francis Group, Boca Raton, FL, 2nd edn., 2007.

45 T. Lindvig, M. L. Michelsen and G. M. Kontogeorgis, *Fluid Phase Equilib.*, 2002, **203**, 247–260.

46 D. C. Kannan, J. L. Duda and R. P. Danner, *Fluid Phase Equilib.*, 2005, **228**–**229**, 321–328.

47 J. Brandrup, E. H. Immergut and E. A. Grulke, *Polymer Handbook*, John Wiley & Sons,

Ltd, New York, 4th edn., 1999.

48 D. van Krevelen and K. te Nijenhuis, *Properties of Polymers*, Elsevier, Amsterdam, 4th edn., 2009.

49 Z. H. Ping, Q. T. Nguyen, S. M. Chen, J. Q. Zhou and Y. D. Ding, *Polymer (Guildf).*, 2001, **42**, 8461–8467.

50 A. Du, D. Koo, G. Theryo, M. A. Hillmyer and R. A. Cairncross, *J. Memb. Sci.*, 2012, **396**, 50–56.

51 P. Blasi, S. S. D'Souza, F. Selmin and P. P. DeLuca, *J. Control. Release*, 2005, **108**, 1–9.

52 C. M. Bell, F. J. Gerner and H. Strathmann, *J. Memb. Sci.*, 1988, **36**, 315–329.

53 B. Bolto, M. Hoang and Z. Xie, *Chem. Eng. Process. Process Intensif.*, 2011, **50**, 227–235.

54 S. P. Kusumocahyo, K. Sano, M. Sudoh and M. Kensaka, *Sep. Purif. Technol.*, 2000, **18**, 141–150.

55 H. Feng, *Polymer (Guildf).*, 2007, **48**, 2988–3002.

56 H. Fujita, A. Kishimoto and K. Matsumoto, *Trans. Faraday Soc.*, 1960, **56**, 424–437.

57 S. C. George and S. Thomas, *Prog. Polym. Sci.*, 2001, **26**, 985–1017.

58 H. Fujita, *Adv. Polym. Sci.*, 1961, **3**, 1–47.

Chapter 5

Isobutylene-rich imidazolium ionomers for use in two-phase partitioning bioreactors

With minor changes to fulfill formatting requirements, this chapter is substantially as it appears in:

S. L. Bacon, A. J. Daugulis and J. S. Parent, *Green Chem.*, 2016, **18**, 6586–6595.

5.1 Abstract

Imidazolium ionomer derivatives of an isobutylene-rich elastomer demonstrated superior absorption characteristics for target molecules of biological interest compared to their non-ionic parent material, while retaining biocompatibility with a range of suspended cell cultures. Halide displacement from brominated poly(isobutylene-co-paramethyl styrene) was used to introduce 0.23 mmol/g-polymer of imidazolium bromide functionality to the polymer, resulting in up to 10-fold improvements in n-octanol and n-butanol partition coefficients (PCs) and up to 4-fold improvements in selectivity (α). In contrast to analogous imidazolium ionic liquids (ILs) that were cytotoxic toward *Saccharomyces cerevisiae*, *Clostridium acetobutylicum* and *Pseudomonas putida*, the ionomers had no effect on suspended cell growth. In addition, these ionomers demonstrated surface antimicrobial activity towards select microorganisms under static conditions with direct surface/microbe contact. Thus, these materials do not affect suspended cell growth while simultaneously reducing cell proliferation at the ionomer interface.

5.2 Graphical Abstract

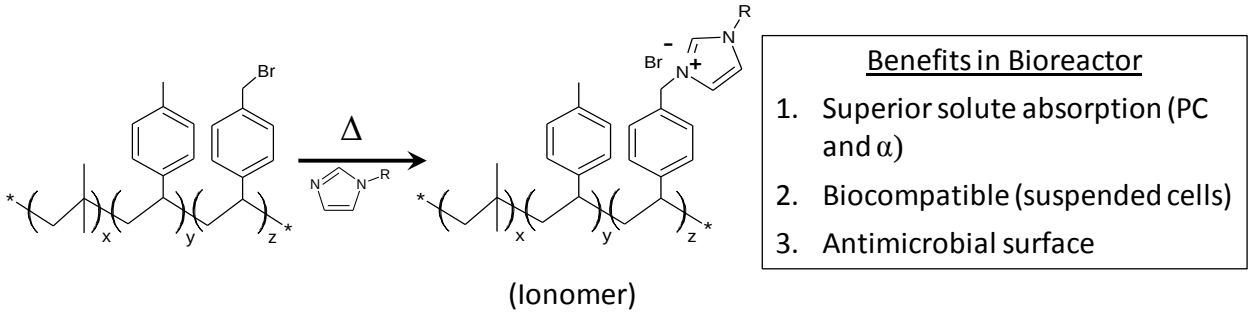

List of Abbreviations:

BIMS – Brominated poly(isobutylene-*co*-paramethylstyrene)

IMS-[BuIm][Br] – n-Butylimidazolium bromide derivative of BIMS

IMS-[HEIm][Br] – 2-Hydroxyethylimidazolium bromide derivative of BIMS

IMS-[BuIm][BF_4] – n-Butylimidazolium tetrafluoroborate derivative of BIMS

[C_{12}BuIm][Br] – 1-Dodecyl-3-butylimidazolium bromide

[C_{12}BuIm][BF_4] – 1-Dodecyl-3-butylimidazolium tetrafluoroborate

5.3 Introduction

Bioprocesses that are hindered by substrate and/or product cytotoxicity can be improved using two-phase partitioning bioreactor (TPPB) technology, which mitigates cell inhibition by sequestering toxic target molecule(s) into an immiscible second phase. TPPB configurations can be applied to the biodegradation of xenobiotics, where the polymer phase serves as a reservoir for delivering a cytotoxic substrate at sub-lethal concentrations, as well as extractive fermentation, where the polymer is used to remove a cytotoxic product from the fermentation medium as it is formed. For bioremediation applications TPPBs have been effectively exploited for the treatment of contaminated gas,[1] aqueous,[2] and soil[3] environments, as has been recently reviewed.[4] In biosynthesis applications, a recent review article has described TPPB advances over the past decade,[5] and another recent review[6] has evaluated the factors that are important in selecting an effective TPPB sequestering phase. Effective TPPB absorbents provide high solute affinity, as quantified by the partition coefficient (PC), and a strong preference for solute absorption versus water uptake, as quantified by selectivity ($\alpha_{i/w}=PC_{solute}/PC_{water}$). The latter is particularly important for extractive fermentation processes (notably for biofuels), whose cost effectiveness and energy requirements can be sensitive to the efficiency of solute recovery processes. Absorbent selection

and design must also include biocompatibility assessments to ensure that biocatalyst growth and metabolism is not adversely affected by the sequestering phase.

Viscoelastic polymers have emerged as promising TPPB materials, demonstrating favourable absorption characteristics, facile separation from the fermentation medium, and biocompatibility towards suspended cell cultures.[7–10] Furthermore, their solid-state physical properties offer operational advantages over low MW organic solvents and oligomeric liquids, which can present foaming, emulsification and volatility problems.[11–14] However, shifting focus from small molecule absorbing phases to polymeric absorbents requires consideration of crystallinity and glass transition temperature (T_g), since neither crystalline domains nor glassy phases are capable of solute uptake.[15,16] TPPB processes involving non-polar solutes (e.g. PAHs, BTEX, styrene) are relatively straightforward, since these target molecules are readily absorbed by non-polar polymers that have low T_g and little affinity for water. In contrast, hydrophilic solutes such as n-butanol require more polar polymers that can be glassy at bioprocessing temperatures, thereby limiting solute removal to surface adsorption.

Separation processes based on ionic liquids (IL)[17–20] have benefited greatly from the ability to adjust solute affinities by varying both cation and anion structure.[21–26] As such, their use in TPPBs has gained recent interest, however, their utility is often limited by microbe cytotoxicity.[27–31] We have found that isobutylene-rich elastomers bearing small amounts of covalently-bound IL functionality (ionomers) provide the absorption characteristics, physical properties and biocompatibility needed to support a broad spectrum of TPPB applications. These ionomers are easy to prepare via nucleophilic displacement of halide from brominated poly(isobutylene-*co*-paramethylstyrene) (BIMS)[32] to yield amorphous, rubbery derivatives comprised of a non-polar isobutylene-rich polymer matrix and aggregated ion-pairs known as multiplets.[33]

This report provides complex viscosity (η^*), PC, $\alpha_{i/w}$, biocompatibility, and surface antimicrobial data for BIMS-based ionomers with a range of cation (butylimidazolium, hydroxyethylimidazolium) and anion (Br^-, BF_4^-) structures (Table 12). Oscillatory rheology measurements of η^* are used to demonstrate differences in the physical properties of viscoelastic ionomers and viscous ILs. This is followed by comprehensive PC and α data for three solutes relevant to TPPBs (n-butanol, n-octanol and styrene) that explore differences in absorption for solutes of different hydrophobicity and types of molecular interaction. Absorbent biocompatibility in a well-mixed TPPB environment is assessed for industrially-relevant microorganisms (*Saccharomyces cerevisiae*, *Pseudomonas putida*, *Clostridium acetobutylicum*) before quantifying surface antimicrobial characteristics by measuring microorganism colony proliferation under prolonged, direct contact with the polymer. This material property is linked to biofilm formation and surface fouling and is pertinent to any material that is in sustained contact with microorganisms.[34–36]

Table 12 – Room temperature properties of ionomer and IL absorbents

Sample ID	Structure	Ion pair concentration (mmol/g)	Physical State	Complex viscosity η^* (Poise)	Equilibrium water absorption (wt%)
BIMS	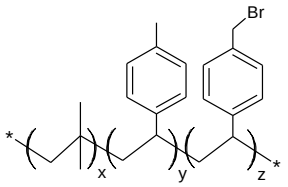	0	Viscoelastic solid	342,000	3.5 ± 1.8
IMS-[HEIm][Br]	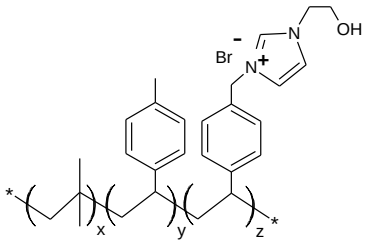	0.23	Viscoelastic solid	1,236,000	11.5 ± 2.2
IMS-[BuIm][Br]	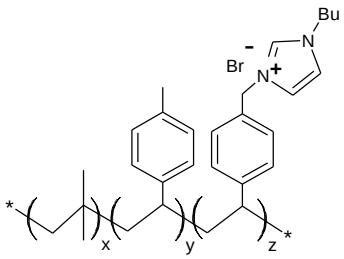	0.23	Viscoelastic solid	807,000	13.3 ± 2.8
IMS-[BuIm][BF_4]	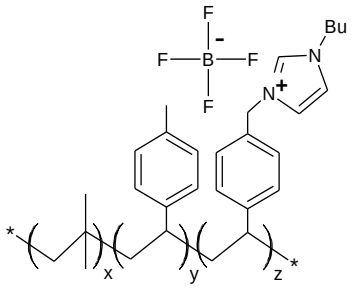	0.23	Viscoelastic solid	642,000	9.2 ± 0.6
[C_{12}BuIm][Br]	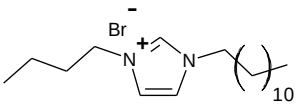	2.68	Viscous liquid	37.3	Water soluble
[C_{12}BuIm][BF_4]	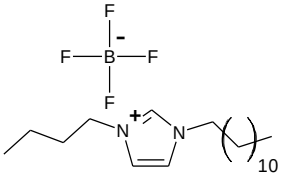	2.63	Viscous liquid	10.6	6.3 ± 0.3

5.4 Experimental

5.4.1 Materials

Butyl imidazole (98%), 1-bromododecane (97%), trifluoroethanol (99%), sodium tetrafluoroborate ($NaBF_4$) (98%), sodium sulfate (Na_2SO_4) (98%), styrene (99%) and n-octanol (99%) were purchased from Sigma-Aldrich (Canada). Methanol (99.8%) and n-butanol (99%) were purchased from Fischer Scientific (Canada). All chemicals were used as received. Brominated poly(isobutylene-*co*-paramethylstyrene) (BIMS) (EXXPRO 3745, 0.23 mmol benzylic bromide functionality/g BIMS) (M_n > 50,000 g/mol) was supplied by Exxon Mobil Chemical (Baytown, Texas) and purified prior to use by dissolving in THF and precipitating in excess acetone, followed by drying *in vacuo* at RT.

5.4.2 Synthesis of IMS-[BuIm][Br] and IMS-[HEIm][Br]

Ionomers were prepared as previously described with minor modifications.[37,38] BIMS (40 g, 9.2 mmol benzylic bromide) was dissolved in toluene (400 mL). Butyl imidazole (2.287 g, 2 eq.) or hydroxyethyl imidazole (2.063 g, 2 eq.) was added to the polymer cement and heated to 100°C under nitrogen for 7 h (IMS-[BuIm][Br]) or 16 h (IMS-[HEIm][Br]). Conversion was measured by ^{1}H-NMR integration of residual brominated paramethylstyrene mers: δ 4.49 (s, 2H), δ 4.45 (s, 2H). The product was recovered from precipitation in excess acetone, milled into thin sheets and dried *in vacuo* at 60°C. Conversion was monitored using the following diagnostic peaks: **IMS-[BuIm][Br]:** ^{1}H-NMR ($CDCl_3$ + 5 wt% CD_3OD): δ 9.99 (s, 1H, -N+-C**H**-N-), δ 5.43 (s, 2H, Ph-**CH_2**-N+-), δ 4.27 (t, 2H, -N-**CH_2**-CH_2-CH_2–CH_3). **IMS-[HEIm][Br]:** ^{1}H-NMR ($CDCl_3$ + 5 wt% CD_3OD): δ 9.55 (s, 1H, -N+-C**H**-N-), δ 5.36 (s, 2H, Ph-**CH_2**-N+-), δ 4.39 (t, 2H, -N-**CH_2**-CH_2-OH).

5.4.3 Synthesis of IMS-[BuIm][BF_4]

Ionomers were prepared as previously described with minor modifications.[37,38] IMS-[BuIm][Br] (40 g, 9.2 mmol bromide) was dissolved in toluene (600 mL). $NaBF_4$ (4.00 g, 36.8 mmol, 4 eq.) was dissolved in ultrapure water (100 mL) and added to the polymer cement. The mixture, which formed an emulsion upon agitation, was stirred for 8 h and then left to settle overnight forming an aqueous phase, a polymer rich phase and a toluene rich phase. The aqueous phase was removed by pipette, then fresh $NaBF_4$ brine was added (4.00 g $NaBF_4$ in 100 mL) and again stirred to emulsion for 8 hours. Removal and replenishment of the brine was repeated twice over until ion exchange was complete within experimental error. The emulsion was precipitated in excess acetone, milled into thin sheets and dried *in vacuo* at 60°C. Conversion was monitored using the following diagnostic peaks: **^{1}H-NMR** ($CDCl_3$ + 5 wt% CD_3OD): δ 9.03 (s, 1H, -N+-C**H**-N-), δ 5.31 (s, 2H, Ph-**CH_2**-N+-), δ 4.19 (t, 2H, -N-**CH_2**-CH_2-CH_2–CH_3). **^{19}F-NMR** ($CDCl_3$ + 5 wt% CD_3OD): δ -152.75 (s, 4F, ^{11}B**F_4**), δ -152.79 (s,4F, ^{10}B**F_4**). Ion exchange conversion was measured by ^{19}F-NMR integration of tetrafluoroborate peaks using a trifluoroethanol internal standard. Note that $^{10}BF_4$ and $^{11}BF_4$ are isotopomers that exist in a 4:1 ratio.

5.4.4 Synthesis of [C_{12}BuIm][Br]

Butyl imidazole (10 g, 80.5 mmol) and 1-bromododecane (24.9 g, 100 mmol, 1.25 eq.) were dissolved in ethyl acetate (25 mL) and stirred for 24 h at reflux under nitrogen. The solution was dried *in vacuo* at 50°C to yield the product, 1-dodecyl-3-butylimidazolium bromide ([C_{12}BuIm][Br]), as an orange oil. The product was washed several times with hexanes to remove residual 1-bromododecane, dried *in vacuo* at 50°C and characterized by ^{1}H-NMR. Yield: 87%. **^{1}H-NMR** ($(CD_3)_2SO$): δ – 9.25 (s, 1H, -N+-C**H**-N-), δ – 7.82 (d, 2H, -N-C**H**=C**H**-N^+-), δ – 4.17 (m, 4H, -N-C**H_2**-CH2-), δ – 1.78 (m, 4H, -N-CH_2-C**H_2**-), δ – 1.23 (m, 20H, -(C**H_2**)$_{10}$-CH_3), δ – 0.90 (t, 3H, -$(CH_2)_3$-C**H_3**), δ – 0.85 (t, 3H, -$(CH_2)_{11}$-C**H_3**)

5.4.5 Synthesis of $[C_{12}BuIm][BF_4]$

$NaBF_4$ (7.6 g, 69.6 mmol, 1.0 eq) was slowly added to a solution of $[C_{12}BuIm][Br]$ (26 g, 69.6 mmol) dissolved in ultrapure water (500 ml) at 70°C under nitrogen. The mixture was stirred for 24 h, with an additional 1.0 eq of $NaBF_4$ (7.6 g) added after 3 h. The ion exchange yielded the product 1-dodecyl-3-butylimidazolium tetrafluoroborate ($[C_{12}BuIm][BF_4]$) as a yellow oil. The oil was dissolved in toluene (50 mL), separated and washed twice with $NaBF_4$ brine (15.2 g, 2 eq in 50 mL). Residual water in the toluene phase was removed using Na_2SO_4 and then dried *in vacuo* at 50°C. The product was characterized by ^{1}H-NMR and ^{19}F-NMR using trifluoroethanol as an internal standard. Yield: 88%. **^{1}H-NMR** ($(CD_3)_2SO$): δ – 9.18 (s, 1H, -N+-C**H**-N-), δ – 7.80 (d, 2H, -N-C**H**-C**H**-N^+-), δ – 4.16 (m, 4H, N-C**H_2**-CH_2-), δ – 1.78 (m, 4H, -N-CH_2-C**H_2**-), δ – 1.24 (m, 20H, -(C**H_2**)$_{10}$-CH_3), δ – 0.90 (t, 3H, -$(CH_2)_3$-C**H_3**), δ – 0.86 (t, 3H, -$(CH_2)_{11}$-C**H_3**). **^{19}F-NMR** ($(CD_3)_2SO$): δ -149.26 (s, 4F, ^{11}B**F_4**)**,** δ -149.31 (s, 4F, ^{10}B**F_4**), δ -76.23 (t, 3F, C**F_3**CH_2OH).

5.4.6 Partition coefficient (PC) experiments

Solute PC tests were performed in triplicate as previously described[16] using aqueous solutions of styrene (0.2 g/L), octanol (0.4 g/L) and butanol (10 g/L) in Type I ultrapure water. For styrene and octanol PC tests, the absorbent phase fraction was 1 wt%. For butanol PCs, the absorbent fraction was 5 wt%. In addition to the polymer mass, a 10 mL aliquot of styrene, octanol or butanol aqueous solution were added to each scintillation vial, sealed tightly with a foil lined cap and allowed to equilibrate in an Innova 4400 incubator shaker at 30°C at 180 rpm for 1 week. Aqueous solute concentrations before and after equilibration with the polymer were measured using a Varian 450-GC gas chromatography unit equipped with a CP-8410 AutoInjector, VF-5ms 30m capillary column and FID detector.

A TA Instruments Q500 thermogravimetric analyzer to determine total water/solute uptake. Polymer/IL samples (10-15 mg) soaked in styrene, octanol or butanol solutions were pat dry and immediately heated in a TA Instruments Q500 thermogravimetric analyzer from ~25°C to 200°C (20°C/min). The samples were held at 200°C (styrene bp 145°C; octanol bp 195°C; butanol bp 118°C) until the rate of mass loss dropped below 0.05 wt%/min.

A mass balance was performed to determine the solute concentration in the polymer phase. Experimental PC values were calculated using aqueous and polymer phase weight fractions (w_i^{aq} and w_i^{poly}) of the solute and water in Equation 29. Standard deviation values were calculated from triplicate samples to establish a mean value for the equilibrium *PC*.

$$PC_i = \frac{w_i^{poly}}{w_i^{aq}} \tag{29}$$

Solute/water selectivity ($\alpha_{i/w}$) was calculated as in Equation 30.

$$\alpha_{i/w} = \frac{PC_i}{PC_w} \tag{30}$$

5.4.7 Microorganisms and media

Saccharomyces cerevisiae was obtained from Alltech (Nicholasville, Kentucky) and cultivated in a medium from Doran and Bailey[39] containing 10 g/L glucose, 5 g/L KH2PO4, 2 g/L yeast extract, 2 g/L $(NH_4)_2SO_4$, 0.4 g/L $MgSO_4 \cdot 7\ H_2O$, and 0.1 g/L $CaCl_2$. *Pseudomonas putida* ATCC 11172 was cultured in the 'LM medium' described by Fujita et al.[40] containing 10 g/L glucose, 10 g/L bacto-peptone, 5 g/L Bacto-yeast, and 5 g/L NaCl. *Clostridium acetobutylicum* ATCC 824 was cultured anaerobically in 'Medium A' described by Barton & Daugulis,[41] modified to 10 g/L

glucose. *p*-aminobenzoic acid and biotin were prepared separately in a 1000x solution and sterilized through a 0.45 μm filter.

5.4.8 Biocompatibility testing

Growth media were freshly prepared and 50 mL added to 125 mL Erlenmeyer flasks using a burette. Foam plugs were added to the flasks, loosely covered with aluminum foil, then the flasks were autoclaved. Once cool, 5 g of sterile IL or polymer (cut into 2mm cubes) was aseptically added to the flasks. To *C. acetobutylicum* cultures, 0.05 mL of sterile *p*-aminobenzoic acid and biotin solution was also added at this point. The *C. acetobutylicum* cultures were then sealed with a sterile fold-over rubber stopper and sparged aseptically for 5 min, alternating between oxygen-free N_2 gas and vacuum every 30 seconds to ensure anaerobic conditions.

Cultures were inoculated with 2 mL of -80°C glycerol stock culture and incubated at 180 rpm and 30°C (*S. cerevisiae* and *P. putida*) or 37°C (*C. acetobutylicum*). After 24 h, cell growth was determined through triplicate optical density measurements at 600 nm (OD_{600}) using a Biochrom Ultrospec 3000 UV/Visible Spectrophotometer, with Type I ultrapure water as a reference. Polymer and IL biocompatibility was determined by comparing OD_{600} to duplicate control cultures.

5.4.9 Antimicrobial surface behaviour

Antimicrobial testing was performed as previously described,[42,43] with minor microbe and polymer-specific modifications. In this work, polymer samples were dissolved (5 wt%) in toluene (BIMS) or 98:2 toluene:hexanol solution (ionomer), cast (1.5 mL) onto glass microscope slides (75 x 25 mm) and allowed to dry *in vacuo* for 48 h. An overnight culture of *S. cerevisiae*, *P. putida* or *C. acetobutylicum* was used to inoculate (10% v/v) 50 mL of fresh media and incubated

at 30°C or 37°C and 180 rpm for 4-6 hours. After centrifugation (3500 rpm, 5 min; IEC 3000R centrifuge), the cells were re-suspended in Type I ultrapure water to an OD_{600} ~ 0.10 (*S. cerevisiae*) or 0.001 (*P. putida, C. acetobutylicum*). The microbial suspension was sprayed onto the test surfaces using a commercial chromatography sprayer (VWR scientific) using sterile nitrogen gas (10 psi). After drying (3-4 min), the glass slide was placed in a petri dish and molten agar (1.5 wt% agar, autoclaved, cooled to 40°C) was carefully added. The petri dish was sealed and incubated at 30°C overnight. To facilitate anaerobic growth of *C. acetobutylicum*, molten agar was sparged with N_2 during cooling and petri dish samples were incubated, unsealed at 37°C under a sterile N_2 environment. Microbial colonies were counted after 24 h using a colony counter. Experiments were performed in duplicate.

5.4.10 Complex viscosity (η*)

Polymers were tested at 30°C using an Advanced Polymer Analyzer 2000 (Alpha Technologies) controlled-strain rheometer equipped with biconical discs operating at 1 Hz and 0.5° arc. Ionic liquids were tested at 25°C using an Anton Paar MCR 702 rheometer equipped with parallel plates operating in the linear viscoelastic region at 1 Hz and 0.1-10% shear strain.

5.5 Results and Discussion

5.5.1 Physical properties of ionomers and ILs

Efficient TPPB operation requires that the two phases are easily separated, with the aqueous fermentation medium recycled immediately, and the non-aqueous phase processed for solute removal/regeneration before being returned to the bioprocess. As described above, polymeric absorbents are well suited to this application, owing to their solid-like characteristics. Consider the complex viscosity (η^*) data listed in Table 12, which quantify the dynamic response of a

material to an applied oscillatory strain. Unlike the steady-shear viscosity measurements used routinely for low molecular weight (MW) liquids, dynamic measurements can be applied to viscous liquids (e.g. ILs) as well as high MW polymers.[10] The tabulated data (Table 12) show that BIMS and its ionic derivatives provide η^* values 4 to 5-orders of magnitude greater than the ILs, clearly establishing them as viscoelastic solids as opposed to viscous liquids.

The small amount of functionality within our ionomers (0.23 mmol/g-polymer) is insufficient to affect the glass transition temperature, which remains unchanged from the BIMS value of approximately T_g= -22°C.[38] As such, these materials are amorphous, rubbery polymers at bioprocessing temperatures. As a result, these materials are capable of absorbing solute throughout their bulk. It should be noted, however, that the morphology of ionomers is more complex than for non-ionic polymers, in that poor solvation of bound ion-pairs results in aggregation of ionic functionality. Evidence of ion-pair association is found in our η^* measurements of BIMS and its imidazolium ionomer derivatives. Depending on ion-pair structure, η^* values increased 1.9 – 3.6-fold over the parent material (Table 12), owing to polymer chain mobility restrictions imposed by the ionic network.[44] These η^* gains approach those generated by covalent crosslinking formulations, yet these ionomers remain completely soluble in suitable organic solvents. The impact of imidazolium-based multiplets on solute uptake is detailed below.

5.5.2 Solute absorption

Biodegradation and biosynthesis are well-established 'green' processes, with the TPPB technology platform offering process intensification benefits that are proportional to absorptive performance (PC and α). TPPB target solutes can span the entire range from hydrophobic (e.g. PAHs, BTEX, styrene) to hydrophilic (e.g. organic acids, alcohols). We selected three solutes – styrene, 1-

octanol, and 1-butanol – to examine the influence of ionic functionality on the absorption of different solute classes. These molecules are also relevant to bioprocessing, in that styrene is a xenobiotic that is amenable to TPPB technology,[45,46] octanol is a widely used reference for assessing compound hydrophobicity (Log $K_{o/w}$),[47] and butanol's development as a renewable biofuel suffers from strong product inhibition.

Solute properties that are often used to interpret thermodynamic equilibrium data are listed in Table 13. Log $K_{o/w}$ values identify butanol as the most hydrophilic compound of the three, while differences between octanol and styrene are not resolved by this measure. Hansen solubility parameters (HSP) are more informative, as they quantify dispersive (δ_D), hydrogen-bonding (δ_H) and polar (δ_P) interactions for pure materials, thereby differentiating styrene from the two alcohols. HSP values for ionomers and ionic liquids are not available. However, data for poly(isobutylene) (PIB), whose composition is very similar to that of BIMS, allow for the calculation of the Hansen Ra distance (Equation 31) from the target solutes to the non-ionic parent material. The smaller the Ra value, the greater the thermodynamic affinity of the polymer for a solute. On this basis, PC data for BIMS acting on the target solutes is expected to follow the order; styrene > octanol > butanol.

Table 13 - Thermodynamic properties of BIMS and solutes of interest

	Log $K_{o/w}$	**δ_D**	**δ_P**	**δ_H**	**Hansen Ra from PIB**
Styrene[a,b]	2.95	18.6	1.0	4.1	3.7
1-Octanol[a,b]	3.00	16.0	5.0	11.2	7.8
1-Butanol[a,b]	0.88	16.0	5.6	15.8	12.3
Poly(isobutylene)[b]	---	16.9	2.5	4.0	---

[a] Log $K_{o/w}$ data sourced from [48]
[b] HSP data sourced from [49,50]

$$Ra = \sqrt{4 * (\delta_{D,1} - 16.9)^2 + (\delta_{P,1} - 2.5)^2 + (\delta_{H,1} - 4.0)^2} \quad (31)$$

These predictions are borne out by experiment, with BIMS providing a styrene PC of 180 ± 6 (Figure 13a). Furthermore, the hydrophobic character of the BIMS polymer backbone is reflected by an $\alpha_{s/w}$ value of 6200 ± 250 (Figure 13b), demonstrating a strong preference for styrene over water. Note that both PC and α for a polymer-solute-water system are not constants, but depend on solute activities in the aqueous and organic phases and, by extension, are functions of mixture composition.[51] The data reported throughout this work were acquired using a standard experimental condition to facilitate comparisons between polymers.

Chemical modification of BIMS to introduce an ion-pair concentration of 0.23 mmol/g-polymer improved styrene uptake at the expense of selectivity, with only minor differences recorded for the various ionomer compositions, as shown in Figure 13-a,d. These data show that ionic functionality that is capable of ion-dipole and hydrogen bonding interactions prefers associating with water over a non-polar solute. In the context of TPPB technology, heightened water uptake is not problematic, since styrene biodegradation is less concerned with absorption selectivity than total absorption capacity.

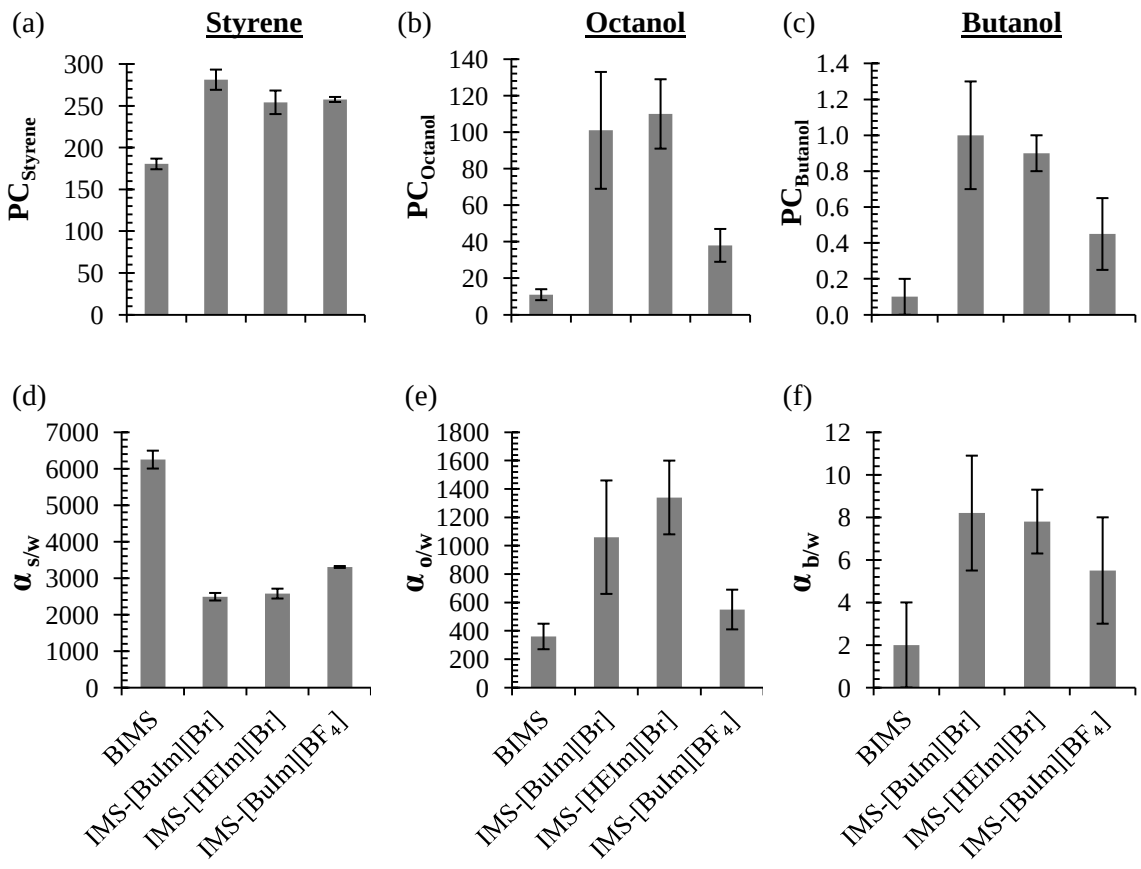

Figure 13 – Partition coefficient (PC) (a,b,c) and solute/water selectivity (α) (d,e,f) for styrene, octanol and butanol in BIMS and its ionic derivatives (0.23 mmol-ion pair/g-polymer)

Although octanol and styrene have similar log $K_{o/w}$ values (log $K_{o/w}$=$[Solute]_{octanol}$/$[Solute]_{aqueous}$; Table 13), they differ markedly in terms of their absorption by BIMS, with an octanol PC of just 11 ± 3 (Figure 13b) and an $\alpha_{o/w}$ value of 360 ± 90 (Figure 13e). This is consistent with the estimated HSP Ra of 7.8 for the BIMS-octanol system. Of greater interest is the effect of imidazolium bromide functionality on octanol absorption, which increased the octanol PC 9.2 - 10-fold and its $\alpha_{o/w}$ value 3 - 3.7-fold. The latter improvement is particularly important, since it demonstrates the potential for imidazolium bromide functionality to increase alcohol absorption selectively over water absorption. Exchange of the Br^- counter ion with BF_4^- compromised both

PC_{OctOH} and $\alpha_{o/w}$, confirming that absorption affinity and selectivity for polar solutes can move in parallel.

The butanol absorption data were consistent with that recorded for octanol, with the imidazolium bromide derivative providing PC_{BuOH} values about 10 times that of BIMS (Figure 13c), and selectivity about 4-fold greater (Figure 13f). The importance of this result to TPPB process efficiency and intensification cannot be overstated. *Clostridium sp.*, a widely used biocatalyst for butanol production, suffers product inhibition at titres of 12-16 g/L, thereby establishing an upper aqueous concentration limit for a TPPB fermentation process.[52,53] Higher PC values mean that less polymer is needed to keep butanol levels below this target, resulting in better volumetric productivity in the bioreactor. Superior selectivity values concentrate butanol in the polymer phase at the expense of water, thereby improving the energy efficiency of butanol purification by a subsequent separation process.[54]

5.5.3 Comparison of solute absorption in ionomers and ionic liquids

Insight into absorptive differences between the ionomers of present interest and IL systems was gained by examining two materials, $[C_{12}BuIm][Br]$ and $[C_{12}BuIm][BF_4]$. Both are viscous liquids at bioprocessing temperatures (Table 12), but the bromide salt is miscible with water and, hence, inappropriate as a TPPB absorbent. Interestingly, IMS-[BuIm][Br] was amongst the best performing ionomers developed in this work (Figure 13). By rendering the ion-pair insoluble with water, covalent binding to an isobutylene-rich backbone made it useful for solute absorption. This suggests that ionomer development efforts can target hydrophilic IL functionality in an effort to promote selective alcohol uptake.

The more hydrophobic tetrafluoroborate salt, $[C_{12}BuIm][BF_4]$, formed an IL phase when mixed with water, and proved highly absorbent toward all three solutes (Table 14). Indeed, it generated

the highest PC and selectivity results recorded in this study. The butanol extraction data are in the range of previous reports on related ILs, $[C_6MIm][BF_4]$ and $[C_8MIm][BF_4]$, which produced similar PC (0.9 and 2.2) and selectivity (3.9 and 12.2) values.[55] Taken together, these results demonstrate the superior absorptive properties of pure ILs relative to ionomer analogues. However, their utility as TPPB absorbents is predicated on their biocompatibility, which is explored below.

Table 14 – Comparison of PC and water/solute selectivity between BIMS, ionomer and IL absorbents

Absorbent	Ion pair conc. (mmol/g)	Styrene		Octanol		Butanol	
		$PC_{Styrene}$	$\alpha_{s/w}$	PC_{OctOH}	$\alpha_{o/w}$	PC_{BuOH}	$\alpha_{b/w}$
BIMS	0	181 ± 6	6200 ± 250	11 ± 3	360 ± 90	0.1 ± 0.1	2 ± 2
IMS-$[BuIm][BF_4]$	0.23	257 ± 3	3300 ± 30	38 ± 9	550 ± 140	0.4 ± 0.2	5 ± 2
IMS-[BuIm][Br]	0.23	281 ± 12	2500 ± 100	101 ± 32	1060 ± 400	1.0 ± 0.3	8 ± 3
$[C_{12}BuIm][BF_4]$	2.63	343 ± 57	6700 ± 1000	311 ± 17	11,200 ± 1100	3.3 ± 0.2	101 ± 9
$[C_{12}BuIm][Br]$	2.68	n/a - soluble		n/a - soluble		n/a - soluble	

5.5.4 Biocompatibility

As defined by IUPAC,[56] biocompatibility refers to the "ability of a material to be in contact with a biological system without producing an adverse effect." In the context of TPPB development, biocompatibility is judged by a material's effect on suspended cell cultures in a well-mixed aqueous medium,[57] typically using a 10 wt% second phase fraction.[58,59] Several indicators of biological activity, including cell growth and glucose consumption, have been exploited successfully for these assessments.[58] In this work we evaluated ILs and ionomers by measuring

cell growth via the optical density (600 nm) of *S. cerevisiae*, *P. putida* and *C. acetobutylicum* in a TPPB environment. These microorganisms are well-represented in literature,[60–62] with *S. cerevisiae* an industrial ethanol-producing yeast (eukaryote) and a pertinent delivery vehicle for genetic engineering, *P. putida* a gram-negative bacterium widely used in bioremediation applications, and *C. acetobutylicum* a common butanol-producing gram-positive bacterium.

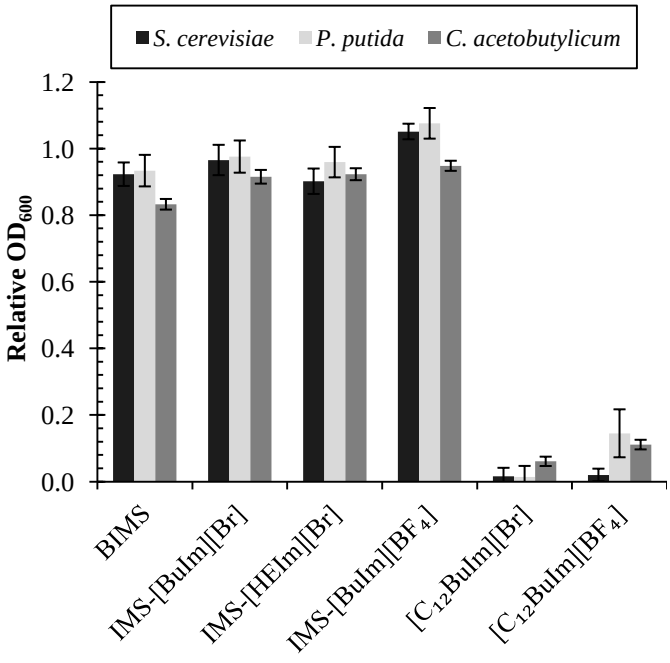

Figure 14 – Optical density (24 h) of suspended cell cultures in contact with 10% (wt/v) BIMS, ionomer or IL

The two ILs ([C_{12}BuIm][Br] and [C_{12}BuIm][BF_4]) were not biocompatible, severely hindering microbial growth relative to a single phase control (Figure 14). These results align with previous reports of [BuMIm][BF_4] toxicity (~1 % (v/v)) towards the yeast *Pichia pastoris* and the bacteria *Escherichia coli* and *Bacillus cereus*.[63] More generally, reports of IL cytotoxicity towards a broad spectrum of microorganisms, mammalian cell lines and aquatic organisms[28,30,64–66] suggest that

some ILs present biocompatibility concerns when used in two-phase bioprocesses. Consequently, while two-phase bioprocesses are generally considered to be 'green', the use of ILs in these cases introduces toxicity precluding their use.

In contrast, covalently grafting the imidazolium functionality in our ionomers substantially eliminated cytotoxicity, as evidenced by the optical density data recorded for all three ionomers, across all cell types. The grafting approach is distinct from previous heterogeneous polymer/IL blends,[67–70] in which a dispersed IL phase is not polymer-bound and can leach into the cell-containing aqueous phase. Altogether, we have demonstrated that IL cytotoxicity can be mitigated by covalently grafting the IL to an insoluble polymer backbone. This approach facilitates the use of a broader selection of ion-pair functionality, particularly those with promising thermodynamic properties that are limited by their water solubility and cytotoxicity in IL form.

5.5.5 Antimicrobial surface properties

The control of microbial growth on surfaces has critical process implications on the operation of TPPBs and related membrane separations (e.g. pervaporation, ultrafiltration, reverse osmosis),[36,71] since biofilm formation can provide a diffusional barrier and compromise the rate of solute transport into the polymer.[72–76] Therefore, antimicrobial surfaces that kill microbes and/or prevent their colonization at the interface have attracted considerable attention.[34,36,77,78] These materials include polymers equipped with imidazolium,[79,80] pyridinium,[42] phosphonium[81] and ammonium functionality,[34] each demonstrating varying degrees of surface antimicrobial activity.

The biocompatibility experiments described above showed that our ionomers had no significant effect on suspended microbe growth that takes place in the bulk aqueous medium (OD_{600}). We have extended these studies by investigating microbe/ionomer interactions directly at the material

interface. This involved a standard antimicrobial surface testing procedure first developed by Tiller et al.[42] and applied successfully elsewhere.[43,82,83] Briefly, a cell suspension was sprayed evenly onto a polymer surface, allowed to dry, and then covered with nutrient-rich agar to ensure direct microbe/polymer contact. After incubation, microbial colonies were counted relative a non-ionic BIMS control slide.

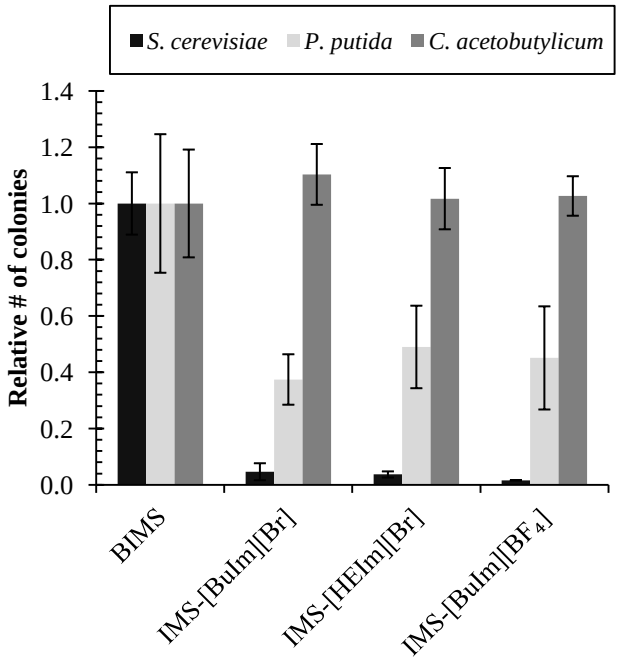

Figure 15 – Antimicrobial activity of the ionomers relative to BIMS (representative images can be found in Appendix A2)

The ionomer surfaces demonstrated the strongest antimicrobial activity toward the yeast *S. cerevisiae*, reducing colony formation between 95 - 98.5% compared to BIMS (Figure 15). Interestingly, they were not as potent towards bacteria, with total *P. putida* colonies reduced by 51 - 64% and no significant change in *C. acetobutylicum* colony proliferation. Reports suggest that antimicrobial activity stems from an ability to disrupt the microorganism's cell wall and/or phospholipid membrane.[42,43,84] Thus, structural differences between microbes may explain the

observed microbe-dependent potency. For example, the thicker and more robust peptidoglycan layer of the gram-positive *C. acetobutylicum* bacterium may enable greater resistance to membrane disruption. In addition to differences in cell structure, material surface charge density can also have an impact on antimicrobial activity. Previous reports suggest that there exists a bacterium-specific threshold below which antimicrobial activity is significantly reduced.[82,85] Given the low levels of ionic functionality (0.23 mmol/g-polymer) in our materials, this may account for the observed microbe-dependent potency.

In all, these results demonstrate that a material can be biocompatible towards suspended cell culture while simultaneously possessing surface antimicrobial behaviour under static conditions. The combination of biocompatibility and antimicrobial properties is ideal for TPPB and membrane-based product recovery techniques, enabling bulk cell growth while minimizing cell proliferation and biofilm formation at the interface.

5.6 Conclusions

Introducing 0.23 mmol/g-polymer of imidazolium-based ionic functionality to an isobutylene-rich elastomer produced ionomers with a broader range of solute absorption characteristics. Partition coefficients for styrene, octanol and butanol were enhanced, but selectivity improvements were limited to alcohol absorption. Whereas imidazolium-based ILs were not biocompatible with suspended cultures of *S. cerevisiae*, *P. putida* and *C. acetobutylicum*, their respective ionomers were suitable for TPPB applications. Furthermore, the ionomers provide surface antimicrobial activity towards some microorganisms under prolonged, direct contact.

5.7 Acknowledgements

We gratefully acknowledge the financial support of DuPont Canada and the Natural Sciences and Engineering Research Council of Canada.

5.8 References

1 C. T. Davidson and A. J. Daugulis, *Appl. Microbiol. Biotechnol.*, 2003, **62**, 297–301.

2 G. P. Prpich, L. Rehmann and A. J. Daugulis, *Biotechnol. Prog.*, 2008, **24**, 839–844.

3 L. Rehmann, G. P. Prpich and A. J. Daugulis, *Chemosphere*, 2008, **73**, 798–804.

4 R. Muñoz, A. J. Daugulis, M. Hernández and G. Quijano, *Biotechnol. Adv.*, 2012, **30**, 1707–1720.

5 W. Van Hecke, G. Kaur and H. De Wever, *Biotechnol. Adv.*, 2014, **32**, 1245–1255.

6 J. T. Dafoe and A. J. Daugulis, *Biotechnol. Lett.*, 2014, **36**, 443–60.

7 M. C. Tomei, M. C. Annesini, S. Rita and A. J. Daugulis, *Environ. Sci. Technol.*, 2010, **44**, 7254–9.

8 D. R. Nielsen and K. J. Prather, *Biotechnol. Bioeng.*, 2009, **102**, 811–21.

9 M. Montes, A. J. Daugulis, M. C. Veiga and C. Kennes, *J. Chem. Technol. Biotechnol.*, 2011, **86**, 47–53.

10 S. L. Bacon, A. J. Daugulis and J. S. Parent, *Chem. Eng. J.*, 2016, **299**, 56–62.

11 G. Quijano, M. Hernandez, F. Thalasso, R. Muñoz and S. Villaverde, *Appl. Microbiol. Biotechnol.*, 2009, **84**, 829–46.

12 A. Arca-Ramos, G. Eibes, M. T. Moreira, G. Feijoo and J. M. Lema, *Chem. Eng. J.*, 2014, **240**, 281–289.

13 L. D. Collins and A. J. Daugulis, *Biotechnol. Bioeng.*, 1997, **55**, 155–162.

14 J. L. Rols, J. S. Condoret, C. Fonade and G. Goma, *Biotechnol. Bioeng.*, 1990, **35**, 427–35.

15 S. L. Bacon, J. S. Parent and A. J. Daugulis, *J. Chem. Technol. Biotechnol.*, 2014, **89**, 948–956.

16 S. L. Bacon, E. C. Peterson, A. J. Daugulis and J. S. Parent, *Biotechnol. Prog.*, 2015, **31**, 1500–7.

17 M. Zawadzki, F. A. e Silva, U. Domańska, J. A. P. Coutinho and S. P. M. Ventura, *Green Chem.*, 2016, **18**, 3527–3536.

18 R. J. Cornmell, C. L. Winder, S. Schuler, R. Goodacre and G. Stephens, *Green Chem.*, 2008, **10**, 685–691.

19 U. Domańska and M. Królikowski, *J. Chem. Thermodyn.*, 2012, **53**, 108–113.

20 K. S. Khachatryan, S. V. Smirnova, I. I. Torocheshnikova, N. V. Shvedene, A. A. Formanovsky and I. V. Pletnev, *Anal. Bioanal. Chem.*, 2005, **381**, 464–470.

21 W. Y. Lou, M. H. Zong and T. J. Smith, *Green Chem.*, 2006, **8**, 147–155.

22 A. B. Pereiro, J. M. M. Araujo, J. M. S. S. Esperanca, I. M. Marrucho and L. P. N. Rebelo, *J. Chem. Thermodyn.*, 2012, **46**, 2–28.

23 L. D. Simoni, A. Chapeaux, J. F. Brennecke and M. A. Stadtherr, *Comput. Chem. Eng.*, 2010, **34**, 1406–1412.

24 H. Zhao, S. Xia and P. Ma, *J. Chem. Technol. Biotechnol.*, 2005, **80**, 1089–1096.

25 P. Steltenpohl and E. Graczová, *Acta Chim. Slovaca*, 2014, **7**, 129–133.

26 P. Dehury, U. Mahanta and T. Banerjee, *Fluid Phase Equilib.*, 2016, (In Press).

27 R. Melgarejo-Torres, C. O. Castillo-Araiza, P. López-Ordaz, N. V. Calleja-Castañeda, J. L. Cano-Velasco, R. M. Camacho-Ruíz, G. J. Lye and S. Huerta-Ochoa, *Chem. Eng. J.*, 2015, **279**, 379–386.

28 O. Dipeolu, E. Green and G. Stephens, *Green Chem.*, 2009, **11**, 397.

29 M. Matsumoto, K. Mochiduki, K. Fukunishi and K. Kondo, *Sep. Purif. Technol.*, 2004, **40**, 97–101.

30 A. Romero, A. Santos, J. Tojo and A. Rodríguez, *J. Hazard. Mater.*, 2008, **151**, 268–273.

31 K. M. Docherty and C. F. Kulpa, Jr., *Green Chem.*, 2005, **7**, 185.

32 J. S. Parent, A. M. J. Porter, M. R. Kleczek and R. A. Whitney, *Polymer (Guildf).*, 2011, **52**, 5410–5418.

33 E. B. Anderson and T. E. Long, *Polymer (Guildf).*, 2010, **51**, 2447–2454.

34 Y. Liu, C. Leng, B. Chisholm, S. Stafslien, P. Majumdar and Z. Chen, *Langmuir*, 2013, **29**, 2897–2905.

35 A. Kugel, S. Stafslien and B. J. Chisholm, *Prog. Org. Coatings*, 2011, **72**, 222–252.

36 I. Francolini, G. Donelli, F. Crisante, V. Taresco and A. Piozzi, in *Biofilm-based healthcare-associated infections: Volume II (Advances in Experimental Medicine and Biology)*, ed. G. Donelli, 2015, vol. 831, pp. 93–117.

37 J. M. Dakin, R. A. Whitney and J. S. Parent, *Ind. Eng. Chem. Res.*, 2014, **53**, 17527–17536.

38 A. R. Cillero, Queen's University, 2014.

39 P. M. Doran and J. E. Bailey, *Biotechnol. Bioeng.*, 1986, **28**, 73–87.

40 M. Fujita, M. Ike and T. Kamiya, *Water Res.*, 1993, **27**, 9–13.

41 W. E. Barton and A. J. Daugulis, *Appl. Microbiol. Biotechnol.*, 1992, **36**, 632–639.

42 J. C. Tiller, C. J. Liao, K. Lewis and A. M. Klibanov, *Proc. Natl. Acad. Sci. U. S. A.*, 2001, **98**, 5981–5985.

43 S. Krishnan, R. J. Ward, A. Hexemer, K. E. Sohn, K. L. Lee, E. R. Angert, D. a. Fischer, E. J. Kramer and C. K. Ober, *Langmuir*, 2006, **22**, 11255–11266.

44 J. S. Parent, A. Liskova, R. A. Whitney and R. Resendes, *J. Polym. Sci. Part A Polym. Chem.*, 2005, **43**, 5671–5679.

45 S. M. Zamir, S. Babatabar and S. A. Shojaosadati, *Chem. Eng. J.*, 2015, **268**, 21–27.

46 P. Parnian, S. M. Zamir and S. A. Shojaosadati, *Chem. Eng. J.*, 2016, **284**, 926–933.

47 OECD, *OECD Guideline for the Testing of Chemicals - Partition Coefficient (n-octanol/water): Shake Flask Method*, Paris, 1995.

48 C. Hansch, A. Leo and D. Hoekman, *Exploring QSAR: Volume 2: Hydrophobic, Electronic, and Steric Constants*, ACS Publications, Washington, 1st edn., 1995.

49 C. M. Hansen, *Hansen Solubility Parameters: A User's Handbook*, Taylor & Francis Group, Boca Raton, FL, 2nd edn., 2007.

50 S. Abbott and H. Yamamoto, HSPiP Computer Program, 2013.

51 S. L. Bacon, J. Scott Parent and A. J. Daugulis, *J. Chem. Technol. Biotechnol.*, 2014, **89**, 948–956.

52 D. T. Jones and D. R. Woods, *Microbiol. Rev.*, 1986, **50**, 484–524.

53 F. Monot, J. R. Martin, H. Petitdemange and R. Gay, *Appl. Environ. Microbiol.*, 1982, **44**, 1318–24.

54 M. Matsumura, H. Kataoka, M. Sueki and K. Araki, *Bioprocess Eng.*, 1988, **3**, 93–100.

55 S. H. Ha, N. L. Mai and Y.-M. Koo, *Process Biochem.*, 2010, **45**, 1899–1903.

56 M. Vert, Y. Doi, K.-H. Hellwich, M. Hess, P. Hodge, P. Kubisa, M. Rinaudo and F. Schué, *Pure Appl. Chem.*, 2012, **84**, 1.

57 R. Muñoz, S. Arriaga, S. Hernández, B. Guieysse and S. Revah, *Process Biochem.*, 2006, **41**, 1614–1619.

58 L. D. Collins and A. J. Daugulis, *Appl. Microbiol. Biotechnol.*, 1999, **52**, 354–359.

59 R. Muñoz, M. Chambaud, S. Bordel and S. Villaverde, *Appl. Microbiol. Biotechnol.*, 2008, **79**, 33–41.

60 S. Ostergaard, L. Olsson and J. Nielsen, *Microbiol. Mol. Biol. Rev.*, 2000, **64**, 34–50.

61 S. Y. Lee, J. H. Park, S. H. Jang, L. K. Nielsen, J. Kim and K. S. Jung, *Biotechnol. Bioeng.*, 2008, **101**, 209–28.

62 I. Poblete-Castro, J. Becker, K. Dohnt, V. M. Dos Santos and C. Wittmann, *Appl. Microbiol. Biotechnol.*, 2012, **93**, 2279–2290.

63 F. Ganske and U. T. Bornscheuer, *Biotechnol. Lett.*, 2006, **28**, 465–469.

64 M. Matsumoto, K. Mochiduki and K. Kondo, *J. Biosci. Bioeng.*, 2004, **98**, 344–7.

65 H. R. Cascon, S. K. Choudhari, G. M. Nisola, E. L. Vivas, D. J. Lee and W. J. Chung, *Sep. Purif. Technol.*, 2011, **78**, 164–174.

66 G. Quijano, A. Couvert and A. Amrane, *Bioresour. Technol.*, 2010, **101**, 8923–8930.

67 S. Heitmann, J. Krings, P. Kreis, A. Lennert, W. R. Pitner, A. Górak and M. M. Schulte, *Sep. Purif. Technol.*, 2012, **97**, 108–114.

68 Y. T. Ong, K. F. Yee, Y. K. Cheng and S. H. Tan, *Sep. Purif. Rev.*, 2014, **43**, 62–88.

69 S. Livi, V. Bugatti, B. G. Soares and J. Duchet-Rumeau, *Green Chem.*, 2014, **16**, 3758.

70 A. Hasanoğlu, *Desalin. Water Treat.*, 2015, **3994**, 1–13.

71 C. G. Kumar and S. . Anand, *Int. J. Food Microbiol.*, 1998, **42**, 9–27.

72 S. F. Zhang, A. Splendiani, L. M. Freitas dos Santos and A. G. Livingston, *Biotechnol. Bioeng.*, 1998, **59**, 80–89.

73 Z. Dong, G. Liu, S. Liu, Z. Liu and W. Jin, *J. Memb. Sci.*, 2014, **450**, 38–47.

74 S. Nakao, F. Saitoh, T. Asakura, T. Kiyoshi and S. Kimura, *J. Membr. Sci.*, 1987, **30**, 273–287.

75 A. Garcia III, E. L. Iannotti and J. L. Fischer, *Biotechnol Bioeng*, 1986, **28**, 785–791.

76 M. Cheryan, *Ultrafiltration Handbook*, Technomic Publishing Co., Inc., Lancaster, PA, 1987.

77 E. R. Kenawy, S. D. Worley and R. Broughton, *Biomacromolecules*, 2007, **8**, 1359–1384.

78 F. Siedenbiedel and J. C. Tiller, *Polymers (Basel).*, 2012, **4**, 46–71.

79 B. Izmaylov, D. Di Gioia, G. Markova, I. Aloisio, M. Colonna and V. Vasnev, *React. Funct. Polym.*, 2015, **87**, 22–28.

80 M. Colonna, C. Berti, E. Binassi, M. Fiorini, S. Sullalti, F. Acquasanta, M. Vannini, D. Di Gioia, I. Aloisio, S. Karanam and D. J. Brunelle, *React. Funct. Polym.*, 2012, **72**, 133–141.

81 A. Kanazawa, T. Ikeda and T. Endo, *Antimicrob. Agents Chemother.*, 1994, **38**, 945–952.

82 J. C. Tiller, S. B. Lee, K. Lewis and A. M. Klibanov, *Biotechnol. Bioeng.*, 2002, **79**, 465–471.

83 D. Park, J. a. Finlay, R. J. Ward, C. J. Weinman, S. Krishnan, M. Paik, K. E. Sohn, M. E. Callow, J. a. Callow, D. L. Handlin, C. L. Willis, D. a. Fischer, E. R. Angert, E. J. Kramer and C. K. Ober, *ACS Appl. Mater. Interfaces*, 2010, **2**, 703–711.

84 L. Timofeeva and N. Kleshcheva, *Appl. Microbiol. Biotechnol.*, 2011, **89**, 475–492.

85 R. Kügler, O. Bouloussa and F. Rondelez, *Microbiology*, 2005, **151**, 1341–1348.

Chapter 6

Imidazolium-based polyelectrolyte absorbents for bioproduct recovery

This chapter has been prepared in draft manuscript form and has not yet been submitted for publication.

6.1 Abstract

Polymerization of vinylimidazolium ionic liquids (ILs) to yield solid, water-insoluble polyelectrolyte absorbents successfully eliminated microbial cytotoxicity concerns while providing excellent separation of polar fermentation products (e.g. n-butanol) from aqueous solution. Although the linear polyelectrolyte P(VC_4ImBr) was water-soluble and inhibitory towards *Saccharomyces cerevisiae*, co-polymerization with a difunctional imidazolium IL successfully eliminated cytotoxicity by rendering the hydrophilic thermosets insoluble. Young's modulus (E) improved up to 50-fold with increasing cross-link density, however, the hydrogels were limited by their poor partition coefficient (PC_{BuOH}) values and n-butanol/water selectivity ($\alpha_{b/w} = PC_{BuOH}/PC_{H2O}$).

Insoluble polyelectrolytes could be alternatively prepared from more hydrophobic ILs bearing longer n-alkyl sidechains (P(V**C**$_{\#}$ImBr) - C_8 to C_{16}) in combination with a range of anions (P(VC_{12}Im**X**) - Cl^-, Br^-, I^- and BF_4^-). The polyelectrolytes were all biocompatible, whereas the IL monomers severely inhibited *S. cerevisiae* growth. The materials possessed good physical properties in aqueous solution, with Young's modulus values increasing with hydrophobicity between 3.0 to 56 MPa. n-Butanol partition coefficient (PC_{BuOH}) and n-butanol/water selectivity ($\alpha_{b/w} = PC_{BuOH}/PC_{H2O}$) were sensitive functions of cation and anion composition, with PC_{BuOH} values up to 7.6 and $\alpha_{b/w}$ up to 78. These materials also demonstrated favorable absorption for several other polar fermentation products, including ethanol, iso-butanol, acetone and 2,3-butanediol.

List of Abbreviations

$[VC_4Im][Br]$ - 1-vinyl-3-butylimidazolium bromide
$[VC_8Im][Br]$ - 1-vinyl-3-octylimidazolium bromide
$[VC_{10}Im][Br]$ - 1-vinyl-3-decylimidazolium bromide
$[VC_{12}Im][Br]$ - 1-vinyl-3-dodecylimidazolium bromide
$[VC_{14}Im][Br]$ - 1-vinyl-3-tetradecylimidazolium bromide
$[VC_{16}Im][Br]$ - 1-vinyl-3-hexadecylimidazolium bromide
$[VC_{12}Im][Cl]$ - 1-vinyl-3-dodecylimidazolium chloride
$[VC_{12}Im][I]$ - 1-vinyl-3-dodecylimidazolium iodide
$[VC_{12}Im][BF_4]$ - 1-vinyl-3-dodecylimidazolium tetrafluoroborate
Bis[VIm][Br]C_{10} - bis(vinylimidazolium bromide)decane
$P(VC_4ImBr)$ - poly(vinylbutylimidazolium bromide)
$P(VC_8ImBr)$ - poly(vinyloctylimidazolium bromide)
$P(VC_{10}ImBr)$ - poly(vinyldecylimidazolium bromide)
$P(VC_{12}ImBr)$ - poly(vinyldodecylimidazolium bromide)
$P(VC_{14}ImBr)$ - poly(vinyltetradecylimidazolium bromide)
$P(VC_{16}ImBr)$ - poly(vinylhexadecylimidazolium bromide)
$P(VC_{12}ImCl)$ - poly(vinyldodecylimidazolium chloride)
$P(VC_{12}ImI)$ - poly(vinyldodecylimidazolium iodide)
$P(VC_{12}ImBF_4)$ - poly(vinyldodecylimidazolium tetrafluoroborate)
AIBN - 2,2′-Azobis(2-methylpropionitrile)
APS - Ammonium persulfate
SMBS - Sodium metabisulfite
OD_{600} - Optical density at 600 nm
PC_i – Partition coefficient (Equation 32)
$\alpha_{i/w}$ – solute/water selectivity (Equation 33)
w_i^{β} –concentration of component 'i' in phase 'β' (g/kg)

6.2 Introduction

The biological synthesis of butanol from biomass feedstocks has attracted considerable attention in recent years as a method of producing renewable fuels, industrial solvents and chemical intermediates.[1–5] Butanol biosynthesis can be severely limited by end-product inhibition at titres between 1-2 wt%,[6] leading to a low product yield, reduced fermentation rates, and increased downstream processing costs.[7] An immiscible extractant can mitigate the effects of end-product inhibition by removing and enriching butanol as it is formed. Effective extractants must possess high butanol affinity, as quantified by the partition coefficient (PC_{BuOH}), and a strong preference for butanol absorption versus water uptake, as quantified by selectivity ($\alpha_{b/w}=PC_{BuOH}/PC_{water}$).[7,8]

Organic solvents have been commonly investigated for use in butanol extractive fermentation, however, their implementation can be limited due to biocompatibility and water solubility concerns, as well as operational challenges stemming from volatility, foaming and emulsification.[9–12] More recently, ionic liquids (ILs) have demonstrated promise in separation processes due to their low vapour pressure, tunable composition and ability to form a range of intermolecular interactions.[13,14] Recent investigations have demonstrated impressive n-butanol sequestration from aqueous solution,[15–17] however, microbial cytotoxicity and water solubility remain critical concerns.[15,18–23] More generally, reports of IL toxicity towards a broad spectrum of organisms [24–28] and enzymes[29,30] may limit their application in 'green' processes.

In contrast to liquid extractants, solid polymers have emerged as promising absorbents due to their widespread biocompatibility and facile solid-liquid separation from the fermentation medium.[31–34] Here, we test the hypothesis that polymerization of IL monomers to prepare solid polyelectrolyte extractants can mitigate cytotoxicity while maintaining bulk absorptive properties. Vinylimidazolium-based materials were selected due to their straightforward synthesis, good thermal stability and demonstrated affinity for polar organics.[28,35–39] The polyelectrolyte

absorbents were evaluated for use in extractive fermentation applications by measuring biocompatibility in a two-phase environment, physical properties (Young's Modulus) and absorptive properties for n-butanol and other polar fermentation products (PC_i; $\alpha_{i/w}$).

6.3 Experimental

6.3.1 Materials

1-Vinylimidazole (98%), 1-bromobutane (99%), 1-bromooctane (99%), 1-bromododecane (97%), 1-bromohexadecane (97%), 1-iododododecane (98%), 1-chlorododecane (97%), 1,10-dibromodecane (97%), sodium tetrafluoroborate ($NaBF_4$) (98%), 2,2′-azobis(2-methylpropionitrile) (AIBN) (98%) and ammonium persulfate (APS) (98%) were purchased from Sigma-Aldrich (Canada). 1-Bromodecane (98%),1-bromotetradecane (98%), sodium metabisulfite (SMBS) (97.7%) and n-butanol (99%) were purchased from Fischer Scientific (Canada). All chemicals were used as received. Type I ultrapure water (18.2 MΩ.cm at 25°C) was used throughout this study.

6.3.2 Synthesis of $[VC_4Im][Br]$, $[VC_8Im][Br]$, $[VC_{10}Im][Br]$ and $[VC_{12}Im][Cl]$

Ionic liquid monomers were prepared as previously described[40] with minor modifications. 1-Vinylimidazole (5.00g, 53.1mmol) and 1.1 eq. of n-alkyl halide (bromobutane 8.01g; bromooctane 11.29g; bromodecane 12.93g; chlorododecane 11.96g) were dissolved in toluene (12.5mL), heated to 90 °C and stirred for 24 h (whereas $[VC_{12}Im][Cl]$ was stirred at 100 °C for 48 h) under nitrogen. After cool down, the upper toluene-rich phase was decanted and the oil was washed with hexanes four times. The final product was dried *in vacuo* and characterized by ^{1}H-NMR.

[VC_4Im][Br]: ^{1}H-NMR ($CDCl_3$): δ 10.95 (s, 1H), δ 7.88 (m, 1H), δ 7.61 (m, 1H), δ 7.49 (dd, 1H), δ 6.03 (dd, 1H), δ 5.40 (dd, 1H), δ 4.42 (t, 2H), δ 1.95 (m, 2H), δ 1.40 (m, 2H), δ 0.97 (t, 3H) (Yield: 95%). **[VC_8Im][Br]:** ^{1}H-NMR ($CDCl_3$): δ 10.90 (s, 1H), δ 7.77 (m, 1H), δ 7.51 (dd, 1H), δ 7.47 (m, 1H), δ 5.96 (dd, 1H), δ 5.41 (dd, 1H), δ 4.42 (t, 2H), δ 1.93 (m, 2H), δ 1.26 (m, 10H), δ 0.86 (t, 3H) (Yield: 70%). **[VC_{10}Im][Br]:** ^{1}H-NMR ($CDCl_3$): δ 11.04 (s, 1H), δ 7.78 (m, 1H), δ 7.51 (dd, 1H), δ 7.48 (m, 1H), δ 5.98 (dd, 1H), δ 5.41 (dd, 1H), δ 4.40 (t, 2H), δ 1.95 (m, 2H), δ 1.24 (m, 14H), δ 0.87 (t, 3H) (Yield: 85%). **[VC_{12}Im][Cl]:** ^{1}H-NMR ($CDCl_3$): δ 11.32 (s, 1H), δ 7.68 (m, 1H), δ 7.56 (dd, 1H), δ 7.48 (m, 1H), δ 5.92 (dd, 1H), δ 5.41 (dd, 1H), δ 4.40 (t, 2H), δ 1.94 (m, 2H), δ 1.26 (m, 18H), δ 0.88 (t, 3H) (Yield: 91%).

6.3.3 Synthesis of bis[VIm][Br]C_{10}

Difunctional ionic liquid cross-linker was prepared as previously described[41] with minor modifications. 1,10-Dibromodecane (3.00 g, 10.0 mmol) and 2.1 eq. of 1-vinylimidazole (1.98 g, 21.0 mmol) were dissolved in ethyl acetate (5 mL) and heated to reflux conditions under nitrogen for 36 h, stirring continuously. Once cooled, the crystal product was ground to a fine powder, washed with ethyl acetate under vacuum filtration, then dried *in vacuo* and characterized by ^{1}H-NMR.

Bis[VIm][Br]C_{10}: ^{1}H-NMR ($CDCl_3$): δ 11.13 (s, 2H), δ 7.71 (m, 2H), δ 7.68 (m, 2H), δ 7.48 (dd, 2H), δ 5.96 (dd, 2H), 5.42 (dd, 2H), 4.46 (t, 4H), 2.02 (m, 4H), 1.39 (m, 12H).

6.3.4 Synthesis of [VC_{12}Im][Br], [VC_{14}Im][Br], [VC_{16}Im][Br], [VC_{12}Im][I]

Ionic liquid monomers were prepared as previously described[40,42] with minor modifications. 1-Vinylimidazole (5.00g, 53.1 mmol) and 1.1 eq. of n-alkyl halide (bromododecane 14.57g; bromotetradecane 16.20g; bromohexadecane 17.84g; iododododecane 17.31g) were dissolved in

ethyl acetate (12.5 mL) and heated to reflux conditions under nitrogen for 24 h, stirring continuously. Once cooled, the crystal product was ground to a fine powder, washed with ethyl acetate under vacuum filtration (for $[VC_{12}Im][Br]$ and $[VC_{12}Im][I]$, the flask was cooled below room temperature to induce crystallization), then dried *in vacuo* and characterized by ^{1}H-NMR. **$[VC_{12}Im][Br]$:** ^{1}H-NMR ($CDCl_3$): δ 10.98 (s, 1H), δ 7.77 (m, 1H), δ 7.51 (dd, 1H), δ 7.48 (m, 1H), δ 5.96 (dd, 1H), δ 5.41 (dd, 1H), δ 4.40 (t, 2H), δ 1.95 (m, 2H), δ 1.24 (m, 18H), δ 0.87 (t, 3H) (Yield: 93%, MP 44-48°C). **$[VC_{14}Im][Br]$:** ^{1}H-NMR ($CDCl_3$): δ 11.13 (s, 1H), δ 7.69 (m, 1H), δ 7.51 (dd, 1H), δ 7.41 (m, 1H), δ 5.95 (dd, 1H), δ 5.42 (dd, 1H), δ 4.41 (t, 2H), δ 1.95 (m, 2H), δ 1.25 (m, 22H), δ 0.88 (t, 3H) (Yield: 95%, MP 58°C). **$[VC_{16}Im][Br]$:** ^{1}H-NMR ($CDCl_3$): δ 11.16 (s, 1H), δ 7.67 (m, 1H), δ 7.51 (dd, 1H), δ 7.39 (m, 1H), δ 5.94 (dd, 1H), δ 5.42 (dd, 1H), δ 4.40 (t, 2H), δ 1.96 (m, 2H), δ 1.25 (m, 26H), δ 0.88 (t, 3H) (Yield: 95%, MP 66°C). **$[VC_{12}Im][I]$:** ^{1}H-NMR ($CDCl_3$): δ 10.74 (s, 1H), δ 7.69 (m, 1H), δ 7.46 (m, 1H), δ 7.43 (dd, 1H), δ 5.98 (dd, 1H), δ 5.46 (dd, 1H), δ 4.43 (t, 2H), δ 1.97 (m, 2H), δ 1.25 (m, 18H), δ 0.88 (t, 3H) (Yield: 97%, MP 49-50°C).

6.3.5 Synthesis of $[VC_{12}Im][BF_4]$

IL anion metathesis was performed as previously described[40] with minor modification. $[VC_{12}Im][Br]$ (15g, 43.7mmol) was slowly added to water (150mL) at room temperature. Once dissolved, sodium tetrafluoroborate (5.276g, 1.1 eq.) was added to the mixture and stirred for 24 h at room temperature to achieve complete anion exchange, verified with ^{19}F-NMR using trifluoroethanol as an internal standard. The product was extracted using dichloromethane (150mL) then washed twice with brine solution (containing one equivalent of $NaBF_4$ in 60mL) then with water (60mL). Dichloromethane was removed by vacuum. The final product was ground into a fine powder, then dried in vacuo and characterized by ^{1}H-NMR and ^{19}F-NMR.

[VC_{12}Im][BF_4]: ^{1}H-NMR ($CDCl_3$): δ 9.14 (s, 1H), δ 7.63 (m, 1H), δ 7.41 (m, 1H), δ 7.15 (dd, 1H), δ 5.82 (dd, 1H), δ 5.40 (dd, 1H), δ 4.26 (t, 2H), δ 1.90 (m, 2H), δ 1.25 (m, 18H), δ 0.88 (t, 3H). ^{19}F-NMR ($CDCl_3$): δ -151.97 (s, 4F, ^{11}B**F_4**), δ -152.02 (s,4F, ^{10}B**F_4**) (Yield: 80%, MP 37-40 °C).

6.3.6 Synthesis of P(VC_4ImBr) and P(VC_{12}ImBr) with APS initiator (methanol/water)

Polymerization was performed as described elsewhere with minor modification.[42] Varying quantities of monomer ([VC_4Im][Br] or [VC_{12}Im][Br]) and cross-linker bis(vinylimidazolium bromide)decane (Bis[VIm][Br]C_{10}), with a combined mass of 5 g, were dissolved in methanol (2mL) and water (0.75mL) with ammonium persulfate (APS; 0.03 mol-initatior/mol-monomer) at room temperature. Sodium meta-bisulfite (SMBS; 0.03 mol-initatior/mol-monomer) in water (0.4mL) was added to the reaction mixture and allowed to react for 24h at room temperature. P(VC_4ImBr) was precipitated in excess acetone, dried in vacuo at 60°C and was characterized by ^{1}H-NMR. P(VC_{12}ImBr) precipitated during polymerization and was washed several times in Type I ultrapure water and was characterized by ^{1}H-NMR. Uncross-linked hydrated monolithic material was pressed in a Wabash press at 30°C for 12h to prepare a bulk solid. P(VC_4ImBr) and P(VC_{12}ImBr) thermosets containing the cross-linker bis[VIm][Br]C_{10} were washed several times in Type I ultrapure water, however, did not dissolve and could not be characterized by ^{1}H-NMR.

P(VC_4ImBr): ^{1}H-NMR ($CDCl_3$): δ 10.02 (br, 1H), δ 8.42 (br, 1H), δ 7.19 (br, 1H), δ 4.96 (br, 1H), δ 4.26 (br, 2H), δ 2.31 (br, 2H), δ 1.97 (br, 2H), δ 1.45 (br, 2H), δ 1.01 (br, 3H).

P(VC_{12}ImBr): ^{1}H-NMR ($CDCl_3$): δ 9.95 (br, 1H), δ 8.37 (br, 1H), δ 7.19 (br, 1H), δ 4.89 (br, 1H), δ 4.21 (br, 2H), δ 2.07 (br, 4H), δ 1.28 (br, 18H), δ 0.90 (br, 3H).

6.3.7 Synthesis of P(VC_8ImBr), P(VC_{10}ImBr), P(VC_{12}ImBr), P(VC_{14}ImBr), P(VC_{16}ImBr), P(VC_{12}ImCl), P(VC_{12}ImI) and P(VC_{12}ImBF_4) with AIBN initiator (toluene/ethanol)

Bulk polymerization was performed as described elsewhere with minor modification.[42] The required monomer (5 g) was dissolved in a 9:1 toluene:ethanol mixture (25mL) at room temperature. 2,2′-Azobis(2-methylpropionitrile) (AIBN; 0.03 mol-initatior/mol-monomer) was added to the mixture and stirred at room temperature until dissolved. The temperature was increased to 90°C, and heating continued under nitrogen and reflux for 5 h. Once cooled to room temperature, the polymer was precipitated from excess acetone (methanol was used to precipitate P(VC_{12}ImBF_4) and allowed to settle. After 24 h, acetone was decanted and fresh acetone was added. Acetone was decanted after another 24 h, and the final product was dried *in vacuo* and characterized by ^{1}H-NMR.

P(VC_8ImBr): ^{1}H-NMR ($CDCl_3$): δ 10.06 (br, 1H), δ 8.51 (br, 1H), δ 7.11 (br, 1H), δ 4.91 (br, 1H), δ 4.21 (br, 2H), δ 2.10 (br, 2H), δ 1.98 (br, 2H), δ 1.29 (br, 10H), δ 0.89 (br, 3H). **P(VC_{10}ImBr):** ^{1}H-NMR ($CDCl_3$): δ 10.06 (br, 1H), δ 8.54 (br, 1H), δ 7.10 (br, 1H), δ 4.94 (br, 1H), δ 4.21 (br, 2H), δ 1.95 (br, 4H), δ 1.27 (br, 14H), δ 0.89 (br, 3H). **P(VC_{12}ImBr):** ^{1}H-NMR ($CDCl_3$): δ 9.95 (br, 1H), δ 8.37 (br, 1H), δ 7.19 (br, 1H), δ 4.89 (br, 1H), δ 4.21 (br, 2H), δ 2.07 (br, 4H), δ 1.28 (br, 18H), δ 0.90 (br, 3H). **P(VC_{14}ImBr):** ^{1}H-NMR ($CDCl_3$): δ 9.97 (br, 1H), δ 8.37 (br, 1H), δ 7.15 (br, 1H), δ 4.90 (br, 1H), δ 4.20 (br, 2H), δ 2.11 (br, 2H), δ 1.98 (br, 2H), δ 1.26 (br, 22H), δ 0.89 (br, 3H). **P(VC_{16}ImBr):** ^{1}H-NMR ($CDCl_3$): δ 9.95 (br, 1H), δ 8.35 (br, 1H), δ 7.14 (br, 1H), δ 4.88 (br, 1H), δ 4.22 (br, 2H), δ 2.05 (br, 4H), δ 1.27 (br, 26H), δ 0.89 (br, 3H). **P(VC_{12}ImCl):** ^{1}H-NMR ($CDCl_3$): δ 10.13 (br, 1H), δ 8.61 (br, 1H), δ 7.12 (br, 1H), δ 4.87 (br, 1H), δ 4.21 (br, 2H), δ 2.16 (br, 2H), δ 1.96 (br, 2H), δ 1.28 (br, 18H), δ 0.90 (br, 3H). **P(VC_{12}ImI):** ^{1}H-NMR ($CDCl_3$): δ 9.95 (br, 1H), δ 8.37 (br, 1H), δ 7.19 (br, 1H), δ 4.89 (br, 1H), δ 4.21 (br, 2H), δ 2.07 (br, 4H), δ 1.28 (br, 18H), δ 0.90 (br, 3H). **P(VC_{12}ImBF_4):** ^{1}H-NMR ($CDCl_3$): δ 8.49 (br, 1H), δ 7.21 (br, 2H), δ 4.09 (br, 3H), δ 1.79 (br, 4H), δ 1.27 (br, 18H), δ 0.89 (br, 3H). ^{19}F-NMR ($CDCl_3$): δ -151.97 (s, 4F, $^{11}BF_4$), δ -152.02 (s, 4F, $^{10}BF_4$).

6.3.8 Partition coefficient and selectivity experiments

Polyelectrolyte absorptive properties were quantified by determining the solute partition coefficient (PC_i) and selectivity in triplicate, as previously described.[28] A 5 wt% polymer phase fraction was used throughout, with initial aqueous solute concentrations between 5 g/L to 50 g/L depending on reported inhibitory concentrations. Aqueous solute concentrations before and after equilibration with the polymer were measured using a Varian 450-GC gas chromatography unit equipped with a CP-8410 AutoInjector, VF-5ms 30m capillary column and FID detector. Equilibration times varied based on polymer properties and physical dimensions and was determined by time-trial experiments.

Equilibrated polymer samples (~0.10 ± 0.02 g; triplicate) were lightly pat dry with a paper towel and dried in aluminum weigh pans to determine total water/solute uptake. Samples were dried at 60 °C and weighed every 12 hours until the polymer mass remained unchanged between time intervals.

A mass balance was performed to determine the solute and water concentration in the polymer phase. Experimental partition coefficient (PC) and selectivity ($\alpha_{i/w}$) values were calculated using aqueous and polymer phase weight fractions (w_i^{aq} and w_i^{poly}) of the solute and water in Equation 32. Standard deviation values were calculated from triplicate samples to establish a mean value for the equilibrium *PC*.

$$PC_i = \frac{w_i^{poly}}{w_i^{aq}} \tag{32}$$

Solute/water selectivity ($\alpha_{i/w}$) was calculated as in Equation 33.

$$\alpha_{i/w} = \frac{PC_i}{PC_w} \tag{33}$$

6.3.9 Young's Modulus (E)

After equilibration with an aqueous solution, polymer samples were lightly dried with a paper towel and assayed in triplicate using a Shore A durometer on a flat level bench at room temperature. In cases where materials fragmented, durometer readings were taking immediately prior to fracture. Young's Modulus (E; MPa) was calculated from durometer readings as previously described.[41]

6.3.10 Polymer imaging

Dry polymer samples were fractured in liquid nitrogen, gold-coated and imaged using a Hitachi S-2300 scanning electron microscope at 600x and 2000x magnification. Images were analyzed using ImageJ software.

6.3.11 Biocompatibility testing

Saccharomyces cerevisiae was obtained from Alltech (Nicholasville, Kentucky) and cultivated in a medium from Doran and Bailey[42] containing 10 g/L glucose, 5 g/L KH_2PO_4, 2 g/L yeast extract, 2 g/L $(NH_4)_2SO_4$, 0.4 g/L $MgSO_4 \cdot 7\ H_2O$, and 0.1 g/L $CaCl_2$.

Polymer biocompatibility was determined as previously described.[28] Briefly, 50 mL of freshly prepared growth medium was added to 125 mL Erlenmeyer flasks and sterilized by autoclave. Once cool, 5 g of sterile polymer or IL monomer was aseptically added to the flasks, inoculated with 2 mL of -80°C glycerol stock culture and incubated at 180 rpm and 30°C for 24 h. Cell growth was determined through triplicate optical density measurements at 600 nm (OD_{600}) using a Biochrom Ultrospec 3000 UV/Visible Spectrophotometer and compared to duplicate control

cultures. [VC_{16}Im][Br] formed a stable emulsion with the fermentation medium and could not be evaluated using this method.

6.4 Results and discussion

6.4.1 Polyelectrolyte biocompatibility

Extractants are classified as biocompatible if they do not produce an adverse or inhibitory effect on microorganisms when contacted with the fermentation medium. In extractive fermentation, biocompatibility is gauged by an extractant's effect on suspended microbial culture growth in a well-mixed aqueous medium, typically using a 10 wt% second phase fraction.[43–45] In the present study, we measured biocompatibility via the optical density (600 nm) of *Saccharomyces cerevisiae*, an industrial ethanol-producing yeast and an important vehicle for genetic engineering that can be manipulated to produce n- and iso-butanol isomers.[46–48]

The data in Figure 16 indicate that all IL monomers used in this study were cytotoxic towards *S. cerevisiae* (dark grey bars), severely inhibiting suspended cell growth compared to the single phase controls (relative $OD_{600} < 0.15$). These results align with previous reports of imidazolium IL toxicity towards a range of microorganisms.[21,22,24] Polymerization of the hydrophilic monomer [VC_4Im][Br] yielded the water-soluble polyelectrolyte P(VC_4ImBr) that possessed a moderately inhibitory effect on *S. cerevisiae* growth under these conditions (light grey bar).

Most notably, Figure 16 demonstrates that all water-insoluble polyelectrolytes studied here were biocompatible with *S. cerevisiae* (black bars), substantially eliminating cytotoxicity concerns associated with the IL monomer. Thus, the data show that polymerization is an effective means of mitigating IL toxicity, provided the resultant material is insoluble in water. The biocompatible

polyelectrolytes can now be evaluated on the basis of material strength and absorptive properties, as described below.

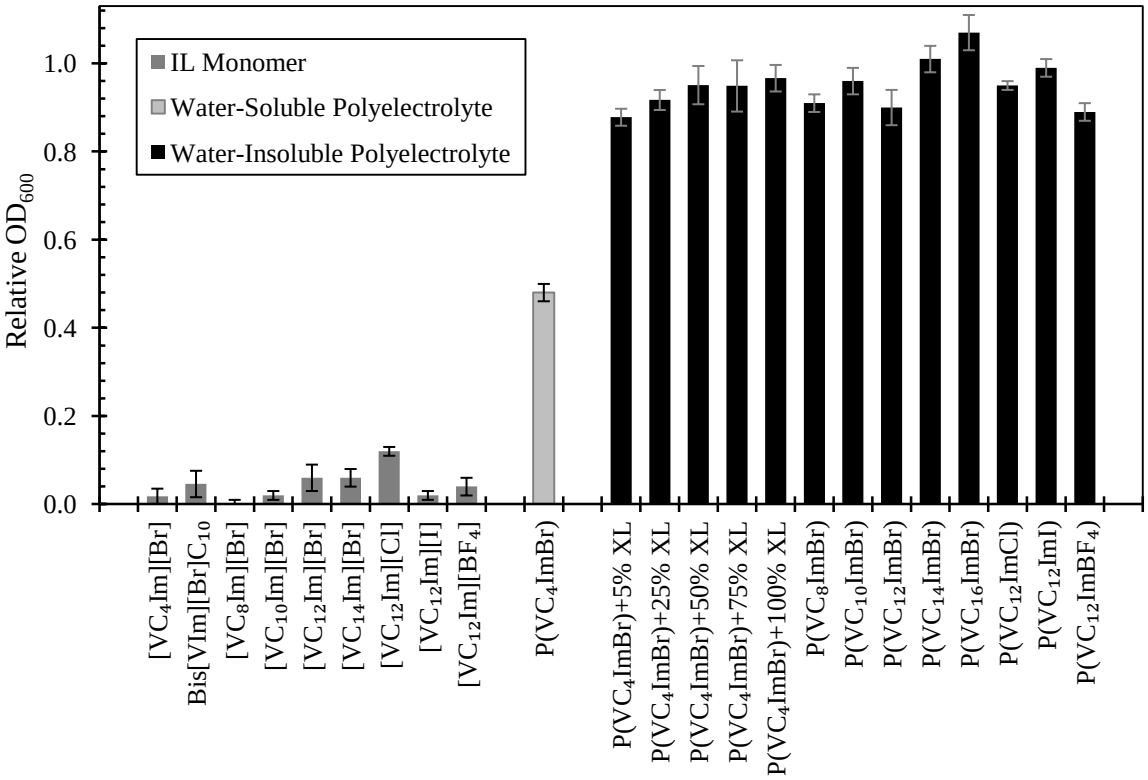

Figure 16 – Optical density (OD_{600}) of *S. cerevisiae* cultures containing 10 wt% IL monomer or polyelectrolyte relative to a single phase control after 24 h.

6.4.2 Hydrophilic formulations – hydrogels

The previous section demonstrated that the hydrophilic polymer P(VC_4ImBr) was water-soluble and not suitable for extractive fermentation applications. Water-solubility concerns were mitigated by preparing thermoset materials of varying cross-link density by co-polymerizing [VC_4Im][Br] with a difunctional IL (bis[VIm][Br]C_{10}). The thermosets remained highly hydrophilic and have been classified accordingly as hydrogels.

A key material property consideration is the solid polymer absorbent's ability to withstand the shear forces imposed in a stirred-tank bioreactor and solid-liquid separation operation. Here, durometry was used as a simple method to estimate the polymer's Young's Modulus (E), a widely-used measure of a material's elastic resistance to an applied deformation. The Young's modulus provides insight into the material's physical strength, with the added benefit of being widely cited for many polymers.[49]

The data in Figure 17-a demonstrate the impact of cross-link density on Young's modulus. With low levels of cross-linker (5 wt%), the hydrogel's small modulus (0.9 ± 0.2 MPa) translated into a weak material that was very susceptible to fracture. The hydrogel was highly swollen with water (Figure 17-d), with the material's large liquid fraction ($w_{BuOH}^{poly} + w_{H2O}^{poly}$ = 900 g/kg) consistent with its low modulus. Increasing cross-link density yielded up to nearly 50-fold improvements in modulus due to the polymer's tighter network and lower liquid content (Figure 17-a,b).

In addition to being insoluble, solid and biocompatible, polymeric extractants should also provide favourable sequestration of the fermentation product. Extractant absorptive performance is commonly quantified by its solute partition coefficient (PC_i) and its solute/water selectivity ($\alpha_{b/w} = PC_{BuOH}/PC_{H2O}$). PC has important implications on the fraction of bioreactor volume occupied by extractant and the overall fermentor productivity, whereas $\alpha_{b/w}$ is directly related to downstream product purification costs.[50]

The effect of hydrogel cross-link density on PC and $\alpha_{b/w}$ for n-butanol is demonstrated in Figure 17-c and Figure 17-d, respectively. The data show that increasing cross-link density improves PC_{BuOH} from 0.75 to 1.2. Similarly, the more tightly cross-linked networks absorbed lower amounts of water, yielding nearly 6-fold improvements in $\alpha_{b/w}$ from 0.75 to 4.4.

Compared to other extractants, however, the absorptive performance of these hydrogels fell short. For reference, oleyl alcohol is a biocompatible organic solvent used extensively in academia and industry with an experimental n-butanol PC of 3.6 ± 0.4 and $\alpha_{b/w}$ = 180 ± 53 (data in Table 16; previous reports align: PC = 3.4 – 3.7 and $\alpha_{b/w}$ = 194).[15,50,51] In general, the hydrogels tested were too hydrophilic, demonstrated by their preferential affinity for water over n-butanol. The following sections describe polyelectrolyte absorbents prepared from more hydrophobic IL monomers in order to improve the material's affinity and selectivity for n-butanol.

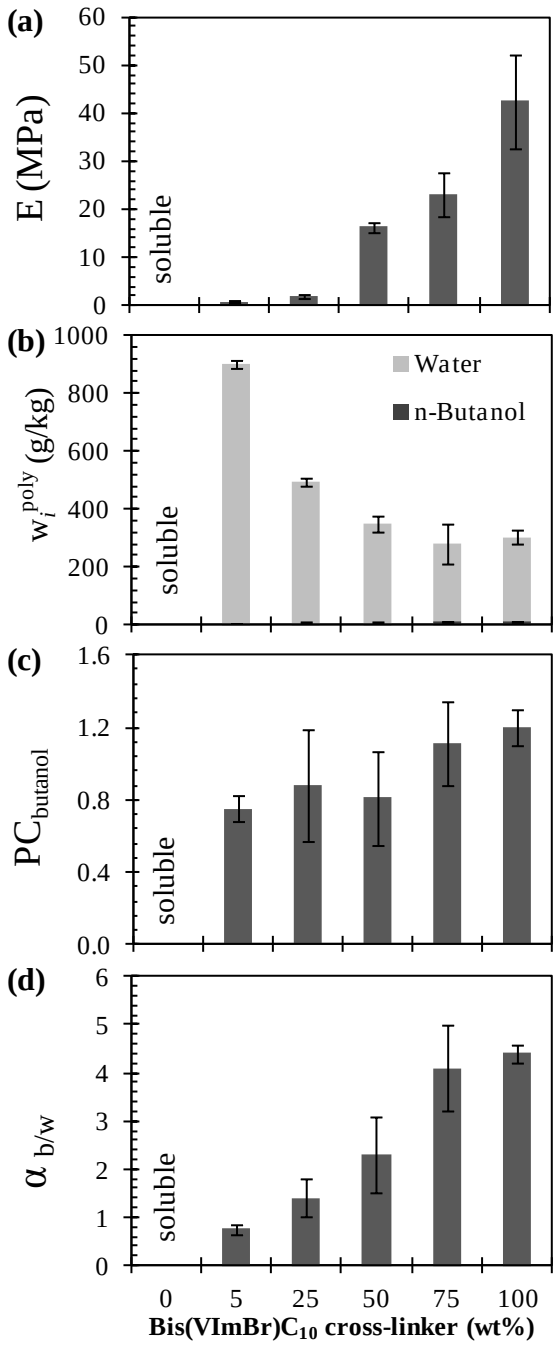

Figure 17 - Properties of P(VC_4ImBr) gels containing varying amounts of Bis[VIm][Br]C_{10} cross-linker (10 g/L initial n-butanol concentration; 5 wt% polymer phase fraction; 30 °C).

6.4.3 Hydrophobic formulations-monoliths

Polymerization of a more hydrophobic IL monomer is an alternate means of preparing a water-insoluble (i.e. biocompatible) polyelectrolyte without requiring cross-linker. This was demonstrated with [VC_{12}Im][Br], wherein polymerization successfully converted a sparingly soluble monomer into a water-insoluble linear polymer. The process of polymerization resulted in minor changes in overall chemical composition, from vinyl to alkyl functionality, however, this is unlikely to account for the observed change in water solubility. Rather, these changes can more likely be attributed to the polymer's lower entropy of mixing that results from its greater molecular weight.[34] A lower entropy of mixing makes polymer dissolution less energetically favorable, which aligns with the observed decrease in water-solubility. Recalling that the highly hydrophilic P(VC_4ImBr) remained soluble in water, these data demonstrate that sufficiently hydrophobic monomers are required to successfully prepare insoluble polymer.

The precipitation polymerization of P(VC_{12}ImBr) from [VC_{12}Im][Br] in an aqueous methanol/water medium further demonstrates these entropy effects. While the IL bearing the C_{12} n-alkyl chain was completely soluble in the medium, polymerization led to instability and, at some critical molecular weight, polymer precipitation.[52,53] SEM imaging of the product revealed a monolith structure composed of small spheres with diameters of 1 to 3 μm (Figure 18). While cross-linker was not required to achieve a water-insoluble material, co-polymerization of [VC_{12}Im][Br] with 5 to 10 wt% of difunctional monomer (bis[VIm][Br]C_{10}) improved modulus by up to ~3-fold (Table 15). Not insignificant, however, are polymer production and processing/re-processing considerations, wherein linear thermoformable materials facilitate the use of a wide range of polymer processing techniques to manufacture forms including pellets, films, membranes and tubing.

Table 15 also demonstrates that the hydrophobic P(VC_{12}ImBr) monoliths registered PC_{BuOH} values 3 to 4-fold larger than the previous hydrophilic hydrogel formulations. Improvements in

butanol/water selectivity were more modest (~2-fold), likely due to the monolith voids filling non-selectively with the test butanol-in-water solution. Thus, while monolith morphology can provide valuable surface area for *adsorptive* resins in chromatography and solid-phase extraction applications,[54,55] it is not beneficial for *absorption*-based separation processes. The influence of collapsing the monolith and producing bulk polyelectrolyte solids on physical and absorptive properties is explored below.

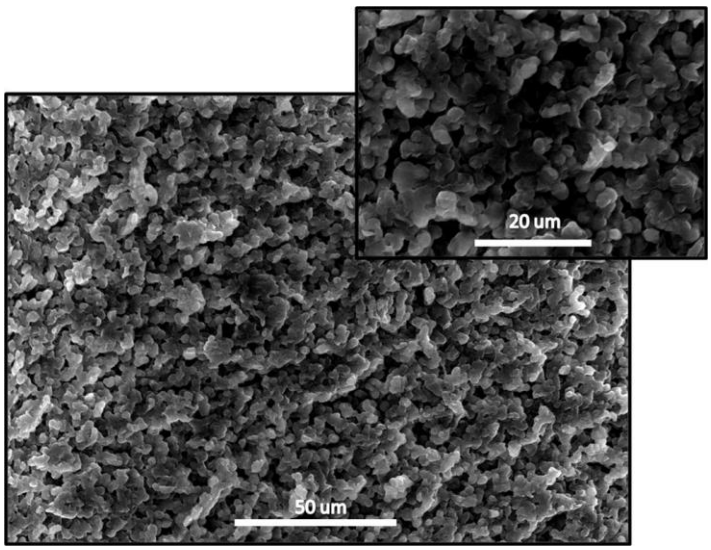

Figure 18 - Monolith structure of P(VC_{12}ImBr) containing 10 wt% bis[VIm][Br]C_{10} cross-linker

Table 15 – Properties of P(VC_{12}ImBr) absorbents (10 g/L initial n-butanol concentration; 5 wt% polymer phase fraction; 30 °C).

Initiator (medium)	**Cross-linker**[a] (wt%)	**Morphology**	$\mathbf{PC_{BuOH}}$	$\boldsymbol{\alpha_{b/w}}$	**E** (MPa)	$\boldsymbol{w_{BuOH}^{poly}}$ (g/kg)	$\boldsymbol{w_{H2O}^{poly}}$ (g/kg)
APS (methanol/water)	-	Monolith	4.4 ± 0.8	10 ± 2	4.5 ± 0.4	34 ± 5	450 ± 20
APS (methanol/water)	5	Monolith	4.3 ± 0.3	10 ± 1	7.6 ± 0.2	34 ± 2	440 ± 19
APS (methanol/water)	10	Monolith	4.1 ± 0.3	11 ± 2	14.0 ± 1.0	33 ± 2	385 ± 9
APS (methanol/water)	-	Collapsed monolith	6.7 ± 0.5	56 ± 5	8.8 ± 1.0	47 ± 2	120 ± 2
AIBN (toluene/ethanol)	-	Continuous bulk	6.9 ± 0.3	56 ± 4	17.2 ± 2.0	51 ± 3	125 ± 4

[a] cross-linker: bis[VIm][Br]C_{10}

6.4.4 Hydrophobic formulations-bulk solids

Eliminating the monolith morphology and associated porosity by pressing the material with 10,000 psi overnight yielded noteworthy improvements in n-butanol absorption (Table 15). The resultant bulk P(VC_{12}ImBr) material possessed among the best absorptive properties for n-butanol (PC_{BuOH} = 6.7 ± 0.5; $\alpha_{b/w}$ = 58 ± 5) reported to date for biocompatible extractants, with a PC nearly 2-fold greater than oleyl alcohol. Table 15 also details the properties of P(VC_{12}ImBr) bulk solids alternatively produced via solution polymerization in toluene/ethanol followed by precipitation in acetone. The absorptive properties were identical between polymerization methods once the thermoformable monolith (i.e. no cross-linker) material was collapsed (Table 15). These data further suggest that initiator type (APS or AIBN; 3 mol%) did not impact absorptive properties.

6.4.5 Effect of alkyl chain length on P($VC_{\#}$ImBr) properties

A homologous series of vinyl imidazolium bromide IL monomers possessing C_8 to C_{16} n-alkyl substituents were polymerized in toluene/ethanol to prepare bulk thermoformable absorbents of varying hydrophobicity. Figure 19-a demonstrates that Young's modulus values increased with longer n-alkyl chain lengths, corresponding to the more hydrophobic materials' lower overall liquid content (Figure 19-b). Interestingly, increasing P($VC_{\#}$ImBr) n-alkyl length increased from C_8 and C_{14} had little influence on PC_{BuOH} (Figure 19-c), but yielded improvements in butanol/water selectivity due to a decreased affinity for water (Figure 19-d).

The data in Figure 19 consequently establish a upper and lower bound for n-alkyl length of C_8 to C_{14} for imidazolium bromide polyelectrolytes. While more hydrophilic materials such as P(VC_4ImBr) were clearly unsuitable due to their high affinity for water, the decline in absorptive performance as n-alkyl length increased from P(VC_{14}ImBr) to P(VC_{16}ImBr) was less clear (Figure 19-c,d). Differential scanning calorimetry of P(VC_{16}ImBr) revealed a melting endotherm at 172 °C, indicating that side-chain crystallization may have formed a non-absorptive domain and limited butanol sequestion.[56]

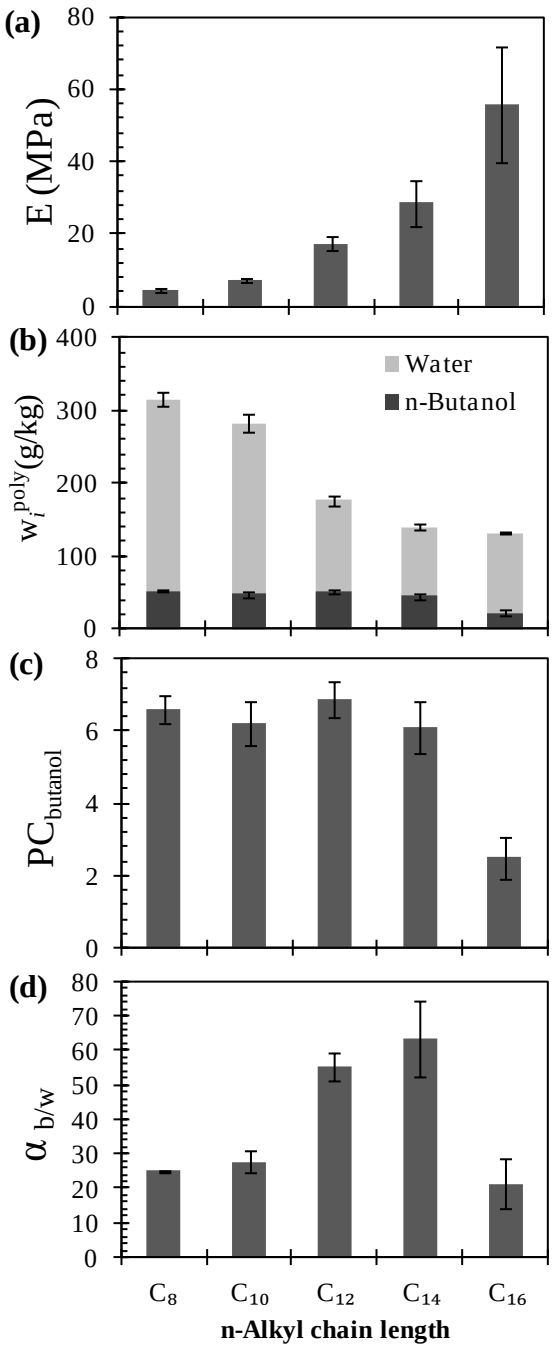

Figure 19 - Effect of imidazolium substituent n-alkyl chain length on P($VC_{\#}$ImBr) properties (10 g/L initial n-butanol concentration; 5 wt% polymer phase fraction; 30 °C).

6.4.6 Effect of anion structure on P(VC_{12}ImX) properties

Polylelectrolytes prepared from [VC_{12}Im][**X**] monomers demonstrate the influence of Cl^-, Br^-, I^- and BF_4^- anion compositions on polyelectrolyte modulus and butanol/water absorption. The relative hydrophobicity of these anions can be described using the Hofmeister series, a measure of a dissociated ion's ability to salt out proteins.[57,58] Accordingly, the anions can be ranked from most hydrophilic to hydrophobic accordingly: $Cl^- > Br^- > I^- > BF_4^-$.

The four linear P(VC_{12}Im**X**) materials were all insoluble in water, with more hydrophilic halide-containing polyelectrolytes ($Cl^- > Br^- > I^-$) possessing lower Young's modulus (Figure 20-a), consistent with their greater liquid content (Figure 20-b). PC_{BuOH} improved with anion hydrophilicity, however, the improvements came at the expense of selectivity (Figure 20-c,d). The highest PC_{BuOH} was reported for P(VC_{12}ImCl) of 7.6 ± 0.7 whereas the highest $\alpha_{b/w}$ was registered for P(VC_{12}ImI) (78 ± 15). In all, these data demonstrate that polymerization of reactive ILs bearing hydrophobic cation side-chains (e.g. C_{12}) facilitates the use of a broader selection of ion-pair functionality, including more hydrophilic halide anions, that possess promising thermodynamic properties but are limited by water-solubility and cytotoxicity in IL form.

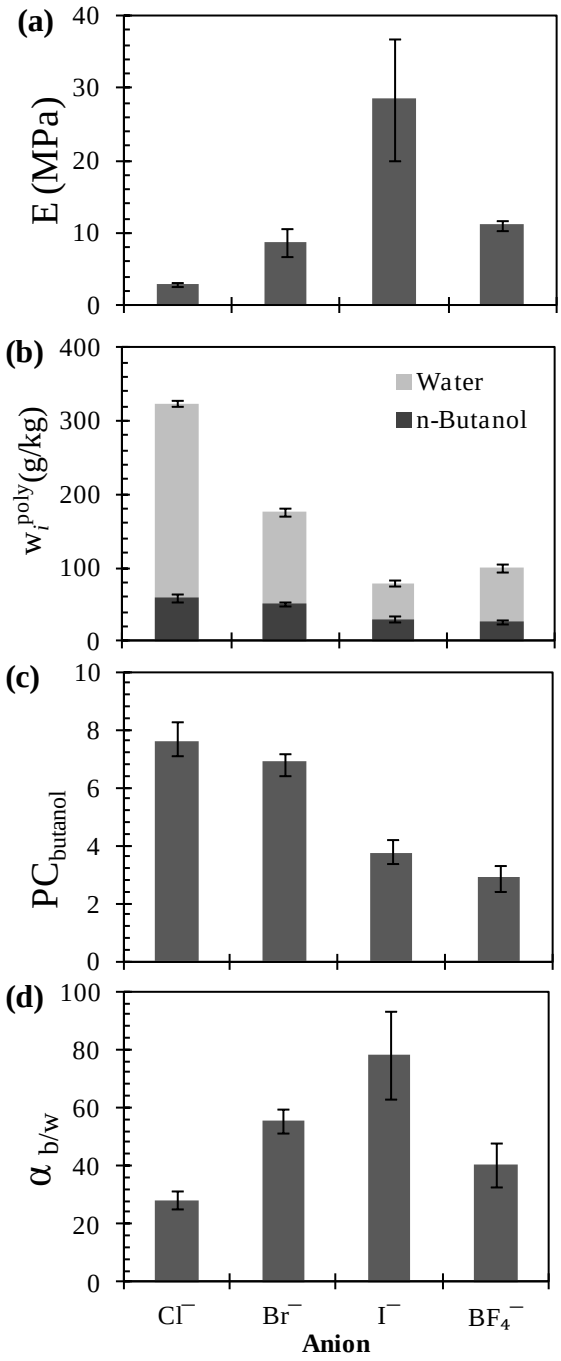

Figure 20 - Effect anion structure P(VC_{12}ImX) properties (10 g/L initial n-butanol concentration; 5 wt% polymer phase fraction; 30 °C).

6.4.7 Extractive fermentation applications

After separating the solid polyelectrolyte from the fermentation medium, the n-butanol/water liquid fraction can be recovered from the polymer for further purification. Downstream, a key element in n-butanol/water separation is the existence of a heterogeneous azeotrope at 57.3 wt% n-butanol (92.3 °C).[59] The presence of this azeotrope prevents further butanol purification using a single distillation column, requiring more complex and capital intensive process configurations. Therefore, the ideal extraction process would sequester a mixture of n-butanol and water with a target selectivity that, once desorbed, yielded a product stream composed of at least 57.3 wt% n-butanol.

Given a 1.0 wt% n-butanol aqueous concentration, we have calculated that an extractant would require $\alpha_{b/w} = 133$ to reach the n-butanol/water azeotrope. More concentrated aqueous n-butanol feeds require lower selectivity values, with 1.5 and 2.0 wt% streams requiring $\alpha_{b/w}$ targets of 88 and 66, respectively, demonstrating the desirability of continued improvements in microbe solvent tolerance through genetic engineering.[6] Importantly, solute PC does not directly influence the ratio of n-butanol/water in the polymer, and underscores that screening extractants based on PC alone does not adequately address all process considerations. However, larger PCs do influence volumetric productivity by requiring less polymer to remove a given quantity of product, thereby occupying less fermentor volume and reducing fixed process costs.

Based on downstream separation considerations, P(VC_{12}ImI) was the best performing material due to its high selectivity for n-butanol ($\alpha_{b/w} = 78$; $PC_{BuOH} = 3.8$). The liquid stream within the polymer was composed of 39 wt% n-butanol, enriched from a 0.81 wt% aqueous solution. The material does fall short in terms of reaching the n-butanol/water azeotropic composition, however, the sensitivity of PC and $\alpha_{b/w}$ towards cation and anion composition (Figure 19 and Figure 20) demonstrates opportunity for further polyelectrolyte optimization.

Several other fermentation processes, including the bioproduction of ethanol, iso-butanol, acetone and 2,3-butanediol also suffer from end-product inhibition. Table 16 demonstrates that the imidazolium polyelectrolytes can achieve good removal of a range of polar products, with P(VC_{12}ImBr) providing significantly improved PC values compared to oleyl alcohol, but lower $\alpha_{o/w}$ values. As each bioprocess may possess varying economic sensitivity to PC and $\alpha_{b/w}$, bioprocess-specific targets should be defined for further material design and optimization.

Table 16 - Sorption of molecules pertinent to extractive fermentation

	Initial solute concentration (g/L)	**PC**	**$\alpha_{i/w}$**	**E** (MPa)
P(VC_{12}ImBr)				
n-Butanol	10	6.9 ± 0.5	56 ± 4	17.2 ± 1.9
iso-Butanol	10	5.6 ± 0.4	40 ± 4	18.8 ± 3.4
Ethanol	10	1.1 ± 0.3	7 ± 2	27.4 ± 8.2
Acetone	5	0.7 ± 0.3	5 ± 2	29.3 ± 5.4
Water	1000	0.14 ± 0.01	-	31.2 ± 8.5
2,3-Butanediol	50	1.1 ± 0.1	8 ± 1	25.1 ± 2.6
Oleyl Alcohol				
n-Butanol	10	3.6 ± 0.4	180 ± 53	n/a
iso-Butanol	10	2.7 ± 0.4	135 ± 29	n/a
Ethanol	10	0.30 ± 0.08	24 ± 7	n/a

6.5 Conclusions

Polymerization of reactive IL monomers successfully mitigated microbial cytotoxicity towards *S. cerevisiae* by reducing material's water solubility. The solid polyelectrolytes possessed excellent bulk absorptive properties, registering among the best n-butanol PC values for biocompatible

extractants and good n-butanol/water selectivity. Adjusting cation and anion composition were demonstrated as potent levers to adjust absorptive performance that could be used to achieve bioprocess-specific separation targets.

6.6 Acknowledgements

We gratefully acknowledge the financial support of DuPont Canada and the Natural Sciences and Engineering Research Council of Canada.

6.7 References

1 N. Qureshi, *Biofuels, Bioprod. Biorefining*, 2008, **2**, 319–330.

2 T. C. Ezeji, N. Qureshi and H. P. Blaschek, *Curr. Opin. Biotechnol.*, 2007, **18**, 220–7.

3 US 2009/0305370 Al, 2009, 111111.

4 US 8,101,808, 2012, 2.

5 B. Ndaba, I. Chiyanzu and S. Marx, *Biotechnol. Reports*, 2015, **8**, 1–9.

6 T. Ezeji, C. Milne, N. D. Price and H. P. Blaschek, *Appl. Microbiol. Biotechnol.*, 2010, **85**, 1697–1712.

7 W. Van Hecke, G. Kaur and H. De Wever, *Biotechnol. Adv.*, 2014, **32**, 1245–1255.

8 J. T. Dafoe and A. J. Daugulis, *Biotechnol. Lett.*, 2014, **36**, 443–60.

9 G. Quijano, M. Hernandez, F. Thalasso, R. Muñoz and S. Villaverde, *Appl. Microbiol. Biotechnol.*, 2009, **84**, 829–46.

10 A. Arca-Ramos, G. Eibes, M. T. Moreira, G. Feijoo and J. M. Lema, *Chem. Eng. J.*, 2014, **240**, 281–289.

11 L. D. Collins and A. J. Daugulis, *Biotechnol. Bioeng.*, 1997, **55**, 155–162.

12 J. L. Rols, J. S. Condoret, C. Fonade and G. Goma, *Biotechnol. Bioeng.*, 1990, **35**, 427–35.

13 A. B. Pereiro, J. M. M. Araujo, J. M. S. S. Esperanca, I. M. Marrucho and L. P. N. Rebelo, *J. Chem. Thermodyn.*, 2012, **46**, 2–28.

14 Y. Kohno and H. Ohno, *Chem. Commun.*, 2012, **48**, 7119–7130.

15 L. Y. Garcia-chavez, C. M. Garsia, B. Schuur and A. B. De Haan, *Ind. Eng. Chem. Res.*, 2012, **51**.

16 H. R. Cascon, S. K. Choudhari, G. M. Nisola, E. L. Vivas, D. J. Lee and W. J. Chung, *Sep. Purif. Technol.*, 2011, **78**, 164–174.

17 S. H. Ha, N. L. Mai and Y.-M. Koo, *Process Biochem.*, 2010, **45**, 1899–1903.

18 R. Melgarejo-Torres, C. O. Castillo-Araiza, P. López-Ordaz, N. V. Calleja-Castañeda, J. L. Cano-Velasco, R. M. Camacho-Ruíz, G. J. Lye and S. Huerta-Ochoa, *Chem. Eng. J.*, 2015, **279**, 379–386.

19 O. Dipeolu, E. Green and G. Stephens, *Green Chem.*, 2009, **11**, 397.

20 M. Matsumoto, K. Mochiduki, K. Fukunishi and K. Kondo, *Sep. Purif. Technol.*, 2004, **40**, 97–101.

21 A. Romero, A. Santos, J. Tojo and A. Rodríguez, *J. Hazard. Mater.*, 2008, **151**, 268–273.

22 K. M. Docherty and C. F. Kulpa, Jr., *Green Chem.*, 2005, **7**, 185.

23 A. G. Fadeev and M. M. Meagher, *Chem. Commun.*, 2001, 295–296.

24 F. Ganske and U. T. Bornscheuer, *Biotechnol. Lett.*, 2006, **28**, 465–469.

25 M. Matsumoto, K. Mochiduki and K. Kondo, *J. Biosci. Bioeng.*, 2004, **98**, 344–7.

26 G. Quijano, A. Couvert and A. Amrane, *Bioresour. Technol.*, 2010, **101**, 8923–8930.

27 R. J. Cornmell, C. L. Winder, S. Schuler, R. Goodacre and G. Stephens, *Green Chem.*, 2008, **10**, 685–691.

28 S. L. Bacon, A. J. Daugulis and J. S. Parent, *Green Chem.*, 2016, **18**, 6586–6595.

29 H. Zhao, O. Olubajo, Z. Song, A. L. Sims, T. E. Person, R. A. Lawal and L. A. Holley, *Bioorg. Chem.*, 2006, **34**, 15–25.

30 H. Zhao, *J. Mol. Catal. B Enzym.*, 2005, **37**, 16–25.

31 M. C. Tomei, M. C. Annesini, S. Rita and A. J. Daugulis, *Environ. Sci. Technol.*, 2010, **44**, 7254–9.

32 D. R. Nielsen and K. J. Prather, *Biotechnol. Bioeng.*, 2009, **102**, 811–21.

33 M. Montes, A. J. Daugulis, M. C. Veiga and C. Kennes, *J. Chem. Technol. Biotechnol.*, 2011, **86**, 47–53.

34 S. L. Bacon, A. J. Daugulis and J. S. Parent, *Chem. Eng. J.*, 2016, **299**, 56–62.

35 J. Yuan and M. Antonietti, *Polymer (Guildf).*, 2011, **52**, 1469–1482.

36 W. J. Horne, M. A. Andrews, K. L. Terrill, S. S. Hayward, J. Marshall, K. A. Belmore, M. S. Shannon and J. E. Bara, *ACS Appl. Mater. Interfaces*, 2015, **7**, 8979–8983.

37 W. Bi, B. Tang and K. H. Row, *Bioprocess Biosyst. Eng.*, 2013, **36**, 651–658.

38 B. Tang, W. Bi and K. H. Row, *Bioresour. Technol.*, 2013, **137**, 25–32.

39 W. Bi, M. Wang, X. Yang and K. H. Row, *J. Sep. Sci.*, 2014, **37**, 1632–1639.

40 H. Ohno and K. Ito, *Chem. Lett.*, 1998, 27, 751–752.

41 A. W. Mix and A. J. Giacomin, *J. Test. Eval.*, 2011, **39**, 1–10.

42 P. M. Doran and J. E. Bailey, *Biotechnol. Bioeng.*, 1986, **28**, 73–87.

43 L. D. Collins and A. J. Daugulis, *Appl. Microbiol. Biotechnol.*, 1999, **52**, 354–359.

44 R. Muñoz, M. Chambaud, S. Bordel and S. Villaverde, *Appl. Microbiol. Biotechnol.*, 2008, **79**, 33–41.

45 R. Muñoz, S. Arriaga, S. Hernández, B. Guieysse and S. Revah, *Process Biochem.*, 2006, **41**, 1614–1619.

46 S. Ostergaard, L. Olsson and J. Nielsen, *Microbiol. Mol. Biol. Rev.*, 2000, **64**, 34–50.

47 S. H. Park, S. Kim and J. S. Hahn, *Appl. Microbiol. Biotechnol.*, 2014, **98**, 9139–9147.

48 E. J. Steen, R. Chan, N. Prasad, S. Myers, C. J. Petzold, A. Redding, M. Ouellet and J. D. Keasling, *Microb. Cell Fact.*, 2008, **7**, 36.

49 J. E. Mark, *Polymer Data Handbook*, Oxford University Press, Cincinnati, 2nd edn., 1999.

50 M. Matsumura, H. Kataoka, M. Sueki and K. Araki, *Bioprocess Eng.*, 1988, **3**, 93–100.

51 W. E. Barton and A. J. Daugulis, *Appl. Microbiol. Biotechnol.*, 1991, **36**, 632–639.

52 J. S. Downey, G. McIsaac, R. S. Frank and H. D. H. Stöver, *Macromolecules*, 2001, **34**, 4534–4541.

53 K. Li and H. D. H. Stöver, *J. Polym. Sci. A*, 1993, **31**, 2473–2479.

54 J. Qin, L. Bai, J. Wang, Y. Ma, H. Liu and S. He, *Anal. Methods*, 2014, **7**, 218–225.

55 Y. Wang, Q. L. Deng, G. Z. Fang, M. F. Pan, Y. Yu and S. Wang, *Anal. Chim. Acta*, 2012, **712**, 1–8.

56 S. L. Bacon, E. C. Peterson, A. J. Daugulis and J. S. Parent, *Biotechnol. Prog.*, 2015, **31**, 1500–7.

57 A. Berthod, M. J. Ruiz-Ángel and S. Carda-Broch, *J. Chromatogr. A*, 2008, **1184**, 6–18.

58 M. K. Potdar, G. F. Kelso, L. Schwarz, C. Zhang and M. T. W. Hearn, *Molecules*, 2015, **20**, 16788–16816.

59 J. Gmehling, J. Menke, J. Krafczyk, K. Fischer, J. Fontaine and H. V Kehiaian, in *Handbook of chemistry and physics*, ed. D. R. Lide, CRC Press, Boca Raton, FL, 2005, pp. 6–160.

Chapter 7

Conclusions and future work

7.1 Conclusions

UNIFAC-vdW-FV and Flory Huggins-based activity models can be used to accurately predict partition coefficient (PC) values for solutes in rubbery, amorphous, non-ionic polymers based on chemical structure and polymer weight distribution. Absorbent polymer selection based on PC encourages the selection of low M_n material, while mechanical strength (G*) and solid/liquid separation considerations favor high M_n solid polymer. Compromises between PC and G* inherent to unimodal molecular weight distribution (MWD) polymers can be mitigated using bimodal MWD formulations, made from mixing very low MW material (organic solvent or oligomer) with a high MW polymer. In addition, crystalline domains and water absorption in polar polymers can influence experimental PC values, with prediction accuracy significantly reduced for these systems.

Ionic liquid (IL) cytotoxicity and water solubility concerns can be mitigated through synthesis of water-insoluble ionic polymers. In one approach, halide displacement of isobutylene-rich elastomers yielded solid ionomers with low levels of ionic functionality that were water-insoluble, biocompatible and possessed good affinity for both polar and non-polar target molecules. Alternatively, polymerization of reactive IL monomers possessing hydrophobic alkyl substituents produced insoluble polyelectrolyte absorbents with a high affinity and selectivity for polar solutes (e.g. alcohols). Varying cation and anion structure produced a group of imidazolium polyelectrolyte absorbents that provided among the largest n-butanol and ethanol PC values reported for biocompatible extractants.

7.2 Future work

There are several promising avenues for future research that have been highlighted in this thesis. In particular, further investigation of polyelectrolyte absorbents and their application in extractive fermentation and TPPBs is required. Sub-topics could include the development of novel polyelectrolyte compositions, consideration of product recovery, and integration of polyelectrolytes into TPPB processes.

The demonstrated capability of IL polymerization to reduce water-solubility and mitigate well-documented microbial cytotoxicity[1–6] presents a unique and promising opportunity to advance the current state-of-the-art in extractive fermentation and TPPBs. Continued investigation into polyelectrolyte composition should focus on the development of materials with improved PC and selectivity as well as lower glass transition temperature (T_g) values. In addition, novel polyelectrolyte structures should continue to focus on thermal stability, good mechanical properties and biocompatibility. The tunability afforded by the polyelectrolyte's structure further enables the development of materials with a specific affinity for other biomolecules, including alcohols, organic acids, flavour/fragrance compounds or pharmaceutical intermediates.

While the thermodynamic models used to describe solute absorption in Chapters 2-4 proved effective for non-ionic polymer selection, they are not easily extended to ionic absorbents at this time. However, *a priori* selection of polyelectrolyte structures based on thermodynamic affinity may be possible using other more recent predictive models such as COSMO-RS.[7–10] Alternatively, heuristic insight into potent chemical structures for alcohol separation may be gained through analysis of ILs previously employed in the literature, for which there are several promising materials.[11,12] Incorporating the polymer science fundamentals described herein may also aid in absorbent selection by focusing on materials with low T_g values and limited crystallinity. Furthermore, the concept of highly bimodal polymer formulations could be applied

to future polyelectrolyte absorbents, wherein a biocompatible low molecular weight solvent or oligomer could be used to improve solute partitioning and diffusivity.

Product recovery from a solid polymer is another interesting research topic that requires attention. Specifically, the characterization of polyelectrolyte diffusivity in a hydrated 'absorptive' mode will help to determine the polymer particle size required based on the biological production rate, as previously described by our group.[13] Solute diffusivity during product recovery is another potential topic of future research, as material properties may be affected by the polymer's decreasing liquid content. Altering desorption temperature may be a means of preventing diffusivity limitations as the liquid content within the polymer is reduced.

A premise of this work is that the presence of a biocompatible absorptive polymer in a TPPB configuration can substantially improve product titer and bioreactor productivity. While this hypothesis has been proven true for a number of biological systems (including the ABE system using organic solvents), quantification of the polyelectrolyte's specific impact on bioreactor performance is required. In particular, optimization of run-time, mode of operation (i.e. batch, fed-batch, continuous) and product titer are interesting and important problems that require further attention.

Similarly important, the effects of the fermentation medium on polyelectrolyte performance have yet to be characterized. The biological production of butanol requires a complex medium consisting of co-products (acetone, ethanol), intermediate metabolites (organic acids), substrate (glucose) and salts, all of which may affect solute partitioning (PC and α). Furthermore, the potential for polyelectrolyte metathesis with ions within the medium requires consideration, however, the development of non-exchangeable cation/anion pairs is currently underway to pre-emptively mitigate this issue.

The ionomers in Chapter 5 possessed antimicrobial surfaces, however, a similar analysis has yet to be performed on the polyelectrolytes of current interest. The higher ionic surface charge density of the polyelectrolytes may provide more potent antimicrobial activity, particularly towards hardy gram-positive bacteria (e.g. *Clostridium acetobutylicum*). Finally, an *in-situ* study is likely required to better quantify the attachment and proliferation of microbes on polymer particles in stirred tank bioreactor and external absorption column configurations.

7.3 References

1 F. Ganske and U. T. Bornscheuer, *Biotechnol. Lett.*, 2006, **28**, 465–469.

2 M. Matsumoto, K. Mochiduki and K. Kondo, *J. Biosci. Bioeng.*, 2004, **98**, 344–7.

3 H. R. Cascon, S. K. Choudhari, G. M. Nisola, E. L. Vivas, D. J. Lee and W. J. Chung, *Sep. Purif. Technol.*, 2011, **78**, 164–174.

4 G. Quijano, A. Couvert and A. Amrane, *Bioresour. Technol.*, 2010, **101**, 8923–8930.

5 R. J. Cornmell, C. L. Winder, S. Schuler, R. Goodacre and G. Stephens, *Green Chem.*, 2008, **10**, 685–691.

6 S. L. Bacon, A. J. Daugulis and J. S. Parent, *Green Chem.*, 2016, **18**, 6586–6595.

7 F. S. Oliveira, J. M. M. Araújo, R. Ferreira, L. P. Rebelo and I. M. Marrucho, *Sep. Purif. Technol.*, 2012, **85**, 137–146.

8 C. M. S. S. Neves, J. F. O. Granjo, M. G. Freire, A. Robertson, N. M. C. Oliveira and J. A. P. Coutinho, *Green Chem.*, 2011, **13**, 1517–1526.

9 M. Diedenhofen and A. Klamt, *Fluid Phase Equilib.*, 2010, **294**, 31–38.

10 D. Rabari and T. Banerjee, *Ind. Eng. Chem. Res.*, 2014, **53**, 18935–18942.

11 L. Y. Garcia-chavez, C. M. Garsia, B. Schuur and A. B. De Haan, *Ind. Eng. Chem. Res.*, 2012, **51**.

12 D. Rabari and T. Banerjee, *Fluid Phase Equilib.*, 2013, **355**, 26–33.

13 M. J. Pittman, M. W. Bodley and A. J. Daugulis, *J. Chem. Technol. Biotechnol.*, 2015, **90**, 1391–1399.

Appendix A1

Supplemental Information to Chapter 2

With minor changes to fulfill formatting requirements, this Appendix is substantially as it appears as Supplemental Information to:

S. L. Bacon, J. S. Parent and A. J. Daugulis, *J. Chem. Technol. Biotechnol.*, 2014, **89**, 948–956.

A1.1 Partition coefficient (PC) predictions for polymer/aqueous TPPB systems

The following provides a methodology for predicting polymer phase activity coefficients using UNIFAC-vdW-FV and the Flory-Huggins model in conjunction with pure component Hildebrand and Hansen solubility parameters.

As discussed in Chapter 2:

$$\text{Partition Coefficient} = \frac{w_i^{poly}}{w_i^{aq}} = \frac{\Omega_i^{aq}}{\Omega_i^{poly}} \tag{A1-1}$$

Where: a_i^{α} is the activity, w_i^{α} is the weight fraction and Ω_i^{α} is the weight fraction activity coefficient.

Aqueous phase weight fraction activity coefficients (Ω_i^{aq}) can be converted from mole fraction infinite dilution activity coefficients ($\gamma_i^{aq,\infty}$) in literature sources.[1–4] Alternatively, models such as NRTL[5] or UNIQUAC[6] can be used in conjunction with published binary system parameters.[7]

Polymer phase weight fraction activity coefficients (Ω_i^{poly}) can be found from literature sources[8–10] or using a predictive model. In Chapter 2, we investigated the use of UNIFAC-vdW-FV[11] and the Flory-Huggins model in conjunction with pure component Hildebrand and Hansen solubility parameters.[12,13] Sample calculations are shown below for the FH-Hildebrand and FH-HSP models. Readers interested in using UNFAC-vdW-FV can utilize the computer program[14] or consult the original derivation.[11]

A1.2 Flory-Huggins Solution Model

The Flory-Huggins solution model is the backbone for both the FH-Hildebrand and FH-HSP models.

$$\ln \gamma_i^{poly,pred} = \ln \frac{\varphi_i}{x_i} + 1 - \frac{\varphi_i}{x_i} + \chi_{ij}\varphi_j^2 \tag{A1-2}$$

Where:

γ^{pred} is the mole fraction activity coefficient (predicted)

x_i is the mole fraction of 'i'

χ_{ij} is the Flory-Huggins interaction parameter

φ_i is the volume fraction of species 'i':

$$\varphi_i = \frac{n_i V_i}{n_i V_i + n_j V_j} = \frac{x_i V_i}{x V_i + x_j V_j} \quad \text{(A1-3)}$$

Where:

n_i is the number of moles of 'i' [mol]

V_i is the molar volume of 'i' [cm^3/mol]:

$$V_i = \frac{MW_i}{\rho_i} \quad \text{(A1-4)}$$

Where:

MW_i is the molecular weight of 'i' [g/mol]

ρ_i is the density of 'i' [g/cm^3]

The mole fraction activity coefficient can be converted to the mass fraction activity coefficient:

$$\Omega_{\mathrm{i}}^{poly,pred} = \left(\frac{x_i}{w_i}\right) \gamma_i^{poly,pred} \quad \text{(A1-5)}$$

A1.3 FH-Hildebrand and FH-HSP

FH-Hildebrand and FH-HSP differ in how the Flory-Huggins interaction parameter (χ_{ij}) is calculated.

For FH-Hildebrand:

$$\chi_{12} = \frac{V_1}{RT}(\delta_1 - \delta_2)^2 + \beta \quad \text{(A1-6)}$$

Where:

V_1 is the solute molar volume [cm^3/mol] (Equation A1-4)

β is correction term generally accepted to equal 0.34

δ is the total solubility parameter [$MPa^{1/2}$]

R is the gas constant – 8.314 [cm^3 MPa K^{-1} mol^{-1}]

T is the temperature in [K]

For FH-HSP:

$$\chi_{12} = \alpha \frac{V_1}{RT}\left[(\delta_{d1} - \delta_{d2})^2 + 0.25\left(\delta_{p1} - \delta_{p2}\right)^2 + 0.25(\delta_{h1} - \delta_{h2})^2\right] \quad \text{(A1-7)}$$

Where:

α is a correction factor, set at α=1

δ_D, δ_P, and δ_H are the dispersive, polar and hydrogen bonding Hansen solubility parameters [$MPa^{1/2}$]

A1.4 Sample Calculations

The activity of *n*-butanol (1) in poly(*n*-butyl acrylate) (2) is used as an example. We will determine the weight fraction activity coefficient ($\Omega_i^{poly,pred}$) using both FH-Hildebrand and FH-HSP. The poly(*n*-butyl acrylate) molecular weight was assumed as 100,000 g/mol. A butanol concentration in the polymer of 0.01 mol/L has also been assumed, representing the upper threshold for the dilute-ideal solution assumption.

The following constants can be defined:

Variable	Description	Value	Equation
[BuOH]	Butanol concentration	0.01 mol/L	n/a
M_1	Butanol molecular weight	74.1 g/mol	n/a
M_2	Polymer molecular weight	100,000 g/mol	n/a
T	Temperature	303 K	n/a
ρ_1	Butanol density	0.810 g/cm^3	n/a
ρ_2	Polymer density (100k g/mol)	1.080 g/cm^3	n/a
δ_1	Butanol solubility parameter	23.2 MPa$^{1/2}$	n/a
δ_2	Polymer solubility parameter	17.6 MPa$^{1/2}$	n/a
$\delta_{1,d}$	Butanol dispersive parameter	16 MPa$^{1/2}$	n/a
$\delta_{1,p}$	Butanol polar parameter	5.7 MPa$^{1/2}$	n/a
$\delta_{1,h}$	Butanol h-bonding parameter	15.8 MPa$^{1/2}$	n/a
$\delta_{2,d}$	Polymer dispersive parameter	16.8 MPa$^{1/2}$	n/a
$\delta_{2,p}$	Polymer polar parameter	2.9 MPa$^{1/2}$	n/a
$\delta_{2,h}$	Polymer h-bonding parameter	4.4 MPa$^{1/2}$	n/a

The first step is to convert [BuOH] to mole fraction, x_i. Consider a system containing a 1 L solution of butanol (1)/poly(butyl acrylate) (2).

In 1 L of polymer-butanol solution, there are n_1= 0.01 mol of butanol, occupying 0.91 cm^3.

0.9991 L of polymer corresponds to:

$$0.9991\ L * 1.08\frac{kg}{L} = 1.079kg\ \rightarrow n_2 = \frac{1.079kg}{100\frac{kg}{mol}} = 0.01079\ mol$$

Therefore the mole fraction of butanol: $x_1 = \frac{n_1}{n_1+n_2} = \frac{0.01}{0.01+0.01079} = 0.481$

The mole fraction of polymer: $x_2 = 1 - x_1 = 0.519$

Using Equations A1-4 and A1-3, the volume fractions φ_i and molar volumes V_i are calculated.

Results are tabulated below.

Variable	Description	Value	Equation
x_1	Mole fraction of butanol	0.481	n/a
x_2	Mole fraction of polymer	0.519	n/a
V_1	Molar volume – butanol	91.5 cm^3/mol	A1-4
V_2	Molar volume – polymer	92,593 cm^3/mol	A1-4
φ_1	Volume fraction – butanol	0.00092	A1-3
φ_2	Volume fraction – polymer	0.9991	A1-3

Flory-Huggins Interaction parameters (χ_{12}) are calculated for the FH-Hildebrand and FH-HSP models

Variable	Description	Value	Equation
χ_{12}	FH-Hildebrand interaction parameter	1.475	A1-6
χ_{12}	FH-HSP interaction parameter	1.275	A1-7

Mole fraction activity coefficients ($\gamma_i^{poly,pred}$) are calculated with Equation A1-2, and converted to mass fraction activity coefficients ($\Omega_i^{poly,pred}$) using Equation A1-5.

Variable	Description	Value	Equation
$\gamma_1^{poly,pred}$	FH-Hildebrand (mole fraction)	0.0225	A1-2
$\boldsymbol{\Omega_1^{poly,pred}}$	**FH-Hildebrand (weight fraction)**	**15.8**	A1-5

$\gamma_1^{poly,pred}$	FH-HSP (mole fraction)	0.0184	A1-2
$\boldsymbol{\Omega_1^{poly,pred}}$	**FH-HSP (weight fraction)**	**12.9**	A1-5

Small discrepancies (<0.1) between the weight fraction activity coefficients ($\Omega_i^{poly,pred}$) calculated above and those published in Chapter 2 are due to the differences in concentrations at which they were evaluated. The results above were calculated at the upper threshold of infinite dilution (0.01 M) while the published values in Chapter 2 were evaluated at <0.0001M.

Appendix A2

Supplemental Information to Chapter 5

With minor changes to fulfill formatting requirements, this Appendix is substantially as it appears as Supplemental Information to:

S. L. Bacon, A. J. Daugulis and J. S. Parent, *Green Chem.*, 2016, **18**, 6586–6595.

A2.1 Ionomer antimicrobial behaviour – representative images

Figures A2-1 to A2-3 are representative experimental images demonstrating the ionomers' antimicrobial surface behaviour relative to the non-ionic parent material (BIMS). Each circular white dot is counted as a single bacterial/yeast colony. The mean number of counted colonies and standard deviation (from duplicate experiments) are presented in Section 5.5.5.

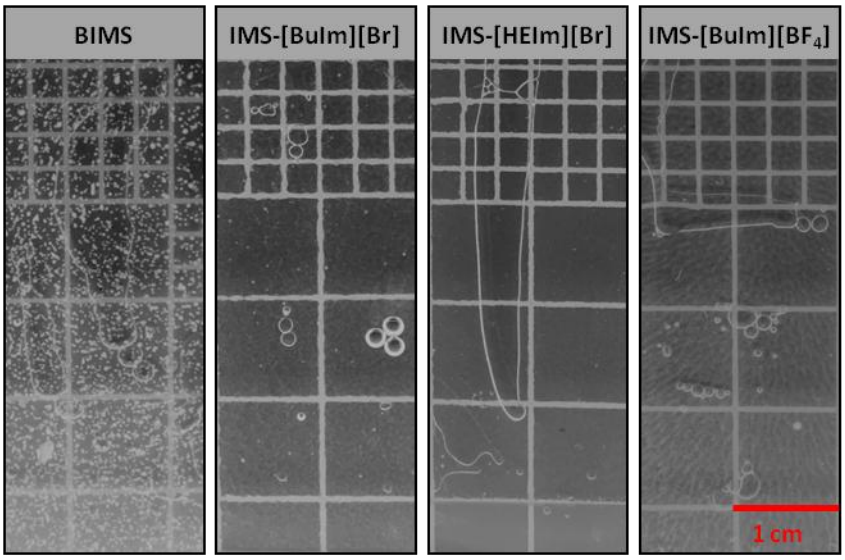

Figure A2-1 - *S. cerevisiae* growth on BIMS and its ionic derivatives

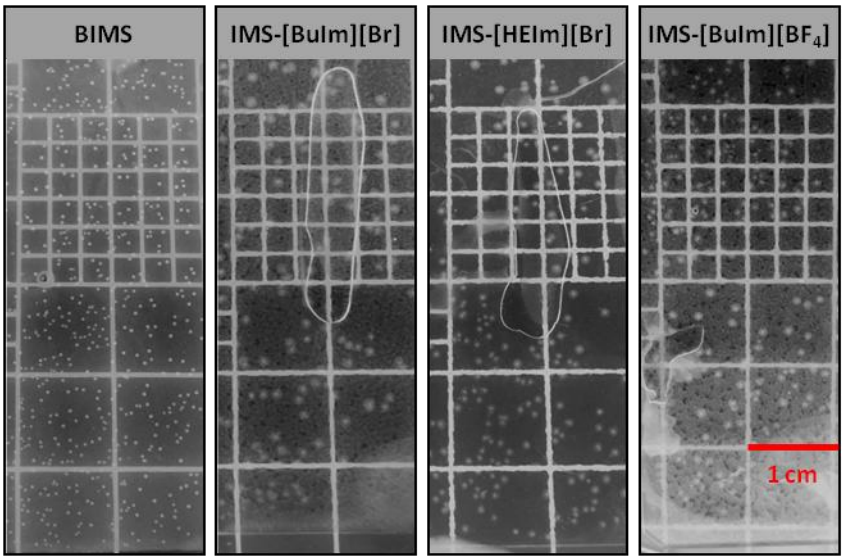

Figure A2-2 - *P.putida* growth on BIMS and its ionic derivatives

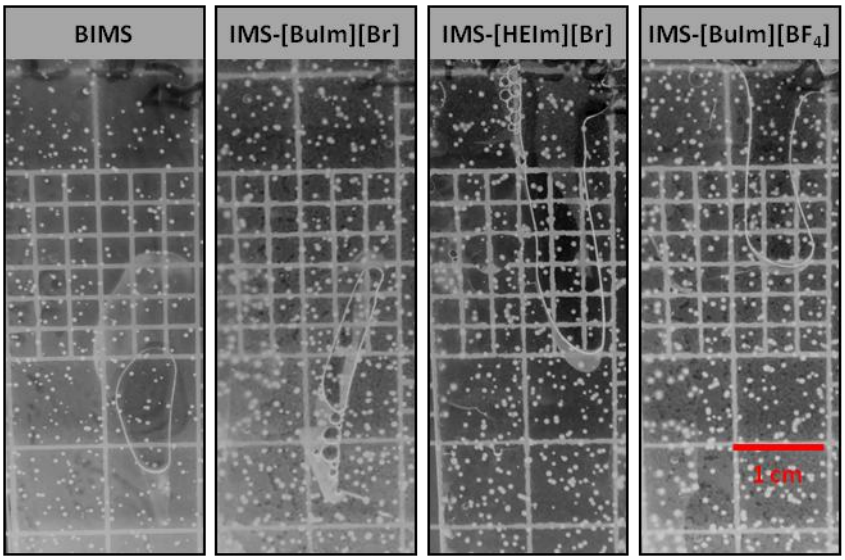

Figure A2-3 - *C. acetobutylicum* growth on BIMS and its ionic derivatives